Understanding Interaction Mechanism of Deformable Droplets in Oil Production

by

Chen Shi

A thesis submitted in partial fulfillment of the requirements for the degree of

Doctor of Philosophy

in

Chemical Engineering

Department of Chemical and Materials Engineering
University of Alberta

Abstract

Interactions mechanisms of deformable air bubbles and liquid droplets play critical roles in many established and modern industrial processes. Understanding the interaction mechanisms of oil droplets and air bubbles is of fundamental and practical importance to solve many challenging issues, especially for oil industries. In this thesis, a state-of-art droplet probe atomic force microscopy (AFM) coupled with reflection interference contrast microscopy (RICM) was applied, for the first time in the world, to simultaneously quantify interaction forces and the spatiotemporal evolution of the thin water film between air bubbles and solid mica surfaces. The measured force results were analyzed using a theoretical model based on Reynolds lubrication theory and augmented Young-Laplace equation to elucidate the intrinsic interaction mechanisms. Stable films sustained by van der Waals force were always observed between air bubbles and hydrophilic mica surfaces, whereas bubbles were found to readily attach onto hydrophobized mica surfaces. An exponential equation was also developed to quantify the hydrophobic attraction involved in asymmetric systems involving deformable droplets and air bubbles.

The validated AFM droplet probe technique and theoretical model were then applied to quantitatively study the interaction mechanisms of (1) oil droplets interacting in aqueous media in the presence or absence of asphaltenes, representing stabilization mechanism of oil-in-water emulsions (2) water droplets interaction in oil media with or without presence of asphaltenes, which represents the stabilization mechanism of water-in-oil emulsion, and (3) oil droplets interacting with solid surfaces in aqueous media, representing the bitumen and oil liberation processes. The force results between oil droplets in water revealed that

the interaction between two pristine oil droplets in water could be described by the classical Derjaguin-Landau-Verwey-Overbeek (DLVO) theory. Adsorption of asphaltenes at oil/water interface was found to result in more negative surface potential of the oil droplets and also induced steric repulsion, both of which inhibited coalescence of oil droplets and contributed to the stability of O/W emulsion. Lower pH could lead to less negative surface potential, and divalent ions (Ca^{2+}) could disrupt the protection of interfacial asphaltenes and induce oil droplets coalescence. For water droplets in oil, rapid coalescence was observed between bare water droplets, while interfacially adsorbed asphaltenes sterically inhibited droplet coalescence and induced interfacial adhesion. The adhesion increased with asphaltenes concentration but drastically decreased after the concentration exceeded ~ 100 mg/L. The addition of poor solvent (heptane) strengthened the interfacial adhesion at low asphaltenes concentration, while the opposite trend was observed for high asphaltenes concentration. Pure heptane was found to destabilize asphaltenes-coated water droplets. Droplet probe AFM was also applied to directly measure the interaction force between oil droplets (i.e. toluene and heptol) with the addition of asphaltenes and mica surfaces with varying hydrophobicity in aqueous media to understand the wetting mechanisms of the oil/water/solid system. For hydrophilic mica surfaces, asphaltenes adsorbed at oil/water interface strengthened electrical double layer repulsion and induced steric repulsion, stabilizing water films and inhibiting oil droplet attachment on the surfaces. For hydrophobized mica surfaces, the hydrophobic attraction overcame the steric hindrance of interfacial asphaltenes, leading to rapid attachment and strong adhesion of oil droplet on the surfaces.

This study provides a novel technique to study the interaction mechanisms of deformable droplets and air bubbles, with the capacity of synchronous measurements of the interaction forces and the drainage dynamics of thin liquid films. Results obtained using this technique for the systems in oil production also provide fundamental insights into the interaction mechanisms of oil and water droplets in complex solution conditions, with valuable implication on the stabilization mechanism of O/W and W/O emulsions and the wetting mechanisms of oil/water/solid systems in presence of asphaltenes.

Preface

Chapter 3 of this thesis has been published as C. Shi, X. Cui, L. Xie, Q. Liu, D.Y.C. Chan, J.N. Israelachvili, and H. Zeng, "Measuring Forces and Spatiotemporal Evolution of Thin Water Films between an Air Bubble and Solid Surfaces of Different Hydrophobicity," *ACS Nano*, vol. 9, issue 1, 2438-2446. I was responsible for the AFM force measurement, data analysis, and the manuscript composition. X. Cui and L. Xie assisted with AFM force measurement. Dr. Q. Liu, Dr. D.Y.C. Chan, and Dr. J.N. Israelachvili contributed to manuscript edits. Dr. Hongbo Zeng was the supervisory author and was involved in concept formation and manuscript composition.

Chapter 4 of this thesis has been published as C. Shi, L. Zhang, L. Xie, X. Lu, Q. Liu, C.A. Mantilla, F.G.A. van den Berg, and H. Zeng, "Interaction Mechanism of Oil-in-Water Emulsions with Asphaltenes Determined Using Droplet Probe AFM," *Langmuir*, vol. 32, issue 9, 2302-2310. I was responsible for extraction of asphaltenes, the AFM force measurement, data analysis, and the manuscript composition. Dr. L. Zhang assisted with AFM force measurement and data analysis. X. Lu assisted with the extraction of asphaltenes and conducted interfacial tension measurement. Dr. Q. Liu, Dr. C.A. Mantilla, and Dr. F.G.A. van den Berg contributed to manuscript edits. Dr. Hongbo Zeng was the supervisory author and was involved in concept formation and manuscript composition.

Chapter 5 of this thesis will be submitted for publication as C. Shi, L. Zhang, L. Xie, Q. Liu, C.A. Mantilla, F.G.A. van den Berg, and H. Zeng, "Nanomechanical insights into the stabilization mechanisms of Water-in-Oil Emulsion due to Asphaltenes." I was responsible for extraction of asphaltenes, the AFM force measurement, data analysis, and

the manuscript composition. Dr. L. Zhang assisted with AFM force measurements and manuscript edit. L. Xie assisted with AFM force measurement and data analysis. Dr. Q. Liu, Dr. C.A. Mantilla, and Dr. F.G.A. van den Berg contributed to manuscript edits. Dr. Hongbo Zeng was the supervisory author and was involved in concept formation and manuscript composition.

Chapter 6 of this thesis will be submitted for publication as C. Shi, L. Zhang, L. Xie, Q. Liu, C.A. Mantilla, F.G.A. van den Berg, and H. Zeng, "Probing the Interaction Mechanisms between Oil Droplet and Solid Surface using Droplet Probe AFM." I was responsible for extraction of asphaltenes, the AFM force measurement, data analysis, and the manuscript composition. Dr. L. Zhang assisted with sample preparation and manuscript edit. L. Xie assisted with contact angle measurement and data analysis. Dr. Q. Liu, Dr. C.A. Mantilla, and Dr. F.G.A. van den Berg contributed to manuscript edits. Dr. Hongbo Zeng was the supervisory author and was involved in concept formation and manuscript composition.

Chapters 1, 2, and 7 are originally written by Chen Shi, and have never been published before.

Acknowledgement

I wish to express my sincere gratitude to Prof. Hongbo Zeng for his excellent and irreplaceable guidance and inspiring encouragement during my graduate study. His brilliant mind shed guiding light for me each time I came across difficulties in these years, and his dedication and passion into scientific research always inspired me to pursue my career and lifelong goal as a dedicated researcher. I also wish to thank Prof. Qingxia Liu for his experienced suggestions throughout the course of this study. His carefulness into each detail during work set an excellent example for me.

I wish to thank all my group members for their solid support and help during my study. I would like to express my special thanks to Mr. Lei Xie, Dr. Jingyi Wang, Dr. Ling Zhang, Mr. Xin Cui for their valuable discussions during progress and contributions to the accomplishment of this work.

The last but not the least, my sincerest gratitude goes to my parents. Without their warm support and encouragement, I would never be able to complete my Ph. D. study.

Table of Contents

List of Tables

List of Figures

List of Acronyms

DLVO   Derjaguin-Landau-Verwey-Overbeek

AFM   Atomic force microscopy

SFA   Surface force apparatus

RICM   Reflection interference contrast microscopy

OTS   Octadecyltrichlorosilane

VDW   Van der Waals

EDL   Electrical double layer

rms   Root-mean-square

DCM   Methylene chloride

List of Symbols

A	Hamaker constant
h	Separation between surfaces
D_{H}	Decay length of hydrophobic force
R_1, R_2	Radius of droplet or bubble
F	Interaction force
φ	Surface potential
κ	Inverse of Debye length
T	Temperature
γ	Interfacial tension

Chapter 1 Introduction

1.1. Interactions of deformable droplets and air bubbles

Deformable droplets or air bubbles are formed by suspending liquid droplets or air bubbles in another immiscible liquid, forming liquid/liquid or air/liquid interface. In contrast to the strong elasticity-controlled deformation energetics of a solid/water interface, the deformation energetics of a liquid/liquid or air/liquid interface is governed by the relatively weak interfacial tension γ, and thereby the shape of the interface is largely controlled by the balance between internal Laplace pressure, which is related to the interfacial tension and the droplet size, and external pressures, including velocity-dependent hydrodynamic pressure due to fluid dynamics and separation-dependent disjoining pressure due to surface forces.[1, 2] Therefore, liquid droplets or air bubbles can readily change their shapes in response to external forces when interacting with other objects. And even tiny forces can result in significant deformation at the liquid/liquid and air/liquid interfaces, especially for those with very low interfacial tension. This convoluted coupling between interfacial deformation and interaction force renders it extremely challenging to accurately determine the absolute local separation between a liquid/liquid or air/liquid interface and another during the interaction, so is the intrinsic interaction mechanisms of deformable liquid droplets and air bubbles.

In general, interaction of deformable liquid droplets or air bubbles can be generalized into three different stages.[3-5] Without losing generality, interaction between an oil droplet and a solid surface in water is shown here as an example as illustrated in Figure 1.1. First,

1

the oil droplet is brought close to the solid surface in water by external forces (e.g. fluid flow, buoyance force). At this stage, the external force exerted on the droplet is negligible and it remains almost spherical with shape unchanged (Figure 1.1A).[4, 6] When the droplet and the solid surface are close enough, the hydrodynamic pressure becomes comparable to the Laplace pressure inside, leading to considerable droplet deformation and formation of a confined thin water film between the solid/water and oil/water interfaces (Figure 1.1B). Due to compensation by droplet deformation, this confined water film is much more difficult to be completely drained out than that between two rigid interfaces. At the final stage when the thickness of the water films decreases to $< \sim 100$ nm, as shown in Figure 1.1C, the disjoining pressure due to surface forces come into effect, ultimately deciding the stability of the water film.[2, 5, 7-10] Fundamentally, attractive surface forces such as van der Waals (VDW) force and hydrophobic force will destabilize the water film and lead to attachment of the oil droplet onto the solid surface, while the thin water film can be stabilized if repulsive surface forces like electrical double layer (EDL) force and steric repulsion dominate the interaction.
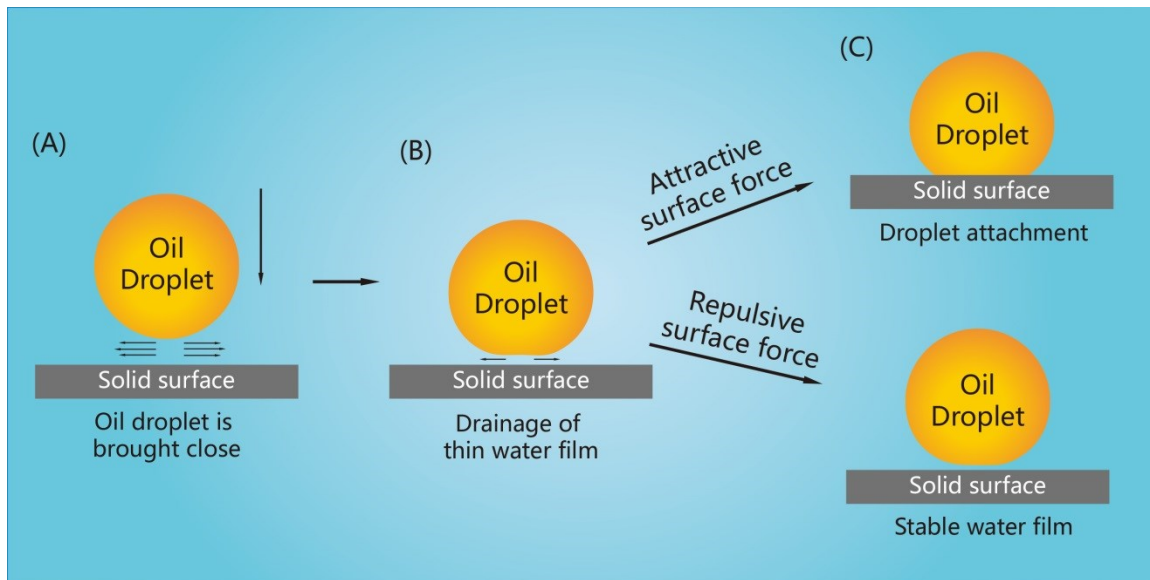
Figure 1.1. Schematic illustration of three different stages of the interaction between an oil droplet and a solid surface in water.

Therefore, a complete understanding of the fundamental interaction mechanisms of deformable droplets and air bubbles requires the essential information on the force-distance profile of the surface forces involved and the corresponding spatiotemporal interfacial deformation during interaction.[11] However, stable and precise manipulation of deformable droplets and bubbles is much more experimentally challenging than solid particles, and the complex convolution between interfacial deformation and surface forces obscures the interpretation of measured force and distance results.

1.2. Approaches to measuring the interaction of deformable droplets and air bubbles

Experimental attempts to measure the interaction of deformable droplets and bubbles can be traced back to be decades ago. In 1934, Taylor investigated the break-up behavior of

emulsion droplets using four-roll mill which could control the movement of suspending droplets through four independently-rotating cylindrical rollers.[12] This four-roll mill was later improved in 1980s to be computer-controlled by Gary Leal.[13-15] This computer-controlled four-roll mill was applied to study the interaction and coalescence behavior between emulsions droplets under different conditions from 2005.[16] It was found that the droplet coalescence was strongly related to velocity,[3] droplet size,[16] viscosity ratio[17] and so on.[18-21] Theoretical model to describe the drainage process of the thin liquid film confined between two droplets or between a droplet and a solid surface was developed in 1980s.[4, 22] Surface forces such as VDW force and EDL force were incorporated within the theoretical models to elucidate the destabilization and stabilization mechanisms of the thin liquid film.[5] Moreover, many other factors, such as viscosity ratio,[23] presence of surfactant,[24] were further investigated to understand their impacts on the film drainage process under different circumstances.

1.2.1. Light interferometer

The evolution of the profile of confined thin water film was studied using light interferometer by observing the light interference patterns. In 1972, for the first time, Blake directly visualized the drainage process of the thin water film confined between an air bubble and a solid silica surface using an apparatus which was later referred to as Scheludko cell.[25, 26] Both bare hydrophilic silica surfaces and methylated hydrophobic silica surfaces were studied. A stable water film was found to be sustained between an air bubble and a hydrophilic silica surface, but the water film rapidly ruptured when thinned to a critical

thickness for the hydrophobized silica surface.[25] A modified Scheludko cell, which was also called thin film pressure balance, was applied to study the drainage process between two air/water interfaces, mimicking the interaction between two air bubbles in water, as shown in Figure 1.2A.[27, 28] With this technique, Yaminsky *et al.* observed different drainage behaviors between two air/water interfaces, which depended on the approach velocity of the air/water interfaces, highlighting the important role of bubble velocity on the interaction mechanisms.[27, 28]
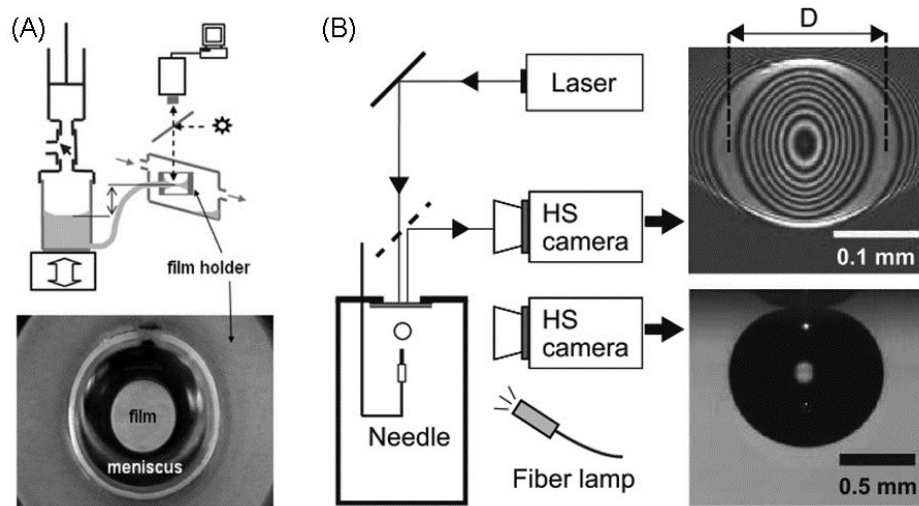
Figure 1.2. (A) Experiment setup of thin film pressure balance for measuring the drainage process between two air/water interfaces (top) and an optical reflection image of a water film between two air/water interfaces (bottom);[27] (B) Schematic of the experimental setup for measuring the drainage process between a rising air bubble and a glass surface (left), and a synchronized top-view high-speed camera was used to record interference fringes between

the glass surface and the bubble surface (right top) and another side-view camera was used to record the bubble position (right bottom). [29]

Free bubble rise method is another conventional method to study the interaction between a rising air bubble and a horizontal solid surface (generally transparent) in water.[30-34] The trajectory of the air bubble that collided with and bounced back from the surface was captured and theoretically modeled. Coupled with light interferometer, the dynamics of the thin water film drainage process between the rising bubble and solid surface were visualized and analyzed, which provided a feasible tool to study the interaction mechanisms of the system.[29, 35, 36] Parkinson et al. used this method to investigate the interaction between a small rising bubble and a hydrophilic titania surface under various aqueous conditions.[35] Theoretical modelling of the measured results revealed the significant impacts of surface forces on the interaction.[36] Using a similar method, Hendrix et al. studied the spatiotemporal evolution of the thin water film confined between an air bubble and a glass surface, and the drainage process could be well explained by a theoretical model based on Reynolds lubrication theory.[29] Recently, the drainage process in an asymmetric system between a rising air bubble and an oil/water meniscus was studied by Li *et al.*[37] By tuning the VDW force to be repulsive or attractive, they successfully demonstrated that a short-ranged hydrophobic attraction should exist in the system to induce water film rupture between the air bubble and oil/water meniscus. All of these techniques have provided valuable information on the drainage process of the confined water film, but the interaction force of

deformable droplets cannot be precisely quantified using these techniques, most likely due to the aforementioned experimental challenges.

1.2.2. Surface force apparatus

The surface force apparatus (SFA) is a unique nanomechanical technique for measuring interaction force between two curved molecularly smooth mica surfaces.[38-40] By using fringes of equal chromatic order (FECO), SFA is able to provide *in situ* high-resolution measurement of the absolute separation between the two interacting surfaces. A modified SFA was reported by Connor in 2001, which changed the top mica surface to be a flat one and replaced the bottom mica surface with a mercury droplet (Figure 1.3A).[41, 42] Their studies focused on the dynamics of the drainage process between the mica surface and the mercury droplet. By changing the electrolyte concentrations and the surface charge of the mercury droplet, they controlled the surface force between the mica surface and mercury droplet to be repulsive and attractive, demonstrating the important role of surface forces in the thin film drainage process and inducing attachment of the droplet onto the solid mica surface.[42] Later, the same experiment technique was applied to study the interaction between a mica surface and an immobilized air bubble in a range of electrolyte solutions with varying concentrations (Figure 1.3B).[43-45] The results demonstrated the negative charge of air bubbles under these conditions and found the strong electrical double layer repulsion could sustain a stable water film between the mica surface and air bubble. However, the experiment focused on the evolution of the thin water film, and the measured force-displacement profiles remained to be further theoretically modeled and explained.[46, 47]
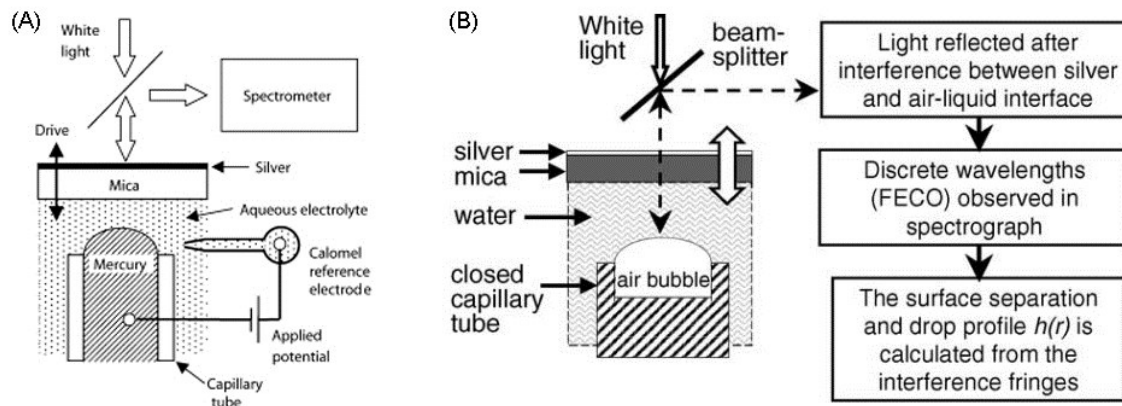
Figure 1.3. Schematic of modified SFA for measuring the interaction between a flat mica surface and (A) a mercury droplet;[42] (B) an air bubble.[44]

1.2.3. Atomic force microscopy

Quantitative force results of interaction involving deformable droplets and air bubbles were first obtained using atomic force microscopy (AFM).[48-50] AFM is one of the most widely used nanomechanical techniques for direct measurement of the interaction force in a wide range of systems. The interaction forces were measured by detecting the deflection of a force-sensing cantilever whose behavior could be treated as a Hooke's spring.[49, 51] Although the information on the absolute separation between interacting objects cannot be directly obtained from AFM measurement, the force-separation profile can be calculated straightforward in systems with only rigid interfaces for their deformation during interaction can be negligible.[50, 52] For interaction involving deformable droplets, however, the

interfacial deformation of the droplets obscures the absolute separation during interaction, so does the force-separation profile. [1, 2, 6, 7, 9, 53, 54]

In 1994, AFM with colloidal probe technique was applied for the first time to quantitate the interaction force between a rigid silica sphere probe and an air bubble immobilized on a substrate, as shown in Figure 1.4A.[1] A spherical colloidal particle, which could be silica, glass, or other minerals, was glued onto tipless cantilever, and then it was driven to interact with an air bubble or oil droplet immobilized on a hydrophobized substrate.[55] Strong repulsion and stable water film was measured between air bubbles and hydrophilic silica particles in water, which could be resulted from repulsive EDL interactions. On the other hand, attachment of solid particles onto the immobilized bubbles or droplets was detected for hydrophobic particles, as indicated by the sudden jump-in behaviors on the measured force curves.[1] Similar method was also applied to measured th interaction between air bubbles and other solid particles.[55-57] Addition of surfactants was found to effectively inhibit attachment of air bubbles on hydrophobized silica particles.[58] This approach using AFM colloidal probe technique makes it possible to directly measure the interaction force between deformable droplets or air bubble and different solid particles, even including real mineral particles.[56] In all of these studies, however, the measured force-displacement data was converted to force-separation results by simply treating the air bubble or oil droplet as a linear Hooke's spring with spring constant equal to the interfacial tension. This assumption was later proven unsuitable in these cases, since the deformation of bubbles or droplets due to external force was non-linear, especially for those with very large deformations.[53, 59, 60] The application of the colloidal probe technique is also limited for the facts that the geometry of the solid particle glued on the tipless cantilever can be extremely irregular and

9

the choice of the particle is highly restricted due to the strict requirement on size, stability and geometry.
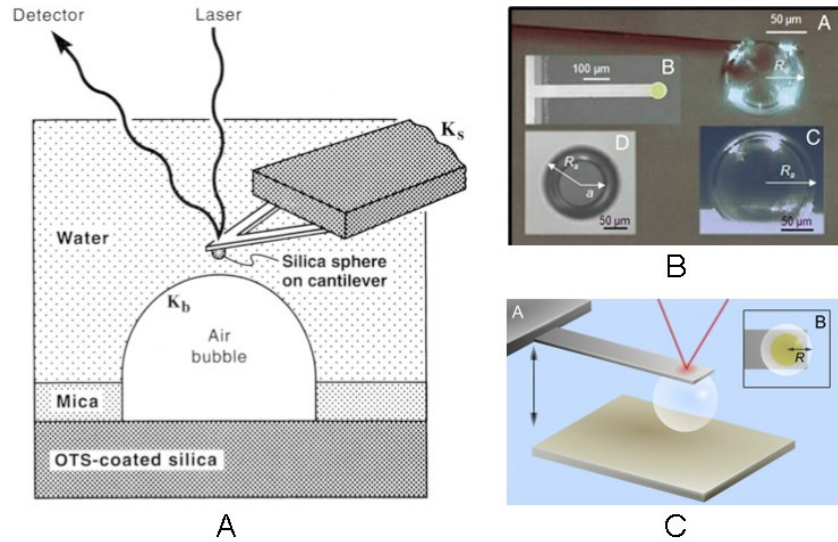
Figure 1.4. (A) Schematic of measuring the interaction between a silica particle and an air bubble using AFM colloidal probe.[1] (B) Measuring interaction between two air bubble using bubble probe AFM;[61] (B) Schematic of measuring interaction between an air bubble using bubble probe AFM.[62]

Precise quantitative investigation of interactions involving deformable droplets or air bubbles was first realized by a newly developed droplet probe AFM technique.[59, 61, 63, 64] Instead of using conventional AFM cantilevers, this droplet probe AFM technique utilized a specialized tipless AFM cantilever to pick up a deformable droplet or air bubble to create a droplet/bubble probe. The created droplet/bubble probe could then be driven to the sample objects to test. Therefore, almost all kinds of surfaces can be used as the substrate with the droplet/bubble probe AFM technique, even including the real mineral substrates. In order to

accurately interpret the force results, a theoretical model based Reynolds lubrication theory and augmented Young-Laplace equation was also developed, which took into consideration both the disjoining pressure from surface forces and non-linear deformation of droplet or bubble during interaction.[65] This theoretical model covered the three regimes of interactions involving deformable droplets or bubbles, and perfectly explained the dynamic force results measured using droplet probe AFM. The validity of the theoretical model was also verified by integrated confocal microscopy. With this novel technique, interaction mechanisms of both symmetric systems, such as between two identical oil droplets or air bubbles in water,[16, 61, 63, 66-69] and asymmetric systems, like between oil droplets and air bubbles,[62, 70] have been successfully elucidated, as shown in Figure 1.4B. The measured force results were analyzed using the aforementioned theoretical model, demonstrating the important roles of both dynamic conditions (e.g. velocity, viscosity)[71] and interfacial properties (e.g. interfacial tension, surfaces forces)[66] on the coalescence behaviors within these systems. Interaction between air bubbles and solid surfaces (e.g. silica, mica, gold) was also studied using this technique (Figure 1.4C), revealing the repulsive VDW force in these systems, which supported thin water films in nanoscale between the bubble and solid surface.[62] This novel method provides a feasible and flexible method to directly obtain quantitative insights into the interaction mechanisms of a wide range of systems involving deformable droplets and air bubbles. However, direct visualization of the thin water film during force measurements is not available for droplet/bubble probe AFM alone.

1.3. Deformable oil droplets and air bubbles in oil industry

1.3.1. Oil-in-water and water-in-oil emulsions

Deformable droplets and bubbles commonly exist in a wide range of industrial process, including mineral flotation,[72, 73] pharmaceutics,[74, 75] and so on. Especially in oil production industry, oil generally co-exists with water and solid particles to form oil-in-water (O/W) emulsion, e.g. oil residue in processing water, or water-in-oil (W/O) emulsion, e.g. water residue in oil froth, depending on the amount ratio between oil and water.[76-78] These emulsions with extremely high stability are highly undesirable, because they are believed to be the major cause for the challenging issues encountered during production of conventional crude oil and oil sands, such as high transportation cost due to increased viscosity. Moreover, emulsified water droplets with size of several micrometers commonly exist in the diluted bitumen froth. These emulsified water droplets contain a large amount of chloride ions, which can cause serious erosion and corrosion production issues in downstream processing equipment including heat exchangers, pipelines and upgrading equipment, and the clay particles in the emulsion can also lead to serious problems such as pipeline plugging.[79-81] Therefore, these emulsions should be destabilized before further treatment, and the residue water and clay particles contained in the emulsions should be removed for enhancing the production quality and efficiency. Understanding the mechanisms by which the O/W and W/O emulsions are stabilized is of both practical and fundamental importance for the oil industries to further devise effective and economic technologies to solve the challenging issues with these emulsions.
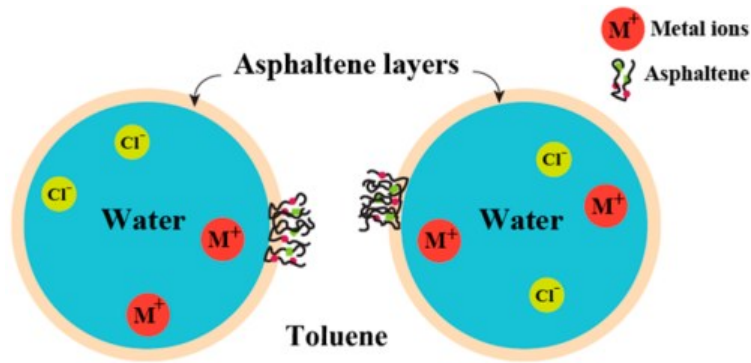
Figure 1.5. Schematic of stabilization of W/O emulsions due to adsorbed asphaltenes and clay particles.[81]

Fundamentally, the stability of the emulsified water or oil droplets is largely determined by the microscopic interaction force between them under complex solution conditions. In general, strong inter-droplet repulsion (e.g. EDL and steric repulsion) and lack of interfacial adhesion will lead to stabilized emulsion, while attractive surface forces (e.g. VDW force and hydrophobic force) and presence of interfacial adhesion can destabilized the emulsions.[2, 7] For the W/O emulsions encountered in oil production industry, the adsorption of asphaltenes and solid clay particles is believed to form a gel-like protective layer around the water droplets (Figure 1.5), providing a strong steric repulsion against droplet coalescence which leads to stabilized W/O emulsions.[78, 81-83] Direct quantitative measurement of the interaction force between emulsion droplets with presence of different surface active components under complex solution conditions will provide valuable insights to the stabilization mechanisms of different kinds of emulsions.

1.3.2. Bitumen flotation

Water-based bitumen extraction from oil sands and air flotation process are the most widely commercialized process for extracting bitumen from open-mined oil sands (Figure 1.6).[84] In the first step in this process, which is also called bitumen liberation process, the oil sands are mixed with hot water and some chemical additives, and the bitumen is liberated from the oil sands grains, forming suspending bitumen droplet in the mixture. Secondly, in the air flotation process, the bitumen-water mixture is then aerated to separate the bitumen droplets from the find solids, which will be diluted with organic solvents and further treated to obtain pure bitumen products.
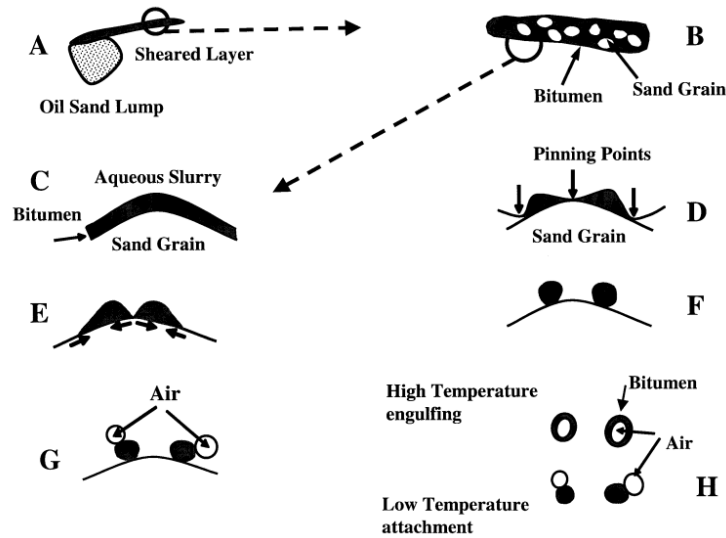
Figure 1.6. Schematic illustration of bitumen liberation process (A~F) and air flotation process (G and H).[84]

Many studies have proven the significant role of the interaction among air bubbles, bitumen droplets and the fine solid particles in determining the bitumen recovery efficiency and efficacy and the quality of the final bitumen products.[85-90] Due to the intrinsic hydrophobicity of bitumen droplets and hydrophilicity of the solid particles, the collecting air bubbles, which are also inherently hydrophobic, will selectively attach onto the bitumen droplets, forming bitumen-bubble aggregates which can float to the top of in the form of a froth rich in bitumen. Meanwhile, the relatively hydrophilic fine solid particles will remain suspending in the water phase for they lack affinity to collecting air bubbles, and thereby the unwanted solid particles can be separated and discarded as tailings. At microscopic scale, the interaction between bitumen droplets and collecting air bubbles directly determines the recovery efficiency of the bitumen, with higher collision and attachment chances corresponding to better bitumen recovery efficiency. Meanwhile, the interaction between fine solid particles and bitumen droplets or air bubbles determines the quality of the bitumen froth. For example, strong attraction and adhesion between solid particles and bitumen droplets will impede the bitumen liberation process and result in relatively high solid content in the bitumen products. In general, to achieve higher bitumen recovery efficiency, larger bitumen droplets and smaller collecting bubbles are highly preferred, for they have relatively high collision and attachment efficiency with each other during flotation processes.[84, 90] Elucidating the intrinsic interaction mechanisms of each step during bitumen flotation will help us find effective ways to further enhance the quality of the bitumen products and the productivity of oil sands industries.

1.3.3. Asphaltenes

The aforementioned issues involving deformable droplets or bubble are closely related with the surface active components during the processes. Of all the surface active components existing in crude oil and bitumen products, asphaltenes is believed to be the most interfacially active and problematic one.[91, 92] Asphaltenes is the heaviest component in all of crude oil and bitumen products.[93-95] Practically, the asphaltenes is separated from crude oil based on the solubility properties, and the components that can be dissolved in aromatic solvents such as toluene but precipitate in paraffinic solvents such as heptane are defined as asphaltenes. Therefore, the asphaltenes is not a pure component with well-defined chemical structures, but a complex mixture consisting of thousands of different molecules with varying structure, shapes and sizes. And the physiochemical properties of asphaltenes varied significantly depending on many parameters such as the source of crude oil, the extraction procedures, and so on. Nevertheless, it has been widely reported that asphaltenes extracted from different crude oil samples share lots of similar colloidal behaviors and interfacial properties, e.g. they all can adsorb at oil/water interfaces and stabilize the W/O emulsions.[96-98]

Although the chemical structure of asphaltenes is still mysterious and under debate, several theoretical models have been reported to explain the molecular and colloidal properties of asphaltenes. Of all the models, the Yen-Mullins model is the most accepted one. In this model, asphaltenes are considered to consist of condensed polyaromatic rings interconnected or decorated with peripheral alkane chains and a considerable amount of heteroatoms including oxygen, nitrogen, sulfur and trace amount of metal ions. The

heteroatoms generally exist in the asphaltenes as polar functional groups including both acidic groups (e.g. carboxylic groups) and basic groups (e.g. amino groups). Hence, the combination of hydrophobic condensed rings and hydrophilic polar groups render the asphaltenes interfacially active, and thereby the asphaltenes molecules can readily adsorb onto the oil/water interface and alter the interfacial properties, which can impact the interactions of the emulsified droplets and ultimately determine the macroscopic properties of the whole system (e.g. emulsion stability).

The adsorption behavior of asphaltenes at oil/water interface and the consequential alteration of interfacial properties have been investigated using a wide range of experiment techniques including interfacial tension and rheology measurement,[97, 99, 100] micropipette,[101, 102] Langmuir-Blodgett trough (L-B trough),[103] and so on.[104] Interfacial tension measurement between water and oil in presence of asphaltenes demonstrated that the asphaltenes could adsorb onto the oil/water interface and lower the interfacial tension, and the adsorption behavior could be affected by asphaltenes types, oil type (e.g. toluene, heptane, pentane), water chemistry (e.g. salt type, salt concentration, pH), temperature, pressure, and so on.[77, 100, 105, 106] Rheological properties of oil/water interfaces with asphaltenes showed a viscoelastic behavior, indicating the asphaltenes might form crosslinked gel-like protective layer at the oil/water interfaces which could effective inhibit coalescence between emulsion droplets.[99, 100, 107] L-B trough experiments showed that the adsorption of asphaltenes at the interface was irreversible, and the formed interfacial layer was rigid to be washed by pure solvent.[103] Micropipette experiment also revealed the significant protective effects of interfacial asphaltenes against droplet coalescence.[102]

The molecular interactions between asphaltenes have also been investigated using nanomechanical techniques including SFA and AFM.[81, 95, 108-110] Measurement of interaction force between asphaltenes surfaces in organic solvents was conducted using AFM and SFA. The asphaltenes was coated on mica or silica surfaces. It was reported that strong repulsion without adhesion was measured between asphaltenes surfaces in toluene, which was believed to be attributed to the steric hindrance between the extending asphaltenes chains in toluene.[81, 95, 110] In heptane, however, much weaker repulsion and strong adhesion and stretching behavior between asphaltenes were measured. Measurement between asphaltenes surfaces in water also provided valuable information on the properties of asphaltenes at the aqueous side.[109, 111, 112] All of these reports provided insights into the molecular interaction mechanisms of asphaltenes under various conditions. However, all the reported force data were based on the interaction between asphaltenes surfaces immobilized on solid substrates, whose mobility and properties could differ significantly from that adsorbed at the real oil/water interfaces. Therefore, a direct and quantitative measurement and understanding of the interaction mechanisms of emulsion droplets with interfacially adsorbed asphaltenes, under various complex solution conditions (e.g. solvent type, pH, ion concentration and the presence of multivalent ions such as Ca^{2+}), is of critical importance to better elucidate the molecular interaction mechanisms of asphaltenes at the real oil/water interface and the stabilization mechanism of both O/W and W/O emulsions.

1.4.Objectives

The fundamental understanding of the interaction mechanisms of deformable droplets and bubbles is still incomplete due to the experimental challenges of measurement of interaction forms and synchronous thin film drainage process. Therefore, the major objective of this thesis is to quantify the interaction mechanisms of deformable droplet and bubble from the aspects of interaction force and thin film drainage by innovatively combining the AFM droplet probe technique, RICM technique and theoretical modeling, and apply this method to quantitatively elucidate the interaction mechanisms of emulsion droplets with presence of asphaltenes under complex solution conditions, with specific focus on the systems encountered in oil productions. The key parameters to be explored include water chemistry, solvent type, and properties of the solid surfaces. The detailed objectives are as follows.

(1) Combine AFM droplet probe technique and RICM technique to directly measure the interaction force and synchronous thin film drainage process between air bubbles and solid surfaces with varying hydrophobicity, which will provide a fundamental understanding of the interaction mechanisms of the deformable droplets and validate the AFM droplet probe technique and theoretical model.

(2) Measure the interaction forces between oil droplets in water in the presence of asphaltenes to elucidate the stabilization mechanisms of O/W emulsions due to asphaltenes. AFM droplet probe technique together with theoretical modeling will be applied to

investigate the interaction forces, and the effects of ion concentration, types of ions (Na^+ and Ca^{2+}), pH, and the asphaltenes concentration in oil droplet will be studied.

(3) Study the interaction between water droplets with interfacially adsorbed asphaltenes in different oil solvents to provide nanoscopic insights into the impacts of interfacial asphaltenes on the stability of W/O emulsions. The parameters to study include asphaltenes concentration, maximum force load, contact time between water droplets, aging time, and solvent type.

(4) Investigate the interaction mechanisms between oil droplets and solid surfaces in aqueous solutions using AFM droplet probe technique to understand the wetting mechanisms of oil/water/solid systems from nanoscopic scale. The impacts of ion concentration, type of oil solvent, asphaltenes concentration in oil and the hydrophobicity of the solid surface will be studied.

1.5. Structure of the Thesis

Chapter 1 introduces the previous approaches to understanding the interaction mechanisms of deformable droplets, and reviews the systems involving deformable droplets in oil productions. The objective of this thesis is also introduced.

Chapter 2 presents the materials and the working principles of the experiment techniques used in this study. The theoretical model used in this thesis is also provided.

Chapter 3 describes the approach to measuring the interaction force and synchronous thin film drainage process in air/water/solid systems by using AFM droplet probe technique and RICM technique. The experiment results and theoretical results are compared to validate the technique and the theoretical model, and the hydrophobic interaction in air/water/solid system is introduced.

Chapter 4 demonstrates the results of interaction forces between oil droplets in aqueous solutions with presence of asphaltenes measured using AFM droplet probe technique, with implication on the stability mechanisms of O/W emulsions due to asphaltenes.

Chapter 5 studies the interaction forces between water droplets in oil solvents with interfacial adsorbed asphaltenes, corresponding to the stability mechanisms of W/O emulsions due to adsorption of asphaltenes.

Chapter 6 presents the study on the interaction between oil droplet and solid mica surfaces in complex aqueous conditions, to provide implications on the wetting mechanisms of oil/water/solid systems in oil productions.

References

(1). Ducker, W. A.; Xu, Z.; Israelachvili, J. N. Measurements of hydrophobic and DLVO forces in bubble-surface interactions in aqueous solutions. *Langmuir* **1994,** 10, 3279-3289.

(2). Israelachvili, J. N., *Intermolecular and surface forces: revised third edition*. Academic press: 2011.

(3). Yang, H.; Park, C. C.; Hu, Y. T.; Leal, L. G. The coalescence of two equal-sized drops in a two-dimensional linear flow. *Physics of Fluids (1994-present)* **2001,** 13, 1087-1106.

(4). Lin, C. Y.; Slattery, J. Thinning of a liquid film as a small drop or bubble approaches a solid plane. *AlChE J.* **1982,** 28, 147-156.

(5). Chen, J.-D. Effects of London—van der Waals and electric double layer forces on the thinning of a dimpled film between a small drop or bubble and a horizontal solid plane. *J. Colloid Interface Sci.* **1984,** 98, 329-341.

(6). Klaseboer, E.; Chevaillier, J. P.; Gourdon, C.; Masbernat, O. Film drainage between colliding drops at constant approach velocity: experiments and modeling. *J. Colloid Interface Sci.* **2000,** 229, 274-285.

(7). Zeng, H., *Polymer adhesion, friction, and lubrication*. John Wiley & Sons: 2013.

(8). Zeng, H.; Shi, C.; Huang, J.; Li, L.; Liu, G.; Zhong, H. Recent experimental advances on hydrophobic interactions at solid/water and fluid/water interfaces. *Biointerphases* **2016,** 11, 018903.

(9). Shi, C.; Chan, D. Y.; Liu, Q.; Zeng, H. Probing the hydrophobic interaction between air bubbles and partially hydrophobic surfaces using atomic force microscopy. *J. Phys. Chem. C* **2014,** 118, 25000-25008.

(10). Shi, C.; Cui, X.; Zhang, X.; Tchoukov, P.; Liu, Q.; Encinas, N.; Paven, M.; Geyer, F.; Vollmer, D.; Xu, Z. Interaction between air bubbles and superhydrophobic surfaces in aqueous solutions. *Langmuir* **2015,** 31, 7317-7327.

(11). Shahalami, M.; Wang, L.; Wu, C.; Masliyah, J. H.; Xu, Z.; Chan, D. Y. Measurement and modeling on hydrodynamic forces and deformation of an air bubble approaching a solid sphere in liquids. *Adv. Colloid Interface Sci.* **2015,** 217, 31-42.

(12). Taylor, G. The formation of emulsions in definable fields of flow. *Proceedings of the Royal Society of London. Series A, Containing Papers of a Mathematical and Physical Character* **1934,** 146, 501-523.

(13). Bentley, B.; Leal, L. An experimental investigation of drop deformation and breakup in steady, two-dimensional linear flows. *J. Fluid Mech.* **1986,** 167, 241-283.

(14). Milliken, W.; Leal, L. Deformation and breakup of viscoelastic drops in planar extensional flows. *Journal of non-newtonian fluid mechanics* **1991,** 40, 355-379.

(15). Acrivos, A., The deformation and break-up of single drops in shear fields. In *Physicochemical Hydrodynamics*, Springer: 1988; pp 1-18.

(16). Hsu, A. S.; Roy, A.; Leal, L. G. Drop-size effects on coalescence of two equal-sized drops in a head-on collision. *Journal of Rheology (1978-present)* **2008,** 52, 1291-1310.

(17). Yoon, Y.; Borrell, M.; Park, C. C.; Leal, L. G. Viscosity ratio effects on the coalescence of two equal-sized drops in a two-dimensional linear flow. *J. Fluid Mech.* **2005,** 525, 355-379.

(18). Baldessari, F.; Leal, L. G. Effect of overall drop deformation on flow-induced coalescence at low capillary numbers. *Physics of Fluids (1994-present)* **2006,** 18, 013602.

(19). Dai, B.; Leal, L. G. The mechanism of surfactant effects on drop coalescence. *Physics of Fluids (1994-present)* **2008,** 20, 040802.

(20). Bremond, N.; Thiam, A. R.; Bibette, J. Decompressing emulsion droplets favors coalescence. *Phys. Rev. Lett.* **2008,** 100, 024501.

(21). Weon, B. M.; Je, J. H. Coalescence preference depends on size inequality. *Phys. Rev. Lett.* **2012,** 108, 224501.

(22). Lin, C. Y.; Slattery, J. Thinning of a liquid film as a small drop or bubble approaches a fluid–fluid interface. *AlChE J.* **1982,** 28, 786-792.

(23). Bazhlekov, I.; Chesters, A.; Van de Vosse, F. The effect of the dispersed to continuous-phase viscosity ratio on film drainage between interacting drops. *Int. J. Multiphase Flow* **2000,** 26, 445-466.

(24). Ivanov, I.; Dimitrov, D.; Somasundaran, P.; Jain, R. Thinning of films with deformable surfaces: diffusion-controlled surfactant transfer. *Chem. Eng. Sci.* **1985,** 40, 137-150.

(25). Blake, T.; Kitchener, J. Stability of aqueous films on hydrophobic methylated silica. *J. Chem. Soc., Faraday Trans. 1* **1972,** 68, 1435-1442.

(26). Velev, O.; Constantinides, G.; Avraam, D.; Payatakes, A.; Borwankar, R. Investigation of thin liquid films of small diameters and high capillary pressures by a miniaturized cell. *J. Colloid Interface Sci.* **1995,** 175, 68-76.

(27). Yaminsky, V. V.; Ohnishi, S.; Vogler, E. A.; Horn, R. G. Stability of aqueous films between bubbles. Part 1. The effect of speed on bubble coalescence in purified water and simple electrolyte solutions. *Langmuir* **2010,** 26, 8061-8074.

(28). Yaminsky, V. V.; Ohnishi, S.; Vogler, E. A.; Horn, R. G. Stability of aqueous films between bubbles. Part 2. effects of trace impurities and evaporation. *Langmuir* **2010,** 26, 8075-8080.

(29). Hendrix, M. H.; Manica, R.; Klaseboer, E.; Chan, D. Y.; Ohl, C.-D. Spatiotemporal evolution of thin liquid films during impact of water bubbles on glass on a micrometer to nanometer scale. *Phys. Rev. Lett.* **2012,** 108, 247803.

(30). Tsao, H. K.; Koch, D. L. Observations of high Reynolds number bubbles interacting with a rigid wall. *Physics of Fluids (1994-present)* **1997,** 9, 44-56.

(31). Klaseboer, E.; Chevaillier, J.-P.; Maté, A.; Masbernat, O.; Gourdon, C. Model and experiments of a drop impinging on an immersed wall. *Physics of Fluids (1994-present)* **2001,** 13, 45-57.

(32). Malysa, K.; Krasowska, M.; Krzan, M. Influence of surface active substances on bubble motion and collision with various interfaces. *Adv. Colloid Interface Sci.* **2005,** 114, 205-225.

(33). Manica, R.; Klaseboer, E.; Chan, D. Y. The hydrodynamics of bubble rise and impact with solid surfaces. *Adv. Colloid Interface Sci.* **2016,** 235, 214-232.

(34). Manica, R.; Klaseboer, E.; Chan, D. Y. The impact and bounce of air bubbles at a flat fluid interface. *Soft matter* **2016,** 12, 3271-3282.

(35). Parkinson, L.; Ralston, J. The interaction between a very small rising bubble and a hydrophilic titania surface. *J. Phys. Chem. C* **2010,** 114, 2273-2281.

(36). Manica, R.; Parkinson, L.; Ralston, J.; Chan, D. Y. Interpreting the dynamic interaction between a very small rising bubble and a hydrophilic titania surface. *J. Phys. Chem. C* **2009,** 114, 1942-1946.

(37). Li, E. Q.; Vakarelski, I. U.; Chan, D. Y.; Thoroddsen, S. T. Stabilization of thin liquid films by repulsive van der Waals force. *Langmuir* **2014,** 30, 5162-5169.

(38). Israelachvili, J.; Min, Y.; Akbulut, M.; Alig, A.; Carver, G.; Greene, W.; Kristiansen, K.; Meyer, E.; Pesika, N.; Rosenberg, K. Recent advances in the surface forces apparatus (SFA) technique. *Rep. Prog. Phys.* **2010,** 73, 036601.

(39). Israelachvili, J.; Pashley, R. The hydrophobic interaction is long range, decaying exponentially with distance. **1982**.

(40). Israelachvili, J. N.; Adams, G. E. Measurement of forces between two mica surfaces in aqueous electrolyte solutions in the range 0–100 nm. *J. Chem. Soc., Faraday Trans. 1* **1978,** 74, 975-1001.

(41). Connor, J. N.; Horn, R. G. Measurement of aqueous film thickness between charged mercury and mica surfaces: A direct experimental probe of the Poisson-Boltzmann distribution. *Langmuir* **2001,** 17, 7194-7197.

(42). Connor, J. N.; Horn, R. G. The influence of surface forces on thin film drainage between a fluid drop and a flat solid. *Faraday Discuss.* **2003,** 123, 193-206.

(43). Connor, J. N.; Horn, R. G. Extending the surface force apparatus capabilities by using white light interferometry in reflection. *Rev. Sci. Instrum.* **2003,** 74, 4601-4606.

(44). Pushkarova, R. A.; Horn, R. G. Surface forces measured between an air bubble and a solid surface in water. *Colloids Surf., A* **2005,** 261, 147-152.

(45). Pushkarova, R. A.; Horn, R. G. Bubble− solid interactions in water and electrolyte solutions. *Langmuir* **2008,** 24, 8726-8734.

(46). Horn, R. G.; Asadullah, M.; Connor, J. N. Thin film drainage: hydrodynamic and disjoining pressures determined from experimental measurements of the shape of a fluid drop approaching a solid wall. *Langmuir* **2006,** 22, 2610-2619.

(47). Clasohm, L. Y.; Connor, J. N.; Vinogradova, O. I.; Horn, R. G. The "wimple": rippled deformation of a fluid drop caused by hydrodynamic and surface forces during thin film drainage. *Langmuir* **2005,** 21, 8243-8249.

(48). Meyer, E. Atomic force microscopy. *Prog. Surf. Sci.* **1992,** 41, 3-49.

(49). Binnig, G.; Quate, C. F.; Gerber, C. Atomic Force Microscope. *Phys. Rev. Lett.* **1986,** 56, 930-933.

(50). Cappella, B.; Dietler, G. Force-distance curves by atomic force microscopy. *Surf. Sci. Rep.* **1999,** 34, 1-104.

(51). Hutter, J. L.; Bechhoefer, J. Calibration of atomic-force microscope tips. *Rev. Sci. Instrum.* **1993,** 64, 1868-1873.

(52). Cui, S.; Manica, R.; Tabor, R. F.; Chan, D. Y. Interpreting atomic force microscopy measurements of hydrodynamic and surface forces with nonlinear parametric estimation. *Rev. Sci. Instrum.* **2012,** 83, 103702.

(53). Chan, D.; Dagastine, R.; White, L. Forces between a rigid probe particle and a liquid interface: I. The repulsive case. *J. Colloid Interface Sci.* **2001,** 236, 141-154.

(54). Dagastine, R.; White, L. Forces between a rigid probe particle and a liquid interface: II. The general case. *J. Colloid Interface Sci.* **2002,** 247, 310-320.

(55). Butt, H.-J. A technique for measuring the force between a colloidal particle in water and a bubble. *J. Colloid Interface Sci.* **1994,** 166, 109-117.

(56). Preuss, M.; Butt, H.-J. Direct measurement of forces between particles and bubbles. *Int. J. Miner. Process.* **1999,** 56, 99-115.

(57). Gillies, G.; Kappl, M.; Butt, H.-J. Direct measurements of particle–bubble interactions. *Adv. Colloid Interface Sci.* **2005,** 114, 165-172.

(58). Preuss, M.; Butt, H.-J. Direct measurement of particle-bubble interactions in aqueous electrolyte: Dependence on surfactant. *Langmuir* **1998,** 14, 3164-3174.

(59). Chan, D. Y. C.; Klaseboer, E.; Manica, R. Theory of non-equilibrium force measurements involving deformable drops and bubbles. *Adv. Colloid Interface Sci.* **2011,** 165, 70-90.

(60). Manica, R.; Connor, J. N.; Dagastine, R. R.; Carnie, S. L.; Horn, R. G.; Chan, D. Y. C. Hydrodynamic forces involving deformable interfaces at nanometer separations. *Phys. Fluids* **2008,** 20, 032101.

(61). Vakarelski, I. U.; Manica, R.; Tang, X.; O'Shea, S. J.; Stevens, G. W.; Grieser, F.; Dagastine, R. R.; Chan, D. Y. Dynamic interactions between microbubbles in water. *Proceedings of the National Academy of Sciences* **2010,** 107, 11177-11182.

(62). Tabor, R. F.; Manica, R.; Chan, D. Y.; Grieser, F.; Dagastine, R. R. Repulsive van der Waals forces in soft matter: why bubbles do not stick to walls. *Phys. Rev. Lett.* **2011,** 106, 064501.

(63). Dagastine, R. R.; Manica, R.; Carnie, S. L.; Chan, D.; Stevens, G. W.; Grieser, F. Dynamic forces between two deformable oil droplets in water. *Science* **2006,** 313, 210-213.

(64). Tabor, R. F.; Grieser, F.; Dagastine, R. R.; Chan, D. Y. Measurement and analysis of forces in bubble and droplet systems using AFM. *J. Colloid Interface Sci.* **2012,** 371, 1-14.

(65). Chan, D. Y.; Klaseboer, E.; Manica, R. Film drainage and coalescence between deformable drops and bubbles. *Soft Matter* **2011,** 7, 2235-2264.

(66). Manor, O.; Chan, D. Y. Influence of Surfactants on the force between two Bubbles. *Langmuir* **2009,** 26, 655-662.

(67). Tabor, R. F.; Wu, C.; Grieser, F.; Dagastine, R. R.; Chan, D. Y. Measurement of the hydrophobic force in a soft matter system. *The Journal of Physical Chemistry Letters* **2013,** 4, 3872-3877.

(68). Tabor, R. F.; Chan, D. Y.; Grieser, F.; Dagastine, R. R. Structural forces in soft matter systems. *The Journal of Physical Chemistry Letters* **2011,** 2, 434-437.

(69). Yoon, Y.; Baldessari, F.; Ceniceros, H. D.; Leal, L. G. Coalescence of two equal-sized deformable drops in an axisymmetric flow. *Physics of Fluids (1994-present)* **2007,** 19, 102102.

(70). Manor, O.; Vakarelski, I. U.; Tang, X.; O'Shea, S. J.; Stevens, G. W.; Grieser, F.; Dagastine, R. R.; Chan, D. Y. Hydrodynamic boundary conditions and dynamic forces between bubbles and surfaces. *Phys. Rev. Lett.* **2008,** 101, 024501.

(71). Dagastine, R. R.; Webber, G. B.; Manica, R.; Stevens, G. W.; Grieser, F.; Chan, D. Y. Viscosity effects on hydrodynamic drainage force measurements involving deformable bodies. *Langmuir* **2010,** 26, 11921-11927.

(72). Xie, L.; Shi, C.; Wang, J.; Huang, J.; Lu, Q.; Liu, Q.; Zeng, H. Probing the Interaction between Air Bubble and Sphalerite Mineral Surface Using Atomic Force Microscope. *Langmuir* **2015,** 31, 2438-2446.

(73). Dai, Z.; Fornasiero, D.; Ralston, J. Particle–bubble attachment in mineral flotation. *J. Colloid Interface Sci.* **1999,** 217, 70-76.

(74). Mura, S.; Nicolas, J.; Couvreur, P. Stimuli-responsive nanocarriers for drug delivery. *Nature materials* **2013,** 12, 991-1003.

(75). Chen, Y.; Chen, H.; Zeng, D.; Tian, Y.; Chen, F.; Feng, J.; Shi, J. Core/shell structured hollow mesoporous nanocapsules: a potential platform for simultaneous cell imaging and anticancer drug delivery. *ACS Nano* **2010,** 4, 6001-6013.

(76). Yang, F.; Tchoukov, P.; Dettman, H.; Teklebrhan, R. B.; Liu, L.; Dabros, T.; Czarnecki, J.; Masliyah, J.; Xu, Z. Asphaltene Subfractions Responsible for Stabilizing Water-in-Crude Oil Emulsions. Part 2: Molecular Representations and Molecular Dynamics Simulations. *Energy & Fuels* **2015,** 29, 4783-4794.

(77). Rocha, J.; Baydak, E.; Yarranton, H. W.; Sztukowski, D.; Ali-Marcano, V.; Gong, L.; Shi, C.; Zeng, H. Role of Aqueous Phase Chemistry, Interfacial Film Properties, and Surface Coverage in Stabilizing Water-in-Bitumen Emulsions. *Energy & Fuels* **2016**.

(78). Tchoukov, P.; Yang, F.; Xu, Z.; Dabros, T.; Czarnecki, J.; Sjöblom, J. Role of asphaltenes in stabilizing thin liquid emulsion films. *Langmuir* **2014,** 30, 3024-3033.

(79). Czarnecki, J.; Tchoukov, P.; Dabros, T.; Xu, Z. Role of asphaltenes in stabilisation of water in crude oil emulsions. *Can. J. Chem. Eng.* **2013,** 91, 1365-1371.

(80). Kilpatrick, P. K. Water-in-crude oil emulsion stabilization: Review and unanswered questions. *Energy & Fuels* **2012,** 26, 4017-4026.

(81). Zhang, L.; Shi, C.; Lu, Q.; Liu, Q.; Zeng, H. Probing Molecular Interactions of Asphaltenes in Heptol Using a Surface Forces Apparatus: Implications on Stability of Water-in-Oil Emulsions. *Langmuir* **2016**.

(82). Harbottle, D.; Chen, Q.; Moorthy, K.; Wang, L.; Xu, S.; Liu, Q.; Sjoblom, J.; Xu, Z. Problematic stabilizing films in petroleum emulsions: Shear rheological response of viscoelastic asphaltene films and the effect on drop coalescence. *Langmuir* **2014,** 30, 6730-6738.

(83). Hannisdal, A.; Ese, M.-H.; Hemmingsen, P. V.; Sjöblom, J. Particle-stabilized emulsions: effect of heavy crude oil components pre-adsorbed onto stabilizing solids. *Colloids Surf., A* **2006,** 276, 45-58.

(84). Masliyah, J.; Zhou, Z. J.; Xu, Z.; Czarnecki, J.; Hamza, H. Understanding water-based bitumen extraction from Athabasca oil sands. *Can. J. Chem. Eng.* **2004,** 82, 628-654.

(85). Taylor, S. D.; Czarnecki, J.; Masliyah, J. Disjoining pressure isotherms of water-in-bitumen emulsion films. *J. Colloid Interface Sci.* **2002,** 252, 149-160.

(86). Gu, G.; Xu, Z.; Nandakumar, K.; Masliyah, J. Influence of water-soluble and water-insoluble natural surface active components on the stability of water-in-toluene-diluted bitumen emulsion. *Fuel* **2002,** 81, 1859-1869.

(87). Moran, K.; Yeung, A. Determining bitumen viscosity through drop shape recovery. *Can. J. Chem. Eng.* **2004,** 82, 813-820.

(88). Liu, J.; Xu, Z.; Masliyah, J. Interaction between bitumen and fines in oil sands extraction system: Implication to bitumen recovery. *Can. J. Chem. Eng.* **2004,** 82, 655-666.

(89). Ren, S.; Masliyah, J.; Xu, Z. Studying bitumen–bubble interactions using atomic force microscopy. *Colloids Surf., A* **2014,** 444, 165-172.

(90). He, L.; Lin, F.; Li, X.; Xu, Z.; Sui, H. Effect of solvent addition on bitumen–air bubble attachment in process water. *Chem. Eng. Sci.* **2015,** 137, 31-39.

(91). Strausz, O. P.; Mojelsky, T. W.; Lown, E. M. The molecular structure of asphaltene: an unfolding story. *Fuel* **1992,** 71, 1355-1363.

(92). Yarranton, H. W.; Hussein, H.; Masliyah, J. H. Water-in-hydrocarbon emulsions stabilized by asphaltenes at low concentrations. *J. Colloid Interface Sci.* **2000,** 228, 52-63.

(93). Mullins, O. C. The asphaltenes. *Annu. Rev. Anal. Chem.* **2011,** 4, 393-418.

(94). Schuler, B.; Meyer, G.; Pena, D.; Mullins, O. C.; Gross, L. Unraveling the molecular structures of asphaltenes by atomic force microscopy. *J. Am. Chem. Soc.* **2015,** 137, 9870-9876.

(95). Natarajan, A.; Xie, J.; Wang, S.; Liu, Q.; Masliyah, J.; Zeng, H.; Xu, Z. Understanding molecular interactions of asphaltenes in organic solvents using a surface force apparatus. *J. Phys. Chem. C* **2011,** 115, 16043-16051.

(96). Cimino, R.; Correra, S.; Del Bianco, A.; Lockhart, T. P., Solubility and phase behavior of asphaltenes in hydrocarbon media. In *Asphaltenes*, Springer: 1995; pp 97-130.

(97). Li, M.; Xu, M.; Ma, Y.; Wu, Z.; Christy, A. A. Interfacial film properties of asphaltenes and resins. *Fuel* **2002,** 81, 1847-1853.

(98). Tanaka, R.; Hunt, J. E.; Winans, R. E.; Thiyagarajan, P.; Sato, S.; Takanohashi, T. Aggregates structure analysis of petroleum asphaltenes with small-angle neutron scattering. *Energy & fuels* **2003,** 17, 127-134.

(99). Rane, J. P.; Pauchard, V.; Couzis, A.; Banerjee, S. Interfacial rheology of asphaltenes at oil–water interfaces and interpretation of the equation of state. *Langmuir* **2013,** 29, 4750-4759.

(100). Sztukowski, D. M.; Yarranton, H. W. Rheology of asphaltene-Toluene/water interfaces. *Langmuir* **2005,** 21, 11651-11658.

(101). Yeung, A.; Dabros, T.; Masliyah, J.; Czarnecki, J. Micropipette: a new technique in emulsion research. *Colloids Surf., A* **2000,** 174, 169-181.

(102). Tsamantakis, C.; Masliyah, J.; Yeung, A.; Gentzis, T. Investigation of the interfacial properties of water-in-diluted-bitumen emulsions using micropipette techniques. *J. Colloid Interface Sci.* **2005,** 284, 176-183.

(103). Zhang, L. Y.; Xu, Z.; Masliyah, J. H. Langmuir and Langmuir-Blodgett films of mixed asphaltene and a demulsifier. *Langmuir* **2003,** 19, 9730-9741.

(104). Langevin, D.; Argillier, J.-F. Interfacial behavior of asphaltenes. *Adv. Colloid Interface Sci.* **2015**.

(105). Hu, C.; Garcia, N. C.; Xu, R.; Cao, T.; Yen, A.; Garner, S. A.; Macias, J. M.; Joshi, N.; Hartman, R. L. Interfacial Properties of Asphaltenes at the Heptol–Brine Interface. *Energy & Fuels* **2015,** 30, 80-87.

(106). Yarranton, H. W.; Alboudwarej, H.; Jakher, R. Investigation of asphaltene association with vapor pressure osmometry and interfacial tension measurements. *Industrial & engineering chemistry research* **2000,** 39, 2916-2924.

(107). Yarranton, H.; Sztukowski, D.; Urrutia, P. Effect of interfacial rheology on model emulsion coalescence: I. Interfacial rheology. *J. Colloid Interface Sci.* **2007,** 310, 246-252.

(108). Wang, S.; Liu, J.; Zhang, L.; Xu, Z.; Masliyah, J. Colloidal interactions between asphaltene surfaces in toluene. *Energy & Fuels* **2008,** 23, 862-869.

(109). Liu, J.; Zhang, L.; Xu, Z.; Masliyah, J. Colloidal interactions between asphaltene surfaces in aqueous solutions. *Langmuir* **2006,** 22, 1485-1492.

(110). Wang, S.; Liu, J.; Zhang, L.; Masliyah, J.; Xu, Z. Interaction forces between asphaltene surfaces in organic solvents. *Langmuir* **2009,** 26, 183-190.

(111). Drummond, C.; Israelachvili, J. Surface forces and wettability. *J. Pet. Sci. Eng.* **2002,** 33, 123-133.

(112). Drummond, C.; Israelachvili, J. Fundamental studies of crude oil–surface water interactions and its relationship to reservoir wettability. *J. Pet. Sci. Eng.* **2004,** 45, 61-81.

Chapter 2 Experiment and Theoretical Model

2.1. Droplet probe AFM

Figure 2.1 shows the schematic of a typical experiment setup of droplet probe AFM for measurement between a droplet and a solid surface. In this study, all the force measurements were conducted using an MFP-3D AFM system (Asylum Research, Santa Barbara, CA) which was mounted on an inverted optical microscopy (Nikon Ti-U). Custom-made rectangular tipless AFM cantilevers with size of $400 \times 70 \times 2$ μm were used for force measurements. This tipless cantilever consists of hydrophilic silicon with a thin circular gold patch (diameter ~ 65 μm, thickness ~ 10 nm) at one end. This gold patch can be hydrophobized using hydrophobic thiol (e.g. 1-decanethiol) to realize stable anchoring of hydrophobic oil droplets or air bubbles on the cantilever.
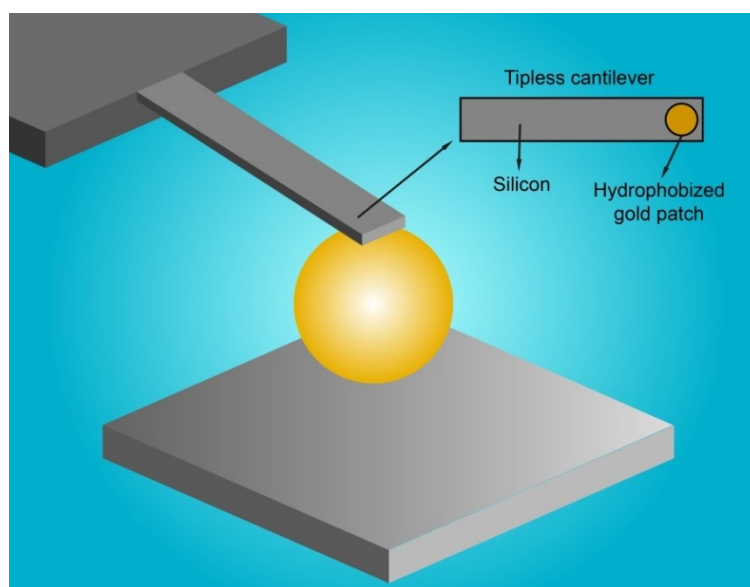
Figure 2.1. Setup of droplet probe AFM for measurement of interaction involving deformable liquid droplets or air bubbles.

Prior to each experiment, the glass substrate of an AFM fluid cell (radius ~ 35 mm) was first mildly hydrophobized by immersing in 10 mM octadecyltrichlorosilane (OTS) in toluene solution for ~5 s to achieve a water contact angle of ~45° in air, providing optimized hydrophobicity for immobilization of oil droplet or air bubbles on the glass substrate. It was noted that too high hydrophobicity would make it difficult to pick up an oil droplet or air bubble using the tipless cantilever, while a substrate with lower hydrophobicity could not immobilize oil droplets or air bubbles. Oil droplets were then immobilized on the substrate through a controlled de-wetting method,[1, 2] or air bubbles were created by carefully injecting air into the AFM fluid cell filled with solution using a custom-made ultra-sharp pipette.[3] For measurement between droplet and solid surface, the sample surface was put into the fluid cell after generation of droplets to avoid potential contamination. A schematic of the typical procedure of force measurement is illustrated in Figure 2.2. The spring constant of the tipless cantilever was first calibrated using Hutter's method.[4] A droplet probe was then created by lowering down the tipless cantilever towards a droplet with suitable size (radius R_0 ~ 60 μm). After droplet attachment, the cantilever was lifted up to detach the droplet from the glass substrate, creating a droplet probe. Then the droplet probe was moved upon another droplet or a solid sample surface for force measurement. The droplet probe was carefully aligned with the droplet or the sample surface by observing through the inverted microscopy to maintain head-on collision. Force measurements were conducted by lowering the droplet probe towards the sample droplet or surface on the substrate for a certain distance and then lifting up the probe. The interaction force F was calculated from the detected

34

deflection of the force-sensing cantilever using Hooke's law. The measured force data F and displacement of the cantilever ΔX were recorded by AFM software, which were used within the theoretical model for further analysis.
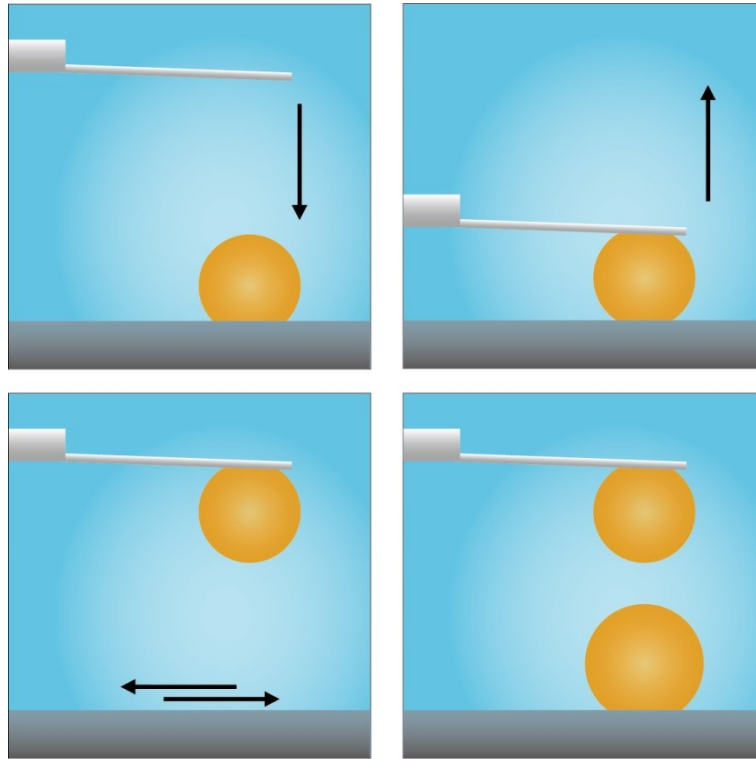
Figure 2.2. Schematic of the typical procedure for measuring interaction force of deformable droplet or bubble using droplet probe AFM.

2.2. Theoretical model

Stokes-Reynolds-Young-Laplace model based on Reynolds lubrication theory and augmented Young-Laplace equation is utilized to interpret the measured force results using droplet probe AFM.[5, 6] Figure 2.3 illustrates the schematics of interaction between two droplets and between a droplet and a solid surface. With immobile boundary conditions assumed at both interfaces during the interaction, the axisymmetric

hydrodynamic drainage process of the water film with thickness $h(r,t)$ confined between two droplets or between a droplet and a solid surface can be described using Reynolds lubrication theory as

$$\frac{\partial h(r,t)}{\partial t} = \frac{1}{12\mu}\frac{\partial}{\partial r}\left(rh^3(r,t)\frac{\partial p(r,t)}{\partial r}\right) \qquad (2.1)$$

where μ is the dynamic viscosity of water film, and $p(r,t)$ is excessive hydrodynamic pressure inside the water film relative to the bulk liquid.
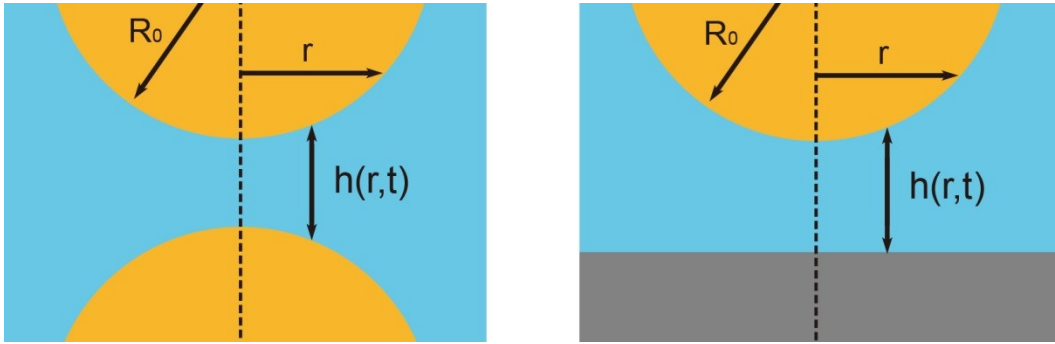
Figure 2.3. Schematic illustration of the interaction region of interaction between (left) two droplets or (right) a droplet and a solid surface.

As mentioned in previous sections, the droplet can readily change shape in response to external interaction forces. Generally, the deformation time of a droplet with size in microns scale can be estimated as $\tau_{def} = \mu_d R_0 / \sigma \sim 10^{-6} s$, which is far less than the practical experiment time (1~10s). Therefore, the deformation of the droplets is treated as a quasi-equilibrium behavior, and deformation occurs almost immediately. Under this

condition, the deformation of the droplet during interaction can be described by the augmented Young-Laplace equation as

$$\frac{n\sigma}{2r}\frac{\partial}{\partial r}\left(r\frac{\partial h(r,t)}{\partial r}\right)=\frac{2\sigma}{R}-p(r,t)-\Pi[h(r,t)] \qquad (2.2)$$

where σ is the interfacial tension, R is the harmonic mean of the interacting droplets, and parameter n equals to 1 for interaction between two droplets, and 2 for interaction between a droplet and a solid surface. $\Pi[h(r,t)]$ is the disjoining pressure, which generally arises from EDL interaction, VDW interaction, hydrophobic interaction, steric interaction and so on. The disjoining pressure due to VDW interaction can be calculated using Hamaker constant as

$$\Pi_{VDW}[h(r,t)]=-\frac{A_H}{6\pi h^3(r,t)} \qquad (2.3)$$

where A_H is the non-retarded Hamaker constant of the system. For symmetric systems (e.g. interaction between two identical droplets), the disjoining pressure due to EDL interaction can be calculated as

$$\Pi_{EDL}[h(r,t)]=64k_B T\rho_0 \tanh^2(\frac{e\varphi}{4k_B T})\exp[-\kappa h(r,t)] \qquad (2.4)$$

where φ is the surface potential of the interface, ρ_0 is the number density of ions in the aqueous solution, and e is the fundamental charge of an electron. For asymmetric systems (e.g. interaction between a droplet and a solid surface), the disjoining pressure due to EDL interaction can be calculated as

$$\Pi_{EDL}[h(r,t)]=\frac{2\varepsilon_0\varepsilon\kappa^2[(e^{+\kappa h}+e^{-\kappa h}\varphi_1\varphi_2-(\varphi_1^2+\varphi_2^2)]}{(e^{+\kappa h}-e^{-\kappa h})^2} \qquad (2.5)$$

where φ_1 and φ_2 are the surface potentials of the two interacting objects. The κ^{-1} is the inverse of Debye length and can be calculated as

$$\kappa = (2\rho_0 e^2 / \varepsilon_0 \varepsilon k_B T)^{1/2} \qquad (2.6)$$

where ε_0 is the permittivity of vacuum and ε is the dielectric constant of the medium.

The initial conditions for interaction between two droplets and between a droplet and a solid surface follow the undeformed spherical droplet shape and can be described as equation 2.7.

$$h(r,t_0) = \begin{cases} h(0,t_0) + \dfrac{r^2}{2R_0}, & \text{droplet-surface interaction} \\[2em] h(0,t_0) + \dfrac{r^2}{R_0}, & \text{droplet-droplet interaction} \end{cases} \qquad (2.7)$$

The overall interaction force $F(t)$ is calculated by integrating over $p(r,t)$ and $\Pi(h(r,t))$ using Derjaguin's approximation as shown in equation 2.8.

$$F(t) = 2\pi \int_0^\infty [p(r,t) + \Pi(h(r,t))] r dr \qquad (2.8)$$

Practically, these equations are solved within the region $(0, r_{max})$, beyond which the local separation $h(r,t)$ is large enough (>100 nm) so that the contribution of disjoining pressure is negligible. And thus, the overall interaction force can be calculated as

$$F(t) = 2\pi \int_0^{r_{max}} [p(r,t) + \Pi(h(r,t))] r dr + 2\pi \int_{r_{max}}^\infty p(r,t) r dr \qquad (2.9)$$

The first integral term on the right-hand side of equation (2.9) generally dominates the overall calculated force and the contribution of the second integral term is comparing small. The boundary conditions of $h(r,t)$ and $p(r,t)$ at $r = 0$ are $\partial h / \partial r = 0$ and $\partial p / \partial r = 0$. The cantilever displacement data $X(t)$ recorded by the AFM software is incorporated in

the boundary condition, equation 2.10, which accounts for the deformation of the interacting droplet and the contact area of the droplet on the cantilever

$$\frac{\partial h(r_{max},t)}{\partial t} = \frac{dX(t)}{dt} + \frac{dF(t)}{2\pi\sigma dt}\left(\frac{2\pi\sigma}{K} - 1 - \frac{1}{2}\ln\left(\frac{1+\cos\theta}{1-\cos\theta}\right) - \ln\left(\frac{r_{max}}{2R}\right)\right) \qquad (2.10)$$

In equation 2.10, θ is the contact angle of the anchored droplet on the cantilever, and K is the spring constant of the tipless cantilever. The boundary condition of the hydrodynamic pressure $p(r,t)$ is $r(\partial p / \partial r) + 4p = 0$ at $r = r_{max}$, for it decays as r^{-4} at $r \to \infty$,

All the equations above are first non-dimensionalized with $h_c = R_0 Ca^{1/2}$, $r_c = R_0 Ca^{1/4}$, $p_c = \sigma / R_0$, $t_c = \mu Ca^{-1/2} / p_c$, and $Ca = \mu V / \sigma$, and then numerically solved after central differentiation in r. General ODEs solvers, such as MATLAB's ode15s, can be used to solve the equations.

Reference

(1). Chan, D.; Dagastine, R.; White, L. Forces between a rigid probe particle and a liquid interface: I. The repulsive case. *J. Colloid Interface Sci.* **2001,** 236, 141-154.

(2). Dagastine, R. R.; Manica, R.; Carnie, S. L.; Chan, D.; Stevens, G. W.; Grieser, F. Dynamic forces between two deformable oil droplets in water. *Science* **2006,** 313, 210-213.

(3). Shi, C.; Chan, D. Y.; Liu, Q.; Zeng, H. Probing the hydrophobic interaction between air bubbles and partially hydrophobic surfaces using atomic force microscopy. *J. Phys. Chem. C* **2014,** 118, 25000-25008.

(4). Hutter, J. L.; Bechhoefer, J. Calibration of atomic-force microscope tips. *Rev. Sci. Instrum.* **1993,** 64, 1868-1873.

(5). Tabor, R. F.; Grieser, F.; Dagastine, R. R.; Chan, D. Y. Measurement and analysis of forces in bubble and droplet systems using AFM. *J. Colloid Interface Sci.* **2012,** 371, 1-14.

(6). Chan, D. Y.; Klaseboer, E.; Manica, R. Film drainage and coalescence between deformable drops and bubbles. *Soft Matter* **2011,** 7, 2235-2264.

Chapter 3 Measuring Forces and Spatiotemporal Evolution of Thin Water Films between an Air Bubble and Solid Surfaces of Different Hydrophobicity

Bubbles are an important component in a wide range of traditional industrial and engineering applications such as foam formation,[1] froth flotation[2] and microfluidic devices[3]. More recently bubbles are found to have important roles as an ultrasound imaging contrast agent,[4-6] in enhancing membrane permeability and molecular uptake,[7-9] as a stimuli-responsive carrier for drug and gene delivery,[4, 10-13] as a water-driven micromotor,[14] as template for synthesis of micro and nanoparticles[15, 16] used in catalysis,[17] in heterogeneous cavitation[18] and in surface cleaning.[19] In many of these applications, the interactions between bubbles and solids of different hydrophobicity in aqueous environments in which electrostatic, hydrophobic, specific ligand-receptor interactions and hydrodynamic interaction are the critical determining factors for achieving desired characteristics and functionality of bubbles.[13, 20-25] Due to the intrinsic hydrophobicity of bubbles, hydrophobic interaction is one of the most important non-specific interactions that guides assembly and adsorption of hydrophobic or amphiphilic molecules and particles at air/water interface.[21-23, 26-28]

The hydrophobic interaction has been recognized for decades, yet its precise physical origin remains to be quantified although different models have been proposed.[27, 29-33] To date, quantitative force measurements of hydrophobic interactions were mainly studied using solid surfaces using the surface force apparatus (SFA) and atomic force microscope

(AFM).[31, 32, 34-40] Exponential function with decay lengths of 0.3 nm to >1.0 nm has been reported for the hydrophobic interaction in different material systems[27, 35, 38] and the presence of nanobubbles on hydrophobic surfaces and dissolved aires have also been found to cause long-range attraction.[37, 41-44] On the other hand, reports on hydrophobic interaction involving deformable bubbles or droplets were rather limited, most likely due to the complex coupling of forces and surface deformation during interaction.[30, 45, 46] In contrast to the strong elasticity-controlled deformation energetics of solid surfaces, weaker surface energy governs the deformation of the air/water interface of bubbles in response to external forces, such as velocity-dependent hydrodynamic force and separation-dependent colloidal forces.[21, 47] Therefore, the drainage process of the thin liquid film confined between an air bubble and a solid surface can be more complex than that confined between two solid surfaces. To achieve a complete understanding of the interaction between air bubbles and solid surfaces, it is of critical importance to make synchronous measurements of interaction forces and visualization of the spatiotemporal evolution of the confined thin water film.

Recently, direct measurement of interaction force between an air bubble and solid surfaces has been successfully achieved using the AFM with the colloidal probe technique[46, 47] and bubble probe technique.[48-50] Repulsive van der Waals forces were observed between an air bubble and hydrophilic surfaces (*e.g.* mica) that stabilizing a confined thin water film,[49, 51] whereas an attractive hydrophobic attraction was found to be responsible for bubble attachment and immobilization on hydrophobic substrates.[48] In such AFM studies, absolute separation between the interacting surfaces and associated deformation can only be obtained indirectly through theoretical modeling. On the other

hand, visualization of the film drainage process and spatial-temporal evolution of the trapped water film between an air bubble and hydrophilic glass without direct force measurements has been accomplished using optical interferometry and the results could be modeled quantitatively.[51-53] However, simultaneous measurements of the interaction force and spatial-temporal evolution of the confined thin liquid film associated with the dynamic interactions of deformable bubble and droplet has not been attempted to date.

In this work, we have integrated the capabilities of atomic force microscope (AFM) with reflection interference contrast microscopy (RICM) (Figure 3.1), and, for the first time, investigated the interaction between an air bubble and mica surfaces with varying degrees of surface hydrophobicity through synchronous measurements of the interaction force and spatial-temporal visualization of the thin film drainage process. The interaction forces were measured with the AFM by driving a cantilever-anchored air bubble towards the solid surface. The fringe patterns that arise from interference between light reflected from the air/water interface of the bubble and the mica/water interface were obtained with RICM and analyzed using an improved mathematical method reported recently. This enables the reconstruction of bubble-water surface profiles with nanometer-scale resolution.[54]

A theoretical model has been applied to interpret the measured forces and predict the evolution of the thin water film profiles during the interaction that can be compared directly with experimental results.[48, 49] The asymmetric hydrophobic interaction between air bubble and hydrophobized solid surface was also quantified for the first time based on the AFM-RICM measurements. More generally, this study demonstrates the feasibility of simultaneously probing interaction force profiles and thin film drainage dynamics

43

involving deformable surfaces based on the AFM. The technique can be readily extended to study the interactions in systems involving deformable bubbles and droplets with the potential to provide guidance for designing bubble-loaded drug molecules and nanoparticles as well as to predict the assembly process of particles on bubble surfaces.

3.1. Results and Discussion

A micrometer-size air bubble (radius $R_0 = 60–100$ µm) anchored on a custom-made AFM tipless rectangular cantilever ($400 \times 70 \times 2$ µm) was used to measure the interaction with mica surfaces with varying degrees of hydrophobicity (Figure 3.1). The air bubble was immobilized on a well-defined circular gold patch (diameter 65 µm, thickness 30 nm) at one end of the cantilever that was hydrophobized with a layer of self-assembled 1-dodecanethiol.[48, 55] The position of the cantilever and hence the air bubble was accurately controlled by a piezo-electric transducer and variation of the actual displacement, $\Delta X(t)$ of the cantilever with time t, was measured and recorded with a linear variable differential transformer (LVDT) that is an integral part of the AFM.[56, 57] The time-dependent interaction force was measured by monitoring the deflection of the cantilever with a known spring constant by detecting the position of a laser beam reflected from the cantilever on a photodiode detector. For a typical measurement, the air bubble was first driven towards ("approach") the mica surface until bubble attachment occurred or until a desired cantilever deflection was reached, whereupon it is then driven away ("retract") from the mica surface. The RICM interference patterns generated with monochromatic green light (wavelength 546.1 nm) were obtained with a Nikon Ti-U

inverted microscope and were recorded with a video camera. The RICM images were processed with the *ImageJ* software (National Institutes of Health, USA) and the film thickness profiles were obtained by analysis of fringe order and light intensity of the interference patterns (see SI Text RICM image analysis).[54] The measurements were repeated at least 10 times at different positions on at least two surfaces with good reproducibility.
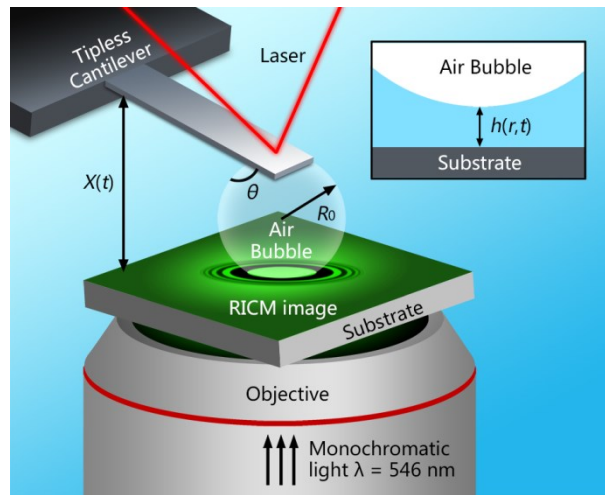
Figure 3.1. Experiment setup of using an AFM coupled with RICM for synchronous measurements of interaction forces and visualization of the spatiotemporal evolution of the confined thin liquid film between an air bubble of radius R_0 and a solid substrate. The air bubble is anchored on a tipless cantilever. The inset shows a schematic of the thin axisymmetric liquid film with thickness $h(r, t)$ between the air bubble and the substrate, where r is the radial coordinate.

3.1.1. Bubble *vs.* hydrophilic mica surface

Before examining interactions between a bubble and mica surfaces with varying degrees of hydrophobicity, we first consider the simpler case of an unmodified hydrophilic mica surface for which all interaction forces are known.[48, 49] This will help establish the experimental protocol and validate the theoretical model used to analyze subsequent experimental results. In Figure 3.2, we show the time variation of the measured force and the profile of the confined water film between an air bubble with radius of 98 μm and a freshly cleaved hydrophilic mica surface in 500 mM NaCl solution at a nominal velocity of $v = 1$ μm/s. At this high salt concentration, the electrical double layer (EDL) interaction between the bubble and the mica surface was highly screened so its contribution, $\Pi_{EDL}(h(r,t))$, to the overall disjoining pressure $\Pi(h(r,t))$ was negligible. The disjoining pressure due to van der Waals (VDW) interaction $\Pi_{VDW}(h(r,t))$, calculated using the full Lifshitz theory is repulsive at all separations (see van der Waals Interaction in SI Text).[58, 59] Therefore, a thin water film is maintained between the air bubble and the hydrophilic mica surface, supported by the repulsive VDW interaction that prevents the air bubble from attaching to hydrophilic mica surface.
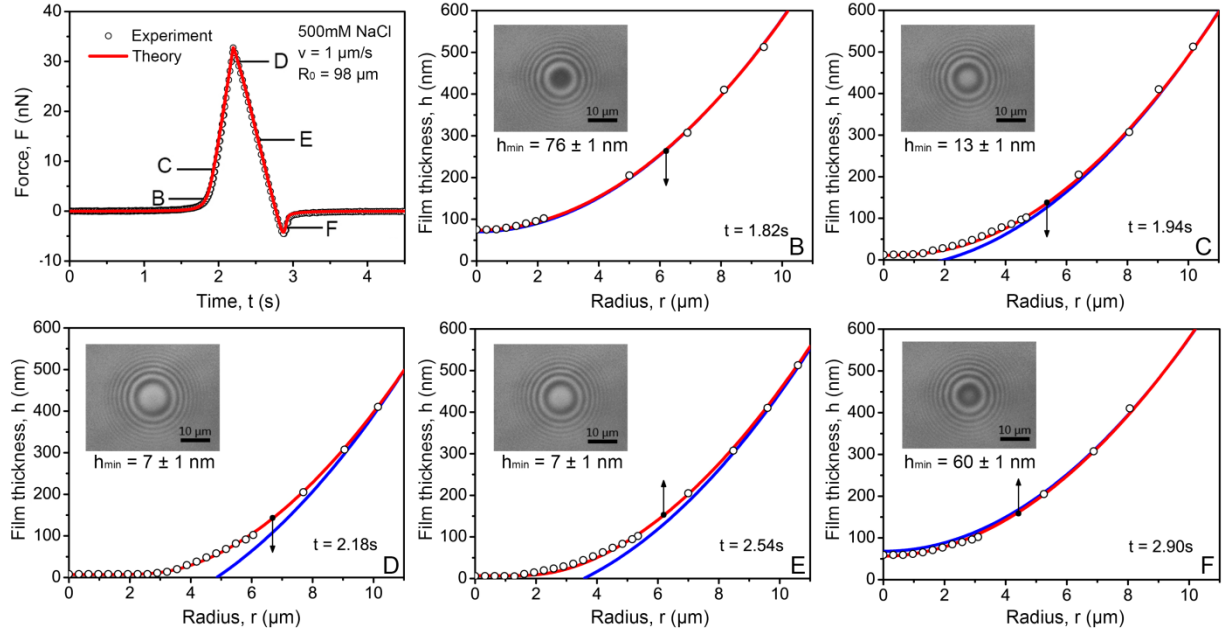
Figure 3.2. Time variations of the force and thin water film profile $h(r, t)$ during interaction between an air bubble and a hydrophilic mica surface in 500 mM NaCl solution. The bubble radius was 98 μm and the nominal driving velocity of bubble was v =1 μm/s. The open circular symbols are experimental results obtained from AFM-RICM measurements and the red solid lines are theoretical predictions. The blue solid lines are the spherical profile from outer part of the air bubble that corresponds to the profile of an undeformed bubble. The insets are interference fringe patterns from which the film profiles were deduced. The arrows indicate the driving direction of the air bubble, towards or away from the substrate. (A) Interaction force F as a function of time t; (B)-(F) confined film profile $h(r, t)$ at selected times indicated on the force curve in (A).

As shown in Figure 3.2, time-dependent interaction force measured by AFM and profiles of the confined thin water film obtained from RICM measurements at different

time (open circular symbols) agreed very well with theoretically predicted results (red solid lines). The RICM interference patterns are shown as insets in Figure 3.2B-3.2F. The symmetry of the inference patterns confirms the assumption of axisymmetric geometry of the confined thin water film during interaction. The initial bubble-mica separation at the time datum $t = 0$ s, was calculated to be $h(r = 0, t = 0) = 3.08 \pm 0.01$ μm by fitting the force curve with theoretical model, the validity of that was verified with AFM coupled with confocal microscope in a previous report[20]. At time $t = 1.82$ s (Figure 3.2B), the cantilever displacement $\Delta X(t)$ measured by the LVDT was 3.02 μm, still less than the initial separation and the profile results, showed that the air bubble remained nearly spherical and the minimum separation, $h(r = 0, 1.82$ s$)$ was about 76 nm. The measured actual $\Delta X(t)$ is larger than $v \times t = 1.82$ μm because the actual instantaneous velocity determined by LVDT $dX(t)/dt$ was slightly different from the nominal driving velocity due to the non-linearity of piezo-electric transducer.[50, 55] At a separation of 76 nm, the magnitude of VDW force was negligible compared to the hydrodynamic interaction that was repulsive during approach because the water confined between the air bubble and mica surface had to be displaced. At time $t = 1.94$ s (Figure 3.2C), $\Delta X(t) = 3.22$ μm, so the air bubble would have made contact with the mica surface if it remained undeformed. However, the film profile shows there was still a finite separation of about 13 nm at $r = 0$ between air bubble and mica, as the bubble is deformed with a flattened central region that is evident on comparing the experimental data (open circles) and theoretical predictions (red solid line) to the undeformed spherical profile (blue solid line). Such deformation was mainly caused by hydrodynamic repulsion as the VDW interaction was

negligible at $h \geqslant 13$ nm. As the bubble was driven even closer to mica, at time $t = 2.18$ s, when $\Delta X(t)$ has exceeded the initial separation $h(r = 0, t = 0)$ by 0.52 μm, the interaction force has reached maximum repulsion with a water film of minimum thickness of 7 nm, confined in a flatten region of about 3 μm in radial extent, as shown in Figure 3.2D. At this stage, no further thinning of the confined water film could be observed even when the cantilever was driven even closer. Therefore, the hydrodynamic interaction in this flattened region was negligible (since $dh/dt \sim 0$) and the thin water film was supported by the disjoining pressure due to the repulsive VDW interaction, calculated to be 1470 Pa at this separation and equal to the Laplace pressure of the air bubble. After the retraction was initiated, in contrast to the solid particle case in which the hydrodynamic force would become attractive immediately, the interaction repulsion force between the air bubble and the mica surface gradually decreased until a maximum hydrodynamic attraction was reached because water needed to be drawn back into the confined film (Figure 3.2A and 3.2E). As shown in Figure 3.2E, at time $t = 2.54$ s, the overall interaction force still remained repulsive during retraction and although the film thickness increased at the outer region of the air bubble due to the retraction, it remained almost unchanged (~7 nm) at the central flattened region while the radial extent of the central flattened region decreased form 3 μm to 2 μm. At time $t = 2.90$ s (Figure 3.2F), an attractive force was measured due to the hydrodynamic suction effect and the bubble showed a slight "pimple" shape, where its central region was closer to the mica surface as compared with the spherical undeformed shape (blue solid line).[48, 50]

At higher velocities, significant bubble deformation and film thinning behavior accompanied by stronger attractive forces can be observed during the retraction process owing to the stronger hydrodynamic suction effect (see SI Text Figure 3.S4). It is evident from the results in Figure 3.2 for the force and the confined film profiles that the VDW repulsion prevented the air bubble from attaching onto hydrophilic mica surface. The RICM experiment results clearly validated the theoretical model that is based on the Reynolds lubrication theory to describe the hydrodynamics of film drainage and the augmented Young-Laplace equation, with the inclusion of the VDW disjoining pressure to describe deformation of the bubble surface.

3.1.2. Bubble *vs.* hydrophobized mica surfaces

Freshly cleaved mica surfaces were hydrophobized with octadecyltrichlorosilane (OTS) by a vapor deposition process under vacuum, and different surface hydrophobicity was achieved by varying deposition duration. The hydrophobicity of the surfaces was characterized by the static water contact angle, θ_w, of sessile water drops on the surfaces. We designate mica surface with different degrees of hydrophobicity by "mica-OTS-45" ($\theta_w = 45°$) and by "mica-OTS-90" ($\theta_w = 90°$) respectively. Figure 3 shows the interaction between an air bubble of radius $R_0 = 75$ μm and the mica-OTS-45 surface and the interaction between an air bubble of radius $R_0 = 81$ μm and the mica-OTS-90 surface. As distinct from the results shown in Figure 3.2, jump-in behaviors (indicated by arrows in Figure 3.3A and 3.3D) where the interaction force drastically turned from positive (repulsive) to negative (attractive), were observed for both mica-OTS-45 and mica-OTS-90 surfaces when the bubble was driven at a low velocity of 1 μm/s towards the mica.

The jump-in behaviors indicated bubble attachment onto the hydrophobized surfaces, which led to strong capillary bridging attraction due to formation of an air capillary bridge between the tipless cantilever and the solid surface. The attachment behaviors were also verified by the evolution of the interference patterns. For both cases, the air bubble could not be detached from the mica surface by retracting the cantilever because of the strong capillary adhesion between the bubble and hydrophobized surface. In fact, for the mica-OTS-90 case, the air bubble could even spontaneously detach from the cantilever during retraction, due to the stronger surface hydrophobicity than mica-OTS-45.

The hydrophobized mica-OTS-45 and mica-OTS-90 surfaces have a root-mean-square (rms) roughness of ~0.3 nm as confirmed by AFM imaging. Since the coated OTS layer on the mica surface was very thin, ~1 nm as reported previously, its effect on the VDW interaction could be neglected for separation larger than 2 nm.[21, 60] As discussed above, the VDW interaction between mica surface and air bubble in water was repulsive at all separations and the EDL interaction was fully suppressed under the concentrated salt solution condition. Therefore, an additional attractive interaction must be responsible for trigging the air bubble attachment – we attribute this to the attractive hydrophobic interaction between the air bubble and the hydrophobized mica. We recognize that interfacial nanobubbles have been observed by AFM imaging on various hydrophobic substrates that could lead to long-ranged attraction between the hydrophobic surfaces.[42-44, 61-66] However, in this work, the RICM image has a normal resolution of ~1 nm and lateral resolution of ~150 nm. Therefore, the presence of nanobubbles with lateral size >150 nm could be excluded by RICM analysis. Tapping mode AFM imaging of the

hydrophobized mica surfaces in 500 mM NaCl (Figure 3.S4) further confirms the absence of nanobubbles on the surfaces. Therefore, interfacial nanobubbles can be ruled out as the source for the observed attraction between an air bubble and hydrophobized mica surfaces in the present study.

Recently, a general interaction free energy per unit area: $W_H(h) = -2\,\gamma\,Hy\,\exp(-h/D_H)$ has been proposed to describe the hydrophobic or hydrophilic interaction between two identical planar surfaces at separation, h where D_H is a characteristic decay length, γ is the interfacial energy of the surfaces and Hy (the so-called Hydra number) is the fraction of the hydrophobic region on the surface that may also depend on solvent conditions.[27, 35, 38] The decay length D_H has been measured to be about 1 nm for solid hydrophobic surfaces, and a shorter decay length of ~ 0.3 nm was also measured between hydrophobic oil droplets very recently.[30, 45]

For the asymmetric interaction between a planar air-water interface and a hydrophobized mica surface, a similar exponential form for the interaction free energy per unit area can be posited: $W_H(h) = -C\,\exp(-h/D_H)$. The constant C can be derived from thermodynamic considerations of the limit $h \to 0$ that creates a solid-air interface with surface energy γ_{SA} from an air-water interface with surface energy γ, and a solid-water interface with surface energy γ_{SW} to give: $C = \gamma + \gamma_{SW} - \gamma_{SA}$. This together with the Young-Duprè equation at the three phase contact line: $\gamma_{SA} = \gamma_{SW} + \gamma\cos\theta_w$ gives $C = \gamma\,(1-\cos\theta_w)$ and results in the following expression for the disjoining pressure between a bubble and a hydrophobized surface.

$$\Pi_H(h) = -dW_H/dh = -[\gamma(1-\cos\theta_w)/D_H]\exp(-h/D_H) \qquad (1)$$

For mica-OTS-45 and mica-OTS-90 surfaces, the constant $C = \gamma (1- \cos\theta_w)$ was determined to be 21 mN/m and 72 mN/m, respectively and the corresponding decay length D_H was found by fitting the force-time data at $v = 1.0$ μm/s shown in Figure 3.3A and 3.3D to be 0.8 ± 0.1 nm for the interaction with the mica-OTS-45 surface and 1.0 ± 0.1 nm for the mica-OTS-90 surface. This fitted hydrophobic disjoining pressure was then used to calculate the confined film profiles at different times. As can be seen in Figure 3.3B and 3.3E, such predicted film profiles agree very well with the experimental data based on the analysis of interference patterns from RICM (SI Figure 3.S5). The critical film thickness before attachment, that is at the point of rupture of the confined water film, was calculated to be ~5.3 nm and ~9.5 nm for mica-OTS-45 case and mica-OTS-90 case, respectively, consistent with the experimental values of ~6 nm and ~11 nm measured by RICM. It is also worth noting that bubble attachment occurs at the critical separation where the disjoining pressure just exceeded the Laplace pressure of the bubble.
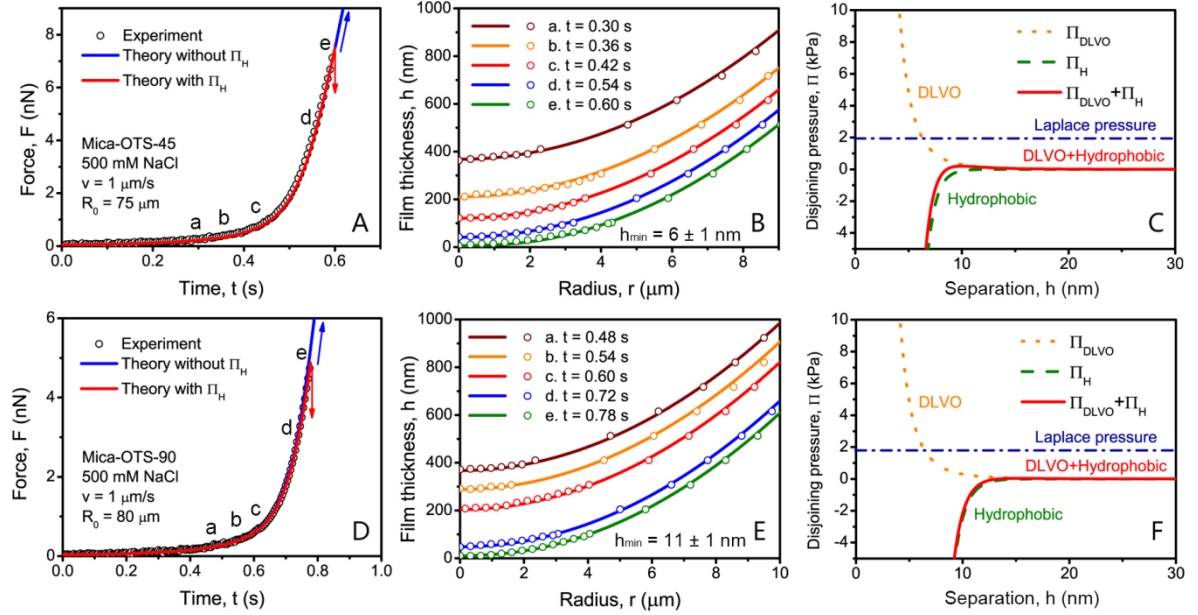
Figure 3.3. Interaction and disjoining pressure profiles between an air bubble and hydrophobized mica surfaces: mica-OTS-45 ($\theta_W = 45°$) (A-C) and mica-OTS-90 ($\theta_W = 90°$) (D-F), in 500 mM NaCl solution. The nominal driving velocity of bubble was $v = 1$ μm/s. In (A) and (D), the red solid lines are predicted theoretical results that included the hydrophobic attractive disjoining pressure (see text) and the blue solid lines are predicted theoretical results without the attractive hydrophobic interaction. The open circular symbols are experimental results obtained from AFM and RICM measurements. (A) and (C): Interaction force F as a function of time; (B) and (E): Evolution of the thin confined water film profile $h(r,t)$; (D) and (F): Variations of components of the disjoining pressure with separation.

The same disjoining pressures for the bubble-hydrophobized mica interaction mica-OTS-45 and mica-OTS-90, without further adjustments, were used to calculate the force

and the film profiles at other drive velocities. In Figure 3.4, we see that such predictions for the force for bubbles approaching mica-OTS-45 and mica-OTS-90 at nominal velocities in the range 5-30 μm/s agree very well with experimental data, and in particular, the model predicted the time of film rupture accurately. It is interesting to note that at these higher nominal drive velocities, water films remain stable on approach to the mica-OTS-45 surface because they are stabilized by higher repulsive hydrodynamic pressure. Film rupture only occurs during the retraction phase (Figures 3.4A and 3.4B) when the hydrodynamic pressure turns attractive and brings the bubble surface close enough to the hydrophobized mica surface to be within range of the attractive hydrophobic disjoining pressure Π_{H}(h). On the other hand, for the mica-OTS-90 surface that has a stronger hydrophobic attraction film rupture occurs during approach at 5 μm/s, whereas a higher repulsive hydrodynamic repulsion at 30 μm/s is needed to prevent film rupture on approach, see Figures 3.4C and 3.4D.
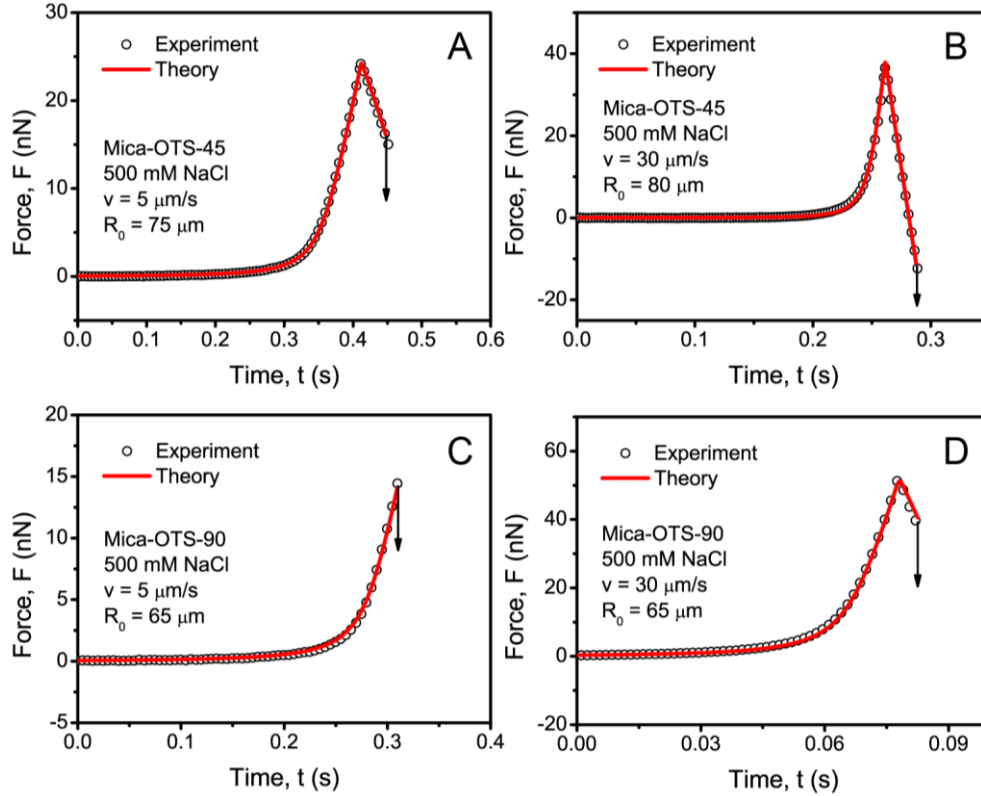
Figure 3.4. Interaction force between a bubble and hydrophobized mica surfaces: mica-OTS-45 ($\theta_w = 45°$) (A and B) and mica-OTS-90 ($\theta_w = 90°$) (C and D), in 500 mM NaCl solution with high velocities. The red solid lines are theoretical predictions. The open circular symbols are experiment force results obtained from AFM measurements. (A) and (C): interaction at a nominal drive velocity of $v = 5$ μm/s; (B) and (D): interaction at a nominal drive velocity of $v = 30$ μm/s.

In this work, the synchronous measurements of interaction forces and visualization of the spatiotemporal evolution of the confined thin water film between air bubble, that is inherently hydrophobic, and hydrohpobized mica surfaces demonstrate the significant role of hydrophobic interaction in this asymmetric system. The excellent agreement

between theoretical predictions and experiment results based on AFM-RICM measurements indicates that $D_H = 0.8 \pm 0.1$ nm and $D_H = 1.0 \pm 0.1$ nm represent the characteristic decay length of hydrophobic interaction between the hydrophobic air bubble and hydrophobized mica-OTS-45 and mica-OTS-90, respectively.[21, 29, 31] The higher the degree of surface hydrophobicity appears to increase the D_H value slightly. It is evident from our results that the characteristic decay length of hydrophobic interaction is influenced by the surface hydrophobicity that affects the structure and orientation of water molecules near the surface.[38, 39] The asymmetric bubble-mica hydrophobic interaction free energy per unit area between the air bubble and the hydrophobic substrate can be described by

$$W_H(h) = -\gamma(1 - \cos\theta_w)\exp(-h/D_H) \tag{2}$$

where γ is surface tension of water, θ_w is the static water contact angle on hydrophobic surface, h is the surface separation, D_H is the characteristic decay length that is system-dependent. Based on the analysis in this work, Equation (2) is most likely applicable as a general potential function for hydrophobic interaction in asymmetric systems where deformable surfaces (*e.g.* air bubble, liquid droplet) are involved.

An attempt to represent the hydrophobic interaction free energy per unit area with a single power law of the form: $W_H(h) = -\gamma(1 - \cos\theta_w)[D_H/(h + D_H)]^n$ failed to provide agreement with experimental data at all drive velocities (see the Supporting Information for details).

In a recent study on the interaction between two hydrophobic drops of fluorocarbon mixture with the same refractive index as water, in which the effects of VDW interaction

was almost eliminated, demonstrated a short-ranged hydrophobic interaction with a characteristic decay length of 0.3 nm,[30, 45] much shorter than that of hydrophobic interaction in solid/water/solid symmetric systems reported previously and the air bubble-water-solid asymmetric system in this work. It is interesting to note when $\theta_w = 180°$, Equation 5 becomes $W_H(h) = -2\gamma \exp(-h/D_H)$, the same as the hydrophobic interaction free energy per unit area reported for the symmetric fluorocarbon/water/fluorocarbon system.

The difference between the observed decay lengths of ~0.3 nm in soft oil/water/oil systems[30, 45] and of 0.8 - 1.0 nm in air/water/solid in this work and elsewhere,[27] might be explained in terms of the difference in the ability of the hydrophobic substrate to respond as interfacial water molecules rearrange their position and orientation to compensate for the loss of hydrogen bonding. The mica surface that has been rendered hydrophobic by the deposition of a thin layer of OTS molecules is rigid, so the first few layers of adjacent water molecules have to restructure as a consequence of the loss of hydrogen bonding compared to water molecules in bulk. On the other hand, in the vicinity of the soft, fluid oil/water interface, both the water and oil molecules in their respective phases near the interface can adjust their structure to accommodate for the loss of hydrogen bonding in the aqueous phase and the change in the surface energetics in the oil phase. As a consequence, the disruption of the of the bulk water structure is expected to extend a shorter distance into the aqueous phase thereby giving rise to the observed shorter decay length, D_H in the hydrophobic interaction free energy per unit area in soft oil/water/oil systems. Indeed as two soft, deformable oil/water interfaces are brought together, it is

expected that the interfacial structure in both the aqueous and the oil phase will change as a function of separation. However, precise quantification of such soft oil/water interfaces will require novel experimental studies and further theoretical modeling.

3.2. Conclusion

In this work, synchronous measurements of the interaction forces and the spatiotemporal evolution of the confined thin water film between air bubble and mica surfaces of different hydrophobicity were quantitatively achieved for the first time using an AFM coupled with RICM. The AFM-RICM experimental results are in complete accord with the theoretical model based on the Reynolds lubrication theory and the augmented Young-Laplace equation by including the effects of disjoining pressure. The excellent agreement between theory and experiments attests that the essential physics for the interaction between bubble and solid substrate has been elucidated. A hydrophobic interaction free energy per unit area of the form: $W_{\mathrm{H}}(h) = -\gamma (1- \cos\theta_w) \exp(-h/D_{\mathrm{H}})$, developed from thermodynamic considerations, is able to quantify the asymmetric interaction between an air bubble and hydrophobic mica substrates in predicting the coalescence attachment of the bubble at AFM drive speeds between 1- 30 µm/s on OTS hydrophobized mica surfaces with water contact angle $\theta_w = 45º$ and 90º. The variation in the decay length, D_{H} observed between the hydrophobic interaction between rigid hydrophobized mica surfaces used here and between soft deformable oil/water interfaces[30, 45] is attributed to the ability of interfacial molecules in the oil phase to accommodate changes in structure (position and orientation) of water molecules near the

interface as a result of the loss of hydrogen bonding. The methodology for synchronous probing interaction force profiles and thin film drainage dynamics involving deformable surfaces can be extended to study the interaction mechanisms of a wide range of systems involving deformable bubbles and liquid droplets. Our results have the potential to provide insights into the basic understanding of the dynamic interaction mechanism between solid surfaces of different hydrophobicity in aqueous media and deformable bubbles/drops/emulsions to more general biological materials that would be useful for designing the loading of bubbles/drops with molecules and particles as targeted delivery systems as well as the assembly of designed structures at soft or hydrophobic interfaces.

3.3. Experiments and Methods

3.3.1. Experiment

A MPF-3D AFM (Asylum Research, Santa Barbara, CA) with a mounted Nikon Ti-U inverted microscope was used to investigate the interaction between air bubble and mica surfaces. A circular glass slide of an AFM fluid cell (radius of 35 mm) was mildly hydrophobized in 10 mM OTS in toluene solution for seconds to obtain a water contact angle of ~ 50° to provide optimized hydrophobicity for immobilizing air bubble on the substrate. The air bubbles were carefully injected with a custom-made glass pipette with ultra-sharp end. The immobilized air bubble was then picked up by a custom-made rectangular silicon AFM cantilever (400 × 70 × 2 μm), which had a strongly hydrohpobized circular gold patch at one end (diameter 65 μm, thickness 30 nm) for secure bubble anchoring.[48-50] Calibration of the cantilever was done before bubble

loading and the spring constant was determined to be 0.3-0.4 N/m using the Hutter and Bechhoefer method.[67] The air bubble was then moved over the mica surface for force measurements.

Mica surfaces were hydrophobized with Octadecyltrichlorosilane (OTS) through a vapor deposition process. A freshly cleaved mica surface was placed in a vacuum desiccator with a small OTS reservoir for different durations to achieve different degrees of hydrophobicity, indicated by the water contact angle of sessile drops. Before use in AFM-RICM experiments, the hydrophobized mica surfaces were washed with large amounts of toluene, ethanol and Milli-Q water sequentially to remove physically adsorbed OTS molecules. The roughness of the hydrophobized mica surfaces was determined by AFM tapping mode imaging, showing very low rms roughness ~ 0.3 nm.

3.3.2. Theoretical model

Since the velocities investigated in this work ranged from 1 to 30 μm/s, corresponding to very small Reynolds numbers ~ 10^{-3}-10^{-4} that indicates the flow is in Stokes flow region, the Reynolds lubrication model[48, 49] can be used for quantitative analysis of the thickness, $h(r,t)$ of the axisymmetric film drainage process

$$\frac{\partial h}{\partial t} = \frac{1}{12\mu r} \frac{\partial}{\partial r}\left(rh^3 \frac{\partial p}{\partial r} \right) .$$ (3)

Here μ is the viscosity of water, $p(r,t)$ is the excess hydrodynamic pressure relative to the bulk solution. Immobile boundary conditions at both air/water and solid/water interfaces were applied in contrast to classic fluid mechanics that suggested that the air/water interface should be fully mobile and could not sustain any shear stress. Recent

work involving air bubble interaction indicated the applicability of the immobile boundary condition at the air/water interface. This could be due to a trace amount of surface active agents, including electrolyte, which can arrest boundary mobility while only lowering the surface tension by as little as 0.1 mN/m.

The augmented Young-Laplace equation

$$\frac{\gamma}{r}\frac{\partial}{\partial r}\left(r\frac{\partial h}{\partial r}\right) = \frac{2\gamma}{R_0} - p - \Pi \tag{4}$$

where R_0 is the radius of the bubble, $(2\gamma/R_0)$ is the Laplace pressure inside the air bubble, and Π is the disjoining pressure, was used to describe the deformation of air bubble during interaction. The contribution to the disjoining pressure Π comprised of the sum of the VDW interaction, calculated based on the full Lifshitz theory and the hydrophobic interaction was described in the main text.

The interaction force $F(t)$ is calculated by integrating $p(r,t)$ and $\Pi(h(r,t))$ based on Derjaguin approximation

$$F(t) = 2\pi \int_0^\infty [p(r,t) + \Pi(h(r,t))]r dr \tag{5}$$

More details of theoretical model are contained in the SI Text.

3.4. Supporting information

AFM force measurement

Force measurement between an air bubble and a solid surface was conducted using an Asylum MFP-3D Atomic Force Microscopy (AFM) following a previously reported procedure[45, 49, 68]. The aqueous solution used in the AFM experiments was prepared using

sodium chloride (NaCl, Fisher Scientific) with highest purity and Milli-Q water (Millipore deionized) with a specific resistivity greater than 18.2 MΩ·cm.

Before force measurement, a custom-made glass pipette with an ultra-sharp end was used to inject air bubbles into an AFM fluid cell filled with the aqueous solution to be tested. The glass substrate of the fluid cell was mildly hydrophobized by immersing in 10 mM octadecyltrichlorosilane (OTS, ACROS Organics) solution in toluene for a few seconds that led to a water contact angle of ~50° on the glass substrate for bubble immobilization. An air bubble with suitable size (typical radius R_0 of 60-100 μm) was picked up with a custom-made rectangular tipless cantilever (400 × 70 × 2 μm) to form an AFM bubble probe, as shown in Figure 3.S1. The tipless cantilever has a circular patch of gold (diameter 65 μm, thickness 30 nm) at the end, which was strongly hydrophobized in 10 mM dedcanethiol solultion in absolute ethanol overnight to facilitate secure and precise anchoring of the air bubble. The spring constant of the unloaded cantilever was determined using the Hutter and Bechhoefer thermal tune method[67]. The effective spring constant of the loaded cantilever was validated using force data for bubble-hydrophilic mica interactions at all drive velocities (see below) and then used for in all experiments with hydrophobized mica.

Force measurements were conducted by driving the cantilever-loaded air bubble towards the solid surface from a large initial separation until bubble attachment occurred or until a desired deflection of cantilever was detected whereupon the cantilever was then driven away from the surface. The driving velocity of the air bubble was controlled by a piezo-actuator of the AFM. Time variation of the cantilever deflection was recoded for each measurement, which could be converted to forces *via* the spring constant. The actual

variation of the cantilever-substrate separation, $X(t)$, with time t, during a force measurement was measured and recorded with a linear variable differential transformer (LVDT) that is part of the AFM. This data was used in the theoretical model for calculation.
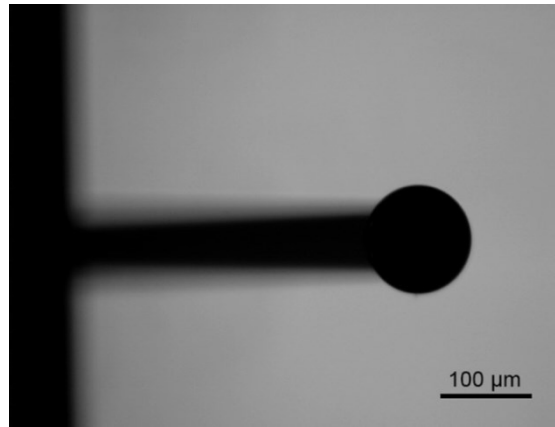
Figure 3.S1. An AFM bubble probe with bubble radius of 60 μm.

Hydrophobization of mica surfaces

Freshly peeled mica surfaces were hydrophobized by exposing to OTS vapor at room temperature (23 °C) under vacuum. Different surface hydrophobicity, characterized by the contact angle θ_w made a sessile drop on the surface, measured through the water, was achieved by varying the exposure time. A 1-hour treatment typically leads to a water contact angle of 45° and 48-72 hours treatment can lead to a water contact angle of 90°. Before each experiment, the hydrophobized mica surfaces were rinsed with toluene, ethanol and Milli-Q water to remove any physically adsorbed OTS molecules. AFM tapping mode imaging was applied to investigate the surface roughness of these hydrophobized mica surfaces that showed rms roughness of ~0.3 nm.

Theoretical model

The Stokes-Reynolds-Young-Laplace model[45, 49, 68] reported before was applied to describe the interaction between air bubble and solid surfaces. Reynolds lubrication theory with immobile boundary condition at both air/water and solid/water interfaces was applied to model the hydrodynamic drainage of the nanoscale water film of thickness, $h(r,t)$ between the air bubble and solid surface,

$$\frac{\partial h}{\partial t} = \frac{1}{12\mu r}\frac{\partial}{\partial r}\left(rh^3\frac{\partial p}{\partial r}\right)$$
(S1)

where μ is the dynamic viscosity of water, $p(r,t)$ is the hydrodynamic pressure. The film is taken to be axisymmetric, and is a good approximation for the present experiments as can be seen from the symmetry of the interference fringes.

The deformation of the bubble surface in response to the hydrodynamic pressure $p(r,t)$ and the disjoining pressure $\Pi(h(r,t))$ is described by the augmented Young-Laplace equation

$$\frac{\gamma}{r}\frac{\partial}{\partial r}\left(r\frac{\partial h}{\partial r}\right) = \frac{2\gamma}{R_0} - p - \Pi \ ,$$
(S2)

where γ is the air-water interfacial tension, R_0 is the bubble radius.

The interaction force $F(t)$ is calculated by integrating over $p(r,t)$ and $\Pi(h(r,t)$

$$F(t) = 2\pi\int_0^\infty [p(r,t) + \Pi(h(r,t))]rdr$$

(S

3)

The equations were solved in a suitable region (0, r_{max}), where the local separation $h(r,t)$ at $r > r_{max}$ was sufficiently large so that the contribution of disjoining pressure could be neglected.[68] Hence, the interaction force can be calculated as

$$F(t) = 2\pi \int_0^{r_{max}} [p(r,t) + \Pi(h(r,t))]r\,dr + 2\pi \int_{r_{max}}^{\infty} p(r,t)r\,dr \tag{S4}$$

In general, the first integral on the right side of Equation (S4) makes the dominant contribution to the calculated force and the impact of the second integral is rather small. In our calculation, the value of r_{max} was also checked to ensure the calculated force was independent on its exact value.

The boundary conditions for $h(r,t)$ and $p(r,t)$ at $r = 0$ are $\partial h / \partial r = 0$ and $\partial p / \partial r = 0$. The actual variation of cantilever displacement $X(t)$ was incorporated in a boundary condition, equation S5, which took in account the deformation of the air bubble during interaction and the pinned contact area of the air bubble on the cantilever [45, 49, 68]

$$\frac{\partial h(r_{max},t)}{\partial t} = \frac{dX(t)}{dt} + \frac{dF(t)}{2\pi\gamma dt}\left(\frac{2\pi\gamma}{K} - 1 - \frac{1}{2}\ln\left(\frac{1+\cos\theta}{1-\cos\theta}\right) - \ln\left(\frac{r_{max}}{2R_0}\right)\right) \tag{S5}$$

Here K is the spring constant of the cantilever, θ is the contact angle of the air bubble on cantilever. The hydrodynamic pressure $p(r,t)$ decays as r^{-4} at $r \to \infty$, leading to the boundary condition $r(\partial p / \partial r) + 4p = 0$ at $r = r_{max}$. The initial condition for $h(r,t)$ follows the undeformed spherical bubble shape.

The equations above were solved numerically with MATLAB after being non-dimensionalized with the scaling parameters: $h_c = R_0 Ca^{1/2}$, $r_c = R_0 Ca^{1/4}$, $p_c = \gamma / R_0$, $t_c = \mu Ca^{-1/2}$, where $Ca = \mu V / \gamma$ is the capillary number and V is the nominal drive velocity. Details of the numerical method are reported previously.

Van der Waals interaction

The VDW disjoining pressure during interaction is calculated using the full Lifshitz theory[58, 595, 6] that includes the effects of electromagnetic retardation. Denoting the air bubble, solid surface and aqueous solution as 1, 2 and 3, the VDW disjoining pressure $\Pi_{VDW}(h)$ between two half spaces at separation h can be calculated as:

$$\Pi_{VDW}(h) = \Pi_{VDW0}(h) - \frac{kT}{\pi c^3} \sum_{n=1}^{\infty} \varepsilon_3^{3/2} \xi_n^3 \int_1^{\infty} p^2 \left[(\Delta_1 \Delta_2 e^{-x} - 1)^{-1} + (\bar{\Delta}_1 \bar{\Delta}_2 e^{-x} - 1)^{-1} \right] dp$$

(S6)

$$\Pi_{VDW0}(h) = -\frac{kT}{2\pi} \int_0^{\infty} p\sqrt{p^2 + \kappa^2} (\Delta_0 - 1)^{-1} dp$$

(S7)

$$\Delta_i = \frac{s_i + p\varepsilon_i / \varepsilon_3}{s_i - p\varepsilon_i / \varepsilon_3} \ , \ \ \bar{\Delta}_i = \frac{s_i + p}{s_i - p} \ , \ \ s_i = \sqrt{\varepsilon_i / \varepsilon_3 - 1 + p^2}$$

$$\Delta_0 = \left(\frac{\sqrt{p^2 + \kappa^2}\,\varepsilon_1(0) + p\varepsilon_3(0)}{\sqrt{p^2 + \kappa^2}\,\varepsilon_1(0) - p\varepsilon_3(0)} \right) \left(\frac{\sqrt{p^2 + \kappa^2}\,\varepsilon_2(0) + p\varepsilon_3(0)}{\sqrt{p^2 + \kappa^2}\,\varepsilon_2(0) - p\varepsilon_3(0)} \right) \exp\left(2\sqrt{p^2 + \kappa^2}\,h \right)$$

$$x = 2p\xi_n \varepsilon_2^{1/2} h/c, \ \ \xi_n = 2\pi n k_B T/\hbar, \ \ \varepsilon_k = \varepsilon_k(i\xi_n)$$

where c is the speed of light in vacuum, k_B is the Boltzmann constant, T is the temperature, $(2\pi\hbar)$ is the Planck's constant, $\varepsilon_k = \varepsilon_k(i\xi_n)$ is the dielectric permittivity, and κ^{-1} is the Debye length. Due to screening by high salt concentration in this study, the effects of zero frequency ($n = 0$) term $\Pi_{VDW0}(h)$ was highly suppressed. The dielectric permittivity of water at imaginary frequencies was taken from previous report[59] and the dielectric permittivity of mica was constructed from Cauchy plot data taken from the literature[697].

RICM image analysis

Monochromatic green light with wavelength λ = 546.1 nm was used for RICM imaging. The RICM interference patterns were obtained by a Nikon Ti-U inverted microscope and were recorded with a video camera. The obtained images were processed with the *ImageJ* software (National Institutes of Health, USA).
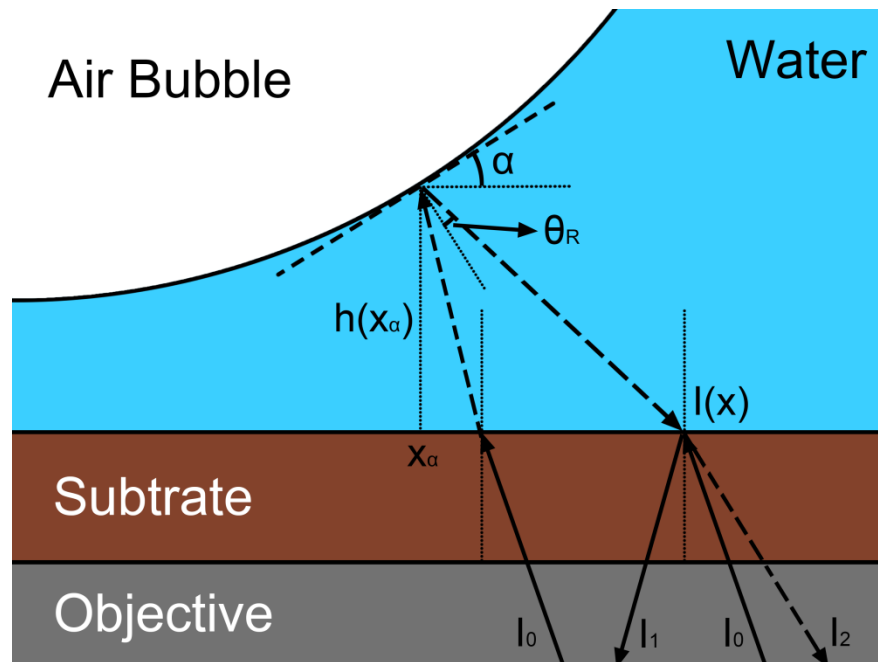
Figure 3.S2. Schematic model of non-planar RICM image formation

Construction of film thickness profile from RICM interference patterns was achieved by an improved mathematical approach[54] that can accurately reconstruct convex object with arbitrary shape by approximating its surface as an ensemble of wedges, as shown in Figure 3.S2. According to the non-planar model, in a system with single interference layer (Figure 3.S3), the light intensity at position x due to interference of light rays I_1 and I_2 can be calculated as

$$I(x) = I_1 + I_2 + 2\sqrt{I_1 I_2} \cos\left(\frac{2\pi}{\lambda}\left(2n_1 h(x_\alpha)\frac{\cos^2(\theta_R)}{\cos(\alpha + \theta_R)}\right) + \delta\right) \qquad \text{(S8)}$$

where α is the inclination angle of the air/water interface at $x = x_\alpha$, θ_R is the reflective angle at the air/water interface, $h(x_\alpha)$ is the thin film thickness at $r = x_\alpha$, $\lambda = 546.1$ nm is the light wavelength, $n_1 = 1.333$ is the refractive index of water and δ is a phase shift due to reflection, which is 0 here since the refractive index of air is less than that of water. According to geometry, x and x_α could be related as

$$x_\alpha = x - h(x_\alpha)\tan(\alpha + \theta_R) \qquad \text{(S9)}$$

A bijective mapping between x and x_α in the interference region has been established and reported including the non-planar effects and effects of illumination and detection zones. To construct the film thickness profile, the Equation S8 is rewritten and a height value h^P is first expressed as

$$h^P = h(x_\alpha)\frac{\cos^2(\theta_R)}{\cos(\alpha + \theta_R)} = \frac{\Delta h_f^P}{\pi}\cos^{-1}\left(\frac{A - I(x)}{B}\right) \qquad \text{(S10)}$$

where $A = (I_{max} + I_{min})/2$, $B = (I_{max} - I_{min})/2$, $\Delta h_f^P = \lambda/4n_1$. Δh_f^P characterizes the height difference between two consecutive fringes. It is noted that in the case of planar parallel interfaces and normal incident light, $h^P = h(x_\alpha)$. Then the inclination angle α and the measured increments of Δh^P and Δx can be related as

$$\sin(\alpha)\cos(\theta_R) = \frac{\Delta h^P}{\Delta x}$$

$$\text{(S11)}$$

in an individual wedge (note the object is approximated as an ensemble of wedges). With the Equations S9-S11, the inclination angles α and reflective angles θ_R in the

interference region can be accurately retrieved by associating Δh^P and Δx, and thus a mapping between position x and α (and θ_R) can be constructed.

Then two different but complementary methods were applied for analyzing the light intensity data. For positions larger than the first extremum, where interference fringes exist, Δx is taken as the distance between the consecutive fringes and $\Delta h^P = \Delta h^P_f$. For the positions inside the first extremum, the light intensity were analysed and transformed so that the Δx is constant and the Δh^P was calculated based on Equation S10. To achieve high resolution, α and θ_R is defined as a function of x and Equation S9 is transformed to a first-order ordinary differential equation as

$$\frac{dx_\alpha}{dx} + x_\alpha F(x) = G(x)$$

$$F(x) = -\frac{d(\tan(\alpha + \theta_R))/dx}{\tan(\alpha + \theta_R) + \tan^2(\alpha + \theta_R)\tan\alpha} \tag{S12}$$

$$G(x) = \frac{\tan(\alpha + \theta_R) - xd(\tan(\alpha + \theta_R))/dx}{\tan(\alpha + \theta_R) + \tan^2(\alpha + \theta_R)\tan\alpha}$$

The above equations can be solved numerically with MATLAB to construct the profile of the thin film. It is noted that the above more rigorous calculation[54, 70, 71] and a simplified approach with assumption of planar parallel interfaces[51, 52, 71] actually provide very similar results in this work, since the maximum inclination in our analysis is very small (<10°).

A procedure to transform RICM interference pattern to thin film profile construction is shown in Figure 3.S3. For the interaction of a bubble and hydrophoized mica surface, the maximum light intensity I_{max}, which indicates zero separation, was measured after

bubble attachment. For interaction with hydrophilic mica surface, I_{max} is not directly available since there is always a thin water film trapped between the air bubble and the mica surface. The I_{max} in this case was obtained by scaling the experiment light intensity values to the variation of intensity with height which is calculated theoretically for stratified planar structures [54].
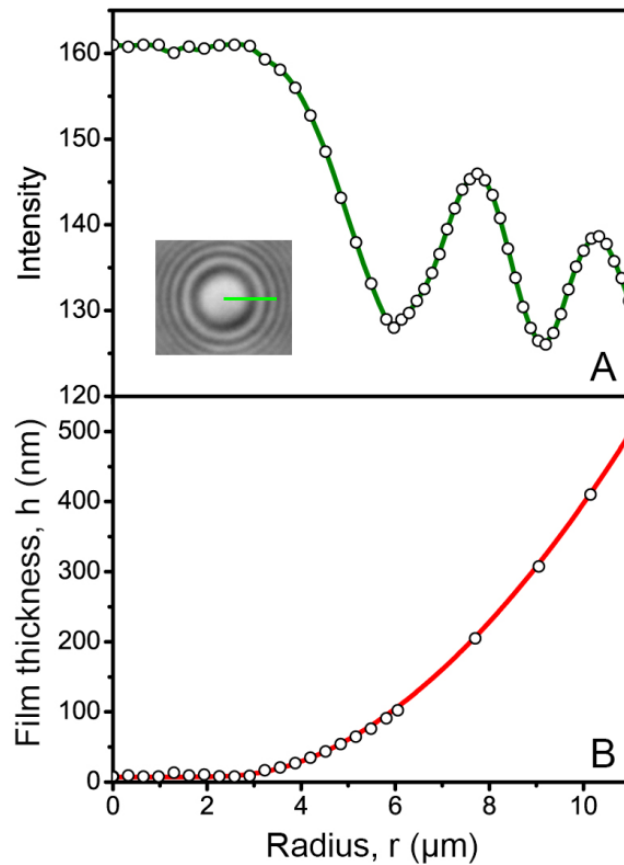
Figure 3.S3. The conversion of the RICM interference pattern to the thin film profile. (A) Profile of light intensity. The open circle symbols are local intensity values and the dark green line has been drawn to guide the eye. The inset shows the interference pattern and the light green line shows the location of the drawn light intensity. (B)

Calculated thin film profile from the intensity pattern where the open circular symbols are RICM experiment results and solid red line is the theoretical prediction from the Stokes-Reynolds-Young-Laplace model.

AFM images of mica and hydrophobized mica surfaces in 500 mM NaCl
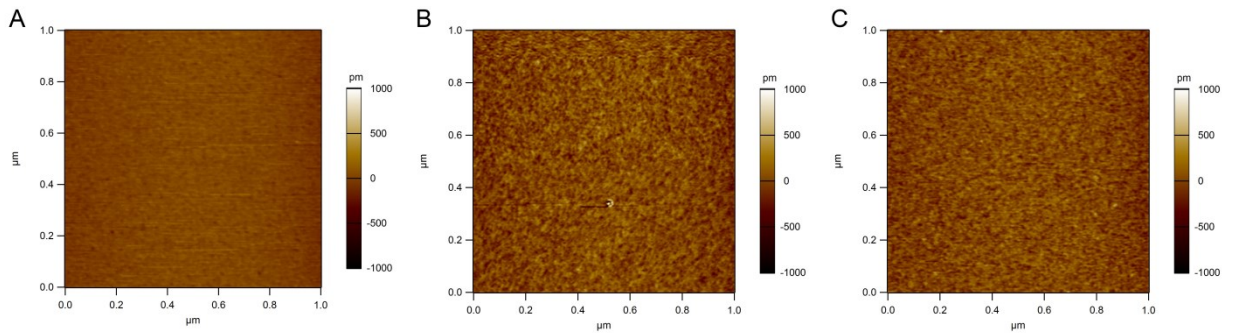
Figure 3.S4. AFM images of (A) freshly cleaved mica (B) mica-OTS-45 and (C) mica-OTS-90 surfaces in 500 mM NaCl.

Interference fringe patterns of thin water film between air bubble and hydrophobized mica surfaces during interaction corresponding to Figure 3 in the main text
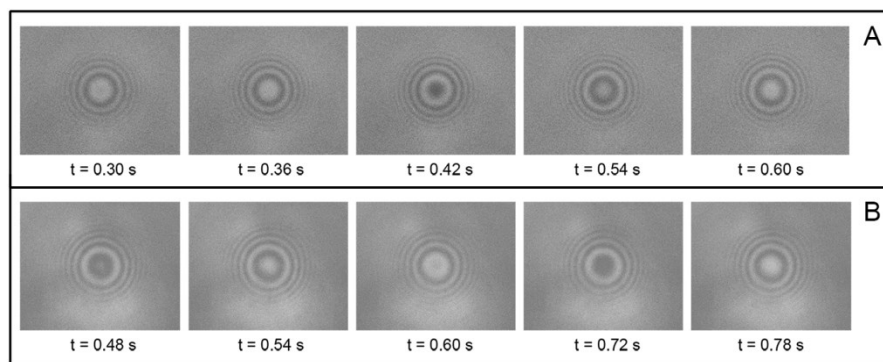
Figure 3.S5. Interference fringe patterns of thin water film between air bubble and (A) mica-OTS-45 and (B) mica-OTS-90 surfaces during interaction of Figure 3 in the main text.

Interaction between air bubble and hydrophilic mica surface at high velocity

When the air bubble is driven at high velocity, the effects of hydrodynamic interaction on the interaction force and thin film drainage process become more evident and cannot be neglected. Figure 3.S6 shows the interaction between an air bubble with radius of 98 μm and hydrophilic mica surface, with a velocity of 10 μm/s. Compared with the force curve in Figure 2A (in the main text), the interaction force with higher velocity shows a much larger attraction during retraction due to the stronger hydrodynamic suction effects since the water has to be drawn back into the thin film. The RICM data and theoretical results of the evolution of the thin water film shown in Figure 3.S6B indicated that the central part of the liquid film continues thinning even after retraction starts, which is a result of hydrodynamic suction effect, indicating bubble attachment could also occur during retracting due to this thinning behaviour.
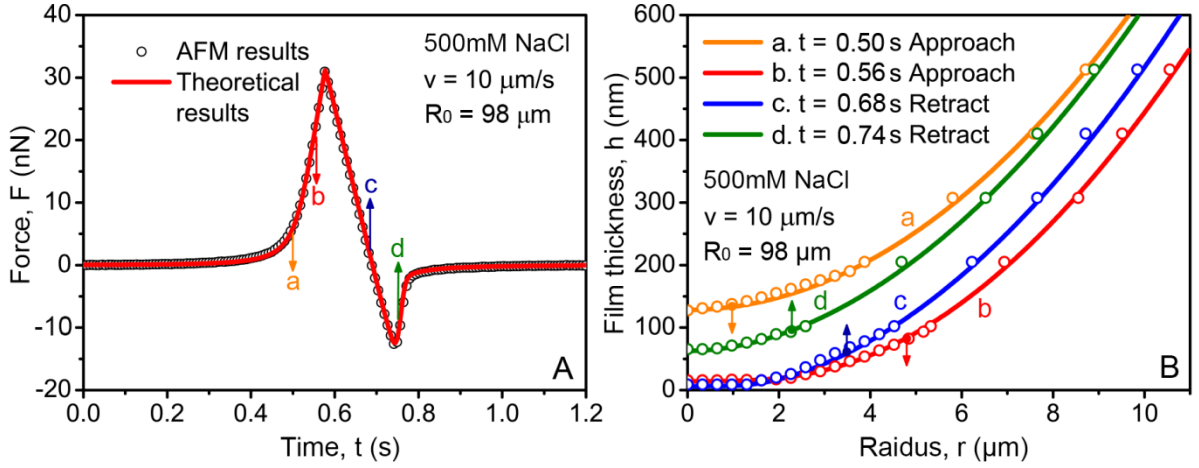
Figure 3.S6. Interaction between an air bubble and hydrophilic mica in 500 mM NaCl solution. The bubble radius is 98 μm. The nominal driving velocity of bubble is 10 μm/s. (A) Variation of the measured force with time measured with the AFM (open circles) and theoretical predictions (line). (B) The film profile deduced from RICM (open circle) and theoretical predictions (solid lines). The arrows indicate the driving direction of the air bubble.

Functional Form of Hydrophobic Interaction

An acceptable functional form of hydrophobic interaction should be able to predict the measured interaction forces and film profiles under all experimental condition. In addition to the exponential form (Equation 1 in main text) of hydrophobic interaction, we have also considered a decaying power of the form

$$\Pi_H(h) = -dW_H(h)/dh = -\frac{n\gamma(1-\cos\theta_w)}{D_H}(\frac{D_H}{h+D_H})^{n+1}$$

(S13)

In this form, both the decay length D_H and the power law index n need to be determined. We found that this power law form for $\Pi_H(h)$ cannot provide agreement with

experimental results at all velocities. For example, as shown in Figure 3.S7A, a decay length D_H = 1 nm and n = 4 could provide a good fit to the experimental force data between an air bubble and mica-OTS-90 surface at nominal velocity v = 1 μm/s including the point of bubble attachment. However, the same parameters for $\Pi_H(h)$ would give an incorrect bubble attachment time at a nominal velocity of v = 30 μm/s (Figure 3.S7B). With a decay length fixed at D_H = 1 nm (Figure 3.S7A), power law form with n = 3 predicted a much earlier attachment, representing a much stronger hydrophobic interaction; whereas the form with n = 5 predicted a delayed attachment. The power law form therefore cannot provide quantitative match with the experiment results.
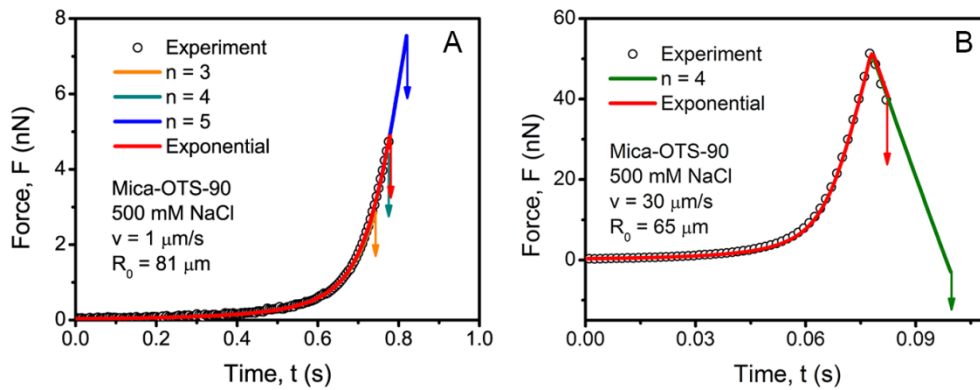
Figure 3.S7. Comparison between the exponential (Equation 1 in main text) and power law forms (Equation S13) of the hydrophobic disjoining pressure. The open circular symbols are experiment results and the solid lines are theoretical prediction with different forms for hydrophobic interaction. (A) Comparison between exponential form and power law form with varying n and D_H = 1 nm, in the case of interaction between an air bubble (R_0 = 81 μm) and mica-OTS-90 surface at nominal velocity v = 1 μm/s; (B) Comparison between exponential form and power law form with n = 4 and D_H = 1 nm, in

the case of interaction between an air bubble (R_0 = 65 μm) and mica-OTS-90 surface at nominal velocity v = 30 μm/s.

References

1.   Durian, D. J.; Weitz, D. A.; Pine, D. J., Multiple Light-Scattering Probes of Foam Structure and Dynamics. *Science* 1991, 252, 686-688.

2.   Ralston, J.; Fornasiero, D.; Hayes, R., Bubble-particle attachment and detachment in flotation. *Int. J. Miner. Process.* 1999, 56, 133-164.

3.   Prakash, M.; Gershenfeld, N., Microfluidic bubble logic. *Science* 2007, 315, 832-835.

4.   Stride, E.; Edirisinghe, M., Novel microbubble preparation technologies. *Soft Matter* 2008, 4, 2350-2359.

5.   Schutt, E. G.; Klein, D. H.; Mattrey, R. M.; Riess, J. G., Injectable microbubbles as contrast agents for diagnostic ultrasound imaging: The key role of perfluorochemicals. *Angew. Chem., Int. Ed.* 2003, 42, 3218-3235.

6.   Lindner, J. R., Microbubbles in medical imaging: current applications and future directions. *Nat. Rev. Drug Discovery* 2004, 3, 527-532.

7.   Prentice, P.; Cuschierp, A.; Dholakia, K.; Prausnitz, M.; Campbell, P., Membrane disruption by optically controlled microbubble cavitation. *Nat. Phys.* 2005, 1, 107-110.

8.   Wrenn, S. P.; Dicker, S. M.; Small, E. F.; Dan, N. R.; Mleczko, M.; Schmitz, G.; Lewin, P. A., Bursting Bubbles and Bilayers. *Theranostics* 2012, 2, 1140-1159.

9.   Chen, K.-J.; Chaung, E.-Y.; Wey, S.-P.; Lin, K.-J.; Cheng, F.; Lin, C.-C.; Liu, H.-L.; Tseng, H.-W.; Liu, C.-P.; Wei, M.-C.; Liu, C.-M.; Sung, H.-W., Hyperthermia-

Mediated Local Drug Delivery by a Bubble-Generating Liposomal System for Tumor-Specific Chemotherapy. *ACS Nano* 2014, 8, 5105-5115.

10.   Lentacker, I.; De Smedt, S. C.; Demeester, J.; Van Marck, V.; Bracke, M.; Sanders, N. N., Lipoplex-loaded microbubbles for gene delivery: A Trojan horse controlled by ultrasound. *Adv. Funct. Mater.* 2007, 17, 1910-1916.

11.   Lentacker, I.; De Smedt, S. C.; Sanders, N. N., Drug loaded microbubble design for ultrasound triggered delivery. *Soft Matter* 2009, 5, 2161-2170.

12.   Mura, S.; Nicolas, J.; Couvreur, P., Stimuli-responsive nanocarriers for drug delivery. *Nat. Mater.* 2013, 12, 991-1003.

13.   Cavalli, R.; Bisazza, A.; Lembo, D., Micro- and nanobubbles: A versatile non-viral platform for gene delivery. *Int. J. Pharm.* 2013, 456, 437-445.

14.   Soler, L.; Magdanz, V.; Fomin, V. M.; Sanchez, S.; Schmidt, O. G., Self-Propelled Micromotors for Cleaning Polluted Water. *ACS Nano* 2013, 7, 9611-9620.

15.   Yec, C. C.; Zeng, H. C., Nanobubbles within a Microbubble: Synthesis and Self-Assembly of Hollow Manganese Silicate and Its Metal-Doped Derivatives. *ACS Nano* 2014, 8, 6407-6416.

16.   Kovalenko, A.; Jouhannaud, J.; Polavarapu, P.; Krafft, M. P.; Waton, G.; Pourroy, G., Hollow magnetic microspheres obtained by nanoparticle adsorption on surfactant stabilized microbubbles. *Soft Matter* 2014, 10, 5147-5156.

17.   Shen, G.; Zhang, X. H.; Ming, Y.; Zhang, L.; Zhang, Y.; Hu, J., Photocatalytic Induction of Nanobubbles on TiO2 surfaces. *J. Phys. Chem. C* 2008, 112, 4029-4032.

18.   Belova, V.; Krasowska, M.; Wang, D.; Ralston, J.; Shchukin, D. G.; Moehwald, H., Influence of adsorbed air at liquid/solid interfaces on heterogeneous cavitation. *Chemical Science* 2013, 4, 248-256.

19.   Liu, G.; Craig, V. S. J., Improved Cleaning of Hydrophilic Protein-Coated Surfaces using the Combination of Nanobubbles and SDS. *Acs Applied Materials & Interfaces* 2009, 1, 481-487.

20.   Lozano, M. M.; Longo, M. L., Microbubbles Coated with Disaturated Lipids and DSPE-PEG2000: Phase Behavior, Collapse Transitions, and Permeability. *Langmuir* 2009, 25, 3705-3712.

21.   Israelachvili, J. N., *Intermolecular and surface forces: revised third edition*. Academic press: 2011.

22.   Dickinson, E.; Ettelaie, R.; Kostakis, T.; Murray, B. S., Factors controlling the formation and stability of air bubbles stabilized by partially hydrophobic silica nanoparticles. *Langmuir* 2004, 20, 8517-8525.

23.   Sanchez-Iglesias, A.; Grzelczak, M.; Altantzis, T.; Goris, B.; Perez-Juste, J.; Bals, S.; Van Tendeloo, G.; Donaldson, S. H., Jr.; Chmelka, B. F.; Israelachvili, J. N.; Liz-Marzan, L. M., Hydrophobic Interactions Modulate Self-Assembly of Nanoparticles. *ACS Nano* 2012, 6, 11059-11065.

24.   Leckband, D., Measuring the forces that control protein interactions. *Annu. Rev. Biophys. Biomol. Struct.* 2000, 29, 1-26.

25.   Tirrell, M.; Kokkoli, E.; Biesalski, M., The role of surface science in bioengineered materials. *Surf. Sci.* 2002, 500, 61-83.

26.   Allan, D. B.; Firester, D. M.; Allard, V. P.; Reich, D. H.; Stebe, K. J.; Leheny, R. L., Linear and nonlinear microrheology of lysozyme layers forming at the air-water interface. *Soft Matter* 2014, 10, 7051-7060.

27.   Donaldson, S. H.; Røyne, A.; Kristiansen, K.; Rapp, M. V.; Das, S.; Gebbie, M. A.; Lee, D. W.; Stock, P.; Valtiner, M.; Israelachvili, J., Developing a general interaction potential for hydrophobic and hydrophilic interactions. *Langmuir* 2014.

28.   Lee, M. H.; Reich, D. H.; Stebe, K. J.; Leheny, R. L., Combined Passive and Active Microrheology Study of Protein-Layer Formation at an Air-Water Interface. *Langmuir* 2010, 26, 2650-2658.

29.   Meyer, E. E.; Rosenberg, K. J.; Israelachvili, J., Recent progress in understanding hydrophobic interactions. *Proc. Natl. Acad. Sci. U. S. A.* 2006, 103, 15739-15746.

30.   Tabor, R. F.; Grieser, F.; Daairtine, R. R.; Chan, D. Y. C., The hydrophobic force: measurements and methods. *Phys. Chem. Chem. Phys.* 2014, 16, 18065-75.

31.   Israelachvili, J.; Pashley, R., THE HYDROPHOBIC INTERACTION IS LONG-RANGE, DECAYING EXPONENTIALLY WITH DISTANCE. *Nature* 1982, 300, 341-342.

32.   Mastropietro, D. J.; Ducker, W. A., Forces between Hydrophobic Solids in Concentrated Aqueous Salt Solution. *Phys. Rev. Lett.* 2012, 108.

33.   Huang, D. M.; Chandler, D., Temperature and length scale dependence of hydrophobic effects and their possible implications for protein folding. *Proc. Natl. Acad. Sci. U. S. A.* 2000, 97, 8324-8327.

34.   Pashley, R. M.; McGuiggan, P. M.; Ninham, B. W.; Evans, D. F., ATTRACTIVE FORCES BETWEEN UNCHARGED HYDROPHOBIC SURFACES - DIRECT MEASUREMENTS IN AQUEOUS-SOLUTION. *Science* 1985, 229, 1088-1089.

35.   Donaldson, S. H., Jr.; Lee, C. T., Jr.; Chmelka, B. F.; Israelachvili, J. N., General hydrophobic interaction potential for surfactant/lipid bilayers from direct force measurements between light-modulated bilayers. *Proc. Natl. Acad. Sci. U. S. A.* 2011, 108, 15699-15704.

36.   Craig, V.; Ninham, B.; Pashley, R., Direct measurement of hydrophobic forces: A study of dissolved air, approach rate, and neutron irradiation. *Langmuir* 1999, 15, 1562-1569.

37.   Faghihnejad, A.; Zeng, H., Hydrophobic interactions between polymer surfaces: using polystyrene as a model system. *Soft Matter* 2012, 8, 2746-2759.

38.   Donaldson, S. H., Jr.; Das, S.; Gebbie, M. A.; Rapp, M.; Jones, L. C.; Roiter, Y.; Koenig, P. H.; Gizaw, Y.; Israelachvili, J. N., Asymmetric Electrostatic and Hydrophobic-Hydrophilic Interaction Forces between Mica Surfaces and Silicone Polymer Thin Films. *ACS Nano* 2013, 7, 10094-10104.

39.   Kristiansen, K.; Stock, P.; Baimpos, T.; Raman, S.; Harada, J. K.; Israelachvili, J. N.; Valtiner, M., Influence of molecular dipole orientations on long-range exponential interaction forces at hydrophobic contacts in aqueous solutions. *ACS Nano* 2014, 8, 10870-7.

40.   Perkin, S.; Kampf, N.; Klein, J., Long-range attraction between charge-mosaic surfaces across water. *Phys. Rev. Lett.* 2006, 96.

41.   Faghihnejad, A.; Zeng, H., Interaction Mechanism between Hydrophobic and Hydrophilic Surfaces: Using Polystyrene and Mica as a Model System. *Langmuir* 2013, 29, 12443-12451.

42.   Carambassis, A.; Jonker, L. C.; Attard, P.; Rutland, M. W., Forces measured between hydrophobic surfaces due to a submicroscopic bridging bubble. *Phys. Rev. Lett.* 1998, 80, 5357-5360.

43.   Thormann, E.; Simonsen, A. C.; Hansen, P. L.; Mouritsen, O. G., Force trace hysteresis and temperature dependence of bridging nanobubble induced forces between hydrophobic surfaces. *ACS Nano* 2008, 2, 1817-1824.

44.   German, S. R.; Wu, X.; An, H.; Craig, V. S. J.; Mega, T. L.; Zhang, X., Interfacial Nanobubbles Are Leaky: Permeability of the Air/Water Interface. *ACS Nano* 2014, 8, 6193-6201.

45.   Tabor, R. F.; Wu, C.; Grieser, F.; Daairtine, R. R.; Chan, D. Y. C., Measurement of the Hydrophobic Force in a Soft Matter System. *J. Phys. Chem. Lett.* 2013, 4, 3872-3877.

46.   Preuss, M.; Butt, H. J., Direct measurement of particle-bubble interactions in aqueous electrolyte: Dependence on surfactant. *Langmuir* 1998, 14, 3164-3174.

47.   Ducker, W. A.; Xu, Z. G.; Israelachvili, J. N., MEASUREMENTS OF HYDROPHOBIC AND DLVO FORCES IN BUBBLE-SURFACE INTERACTIONS IN AQUEOUS-SOLUTIONS. *Langmuir* 1994, 10, 3279-3289.

48.   Shi, C.; Chan, D. Y.; Liu, Q.; Zeng, H., Probing Hydrophobic Interaction between Air Bubble and Partially Hydrophobic Surfaces Using Atomic Force Microscopy. *J. Phys. Chem. C* 2014, 118, 25000-25008.

49.   Tabor, R. F.; Manica, R.; Chan, D. Y. C.; Grieser, F.; Daairtine, R. R., Repulsive van der Waals Forces in Soft Matter: Why Bubbles Do Not Stick to Walls. *Phys. Rev. Lett.* 2011, 106.

50.   Vakarelski, I. U.; Manica, R.; Tang, X.; O'Shea, S. J.; Stevens, G. W.; Grieser, F.; Daairtine, R. R.; Chan, D. Y. C., Dynamic interactions between microbubbles in water. *Proc. Natl. Acad. Sci. U. S. A.* 2010, 107, 11177-11182.

51.   Manica, R.; Parkinson, L.; Ralston, J.; Chan, D. Y. C., Interpreting the Dynamic Interaction between a Very Small Rising Bubble and a Hydrophilic Titania Surface. *J. Phys. Chem. C* 2010, 114, 1942-1946.

52.   Hendrix, M. H. W.; Manica, R.; Klaseboer, E.; Chan, D. Y. C.; Ohl, C.-D., Spatiotemporal Evolution of Thin Liquid Films during Impact of Water Bubbles on Glass on a Micrometer to Nanometer Scale. *Phys. Rev. Lett.* 2012, 108.

53.   Parkinson, L.; Ralston, J., The Interaction between a Very Small Rising Bubble and a Hydrophilic Titania Surface. *J. Phys. Chem. C* 2010, 114, 2273-2281.

54.   Contreras-Naranjo, J. C.; Ugaz, V. M., A nanometre-scale resolution interference-based probe of interfacial phenomena between microscopic objects and surfaces. *Nat. Commun.* 2013, 4.

55.   Tabor, R. F.; Grieser, F.; Daairtine, R. R.; Chan, D. Y. C., Measurement and analysis of forces in bubble and droplet systems using AFM. *J. Colloid Interface Sci.* 2012, 371, 1-14.

56.   Daairtine, R. R.; Manica, R.; Carnie, S. L.; Chan, D. Y. C.; Stevens, G. W.; Grieser, F., Dynamic forces between two deformable oil droplets in water. *Science* 2006, 313, 210-213.

57.   Manor, O.; Vakarelski, I. U.; Stevens, G. W.; Grieser, F.; Daairtine, R. R.; Chan, D. Y. C., Dynamic Forces between Bubbles and Surfaces and Hydrodynamic Boundary Conditions. *Langmuir* 2008, 24, 11533-11543.

58.   Ninham, B. W.; Parsegia.Va, VANDERWAALS FORCES - SPECIAL CHARACTERISTICS IN LIPID-WATER SYSTEMS AND A GENERAL METHOD OF CALCULATION BASED ON LIFSHITZ THEORY. *Biophys. J.* 1970, 10, 646-&.

59.   Daairtine, R. R.; Prieve, D. C.; White, L. R., The dielectric function for water and its application to van der Waals forces. *J. Colloid Interface Sci.* 2000, 231, 351-358.

60.   Grabbe, A., DOUBLE-LAYER INTERACTIONS BETWEEN SILYLATED SILICA SURFACES. *Langmuir* 1993, 9, 797-801.

61.   Borkent, B. M.; Dammer, S. M.; Schoenherr, H.; Vancso, G. J.; Lohse, D., Superstability of surface nanobubbles. *Phys. Rev. Lett.* 2007, 98.

62.   Walczyk, W.; Schoenherr, H., Closer Look at the Effect of AFM Imaging Conditions on the Apparent Dimensions of Surface Nanobubbles. *Langmuir* 2013, 29, 620-632.

63.   Walczyk, W.; Schoen, P. M.; Schoenherr, H., The effect of PeakForce tapping mode AFM imaging on the apparent shape of surface nanobubbles. *J. Phys.: Condens. Matter* 2013, 25.

64.   Zhang, X. H.; Zhang, X. D.; Lou, S. T.; Zhang, Z. X.; Sun, J. L.; Hu, J., Deairsing and temperature effects on the formation of nanobubbles at the mica/water interface. *Langmuir* 2004, 20, 3813-3815.

65.   Walczyk, W.; Schoenherr, H., Characterization of the Interaction between AFM Tips and Surface Nanobubbles. *Langmuir* 2014, 30, 7112-7126.

66.   Walczyk, W.; Hain, N.; Schoenherr, H., Hydrodynamic effects of the tip movement on surface nanobubbles: a combined tapping mode, lift mode and force volume mode AFM study. *Soft Matter* 2014, 10, 5945-5954.

67.   Hutter, J. L.; Bechhoefer, J., CALIBRATION OF ATOMIC-FORCE MICROSCOPE TIPS. *Rev. Sci. Instrum.* 1993, 64, 1868-1873.

68.   Chan, D. Y. C.; Klaseboer, E.; Manica, R., Film drainage and coalescence between deformable drops and bubbles. *Soft Matter* 2011, 7, 2235-2264.

69.   Bailey, A. I.; Kay, S. M., MEASUREMENT OF REFRACTIVE INDEX AND DISPERSION OF MICA EMPLOYING MULTIPLE BEAM INTERFERENCE TECHNIQUES. *Br. J. Appl. Phys.* 1965, 16, 39-44.

70.   Contreras-Naranjo, J. C.; Silas, J. A.; Ugaz, V. M., Reflection interference contrast microscopy of arbitrary convex surfaces. *Appl. Opt.* 2010, 49, 3701-3712.

71.   Wiegand, G.; Neumaier, K. R.; Sackmann, E., Microinterferometry: three-dimensional reconstruction of surface microtopography for thin-film and wetting studies by reflection interference contrast microscopy (RICM). *Appl. Opt.* 1998, 37, 6892-6905.

Chapter 4 Interaction Mechanism of Oil-in-Water Emulsions with Asphaltenes Determined using Droplet Probe AFM

4.1.   Introduction

Formation and stabilization of emulsions with adsorbed interface-active components at oil/water interface have long been of fundamental and practical interest, which are widely involved in many established and modern industrial and biological processes, such as oil sands extraction,[1-3] synthesis of nano/micro-particles with novel structures,[4-7] controllable and programmable drug and gene delivery.[8-10] Thermodynamically, amphiphilic molecules can readily adsorb onto the oil/water interface, altering the properties of the interface (*e.g.* interfacial tension) and changing the surface interactions between the emulsion droplets in the suspending fluid.[11-14] The stability of emulsion droplets is highly dependent on their surface interactions and interfacial properties. Generally, attractive interactions such as van der Waals (VDW) interaction and bridging adhesion due to the presence of polymer flocculants can lead to coagulation and coalescence of the emulsion droplets; while repulsive interactions, such as electrical double layer (EDL) repulsion (in aqueous media) and steric repulsion due to the presence of interface-active materials can enhance the emulsion stability.[3, 13, 15-17] Therefore, quantitative understanding of the surfaces interactions at oil/water interface with/without adsorbed interface-active molecules will help elucidate the stabilization mechanisms of the emulsions. However, quantification of the surface forces at deformable oil/water interfaces is much less

reported as compared to those at solid/liquid interfaces, mainly due to the experimental difficulties such as stable and accurate manipulation of droplet motion and precise interpretation of the measured force-distance data.[18, 19]

Stable water-in-oil (W/O) and oil-in-water (O/W) emulsions are generally undesired because they cause challenging issues in production of conventional crude oil and oil sands.[2, 3, 20-23] Emulsified water droplets of several tens of micrometers are commonly encountered in the naphtha-diluted bitumen froth extracted from oil sands using a water-based extraction method.[3, 20, 21, 24-26] These emulsified water droplets are extremely stable against coalescence and can cause serious processing problems to downstream equipment, *e.g.* fouling and corrosion in heat exchangers, pipelines and upgrading equipment.[1, 20, 27] On the other hand, bitumen droplets in the form of O/W emulsions can appear in processes such as bitumen extraction and flotation.[2, 28-31] To achieve higher bitumen recovery efficiency, larger bitumen drops are preferred which have relatively high collision and attachment efficiency with the collecting air bubbles in bitumen flotation. Stable O/W emulsions present in process water and tailings water in bitumen extraction also cause challenging issues (e.g. fouling) in water treatment process. Therefore, undesired O/W and W/O emulsions can significantly increase the operating cost in oil production.

Adsorption of natural interface-active components in crude oil and bitumen onto oil/water interface has been reported to be a major stabilization mechanism of W/O and O/W emulsions, in which asphaltenes are generally accepted to play an important role.[20, 21, 24-27, 32-34] Asphaltenes commonly exist in crude oil and bitumen products as the heaviest components, defined operationally as a solubility class that are soluble in

aromatic solvents (e.g. toluene) but precipitate in paraffinic solvents (e.g. pentane, heptane).[27, 33-35] This solubility-based definition suggests that asphaltenes do not consist of a well-defined group of chemicals, but a complex mixture of molecules. Nevertheless, asphaltenes extracted from different oil samples have been reported to share similar colloidal behaviors and surface properties. Several theoretical models such as the Yen-Mullins model have been proposed to explain the molecular and colloidal properties of asphaltenes.[27, 33-35] Generally, asphaltene molecules are considered to consist of condensed polyaromatic rings and peripheral alkane chains containing a considerable amount of polar functional groups including both acids (*e.g.* carboxyl groups) and bases (*e.g.* amino groups),[27, 33-36] which render asphaltene molecules interface active. Therefore, the asphaltenes molecules are able to adsorb and build up at oil/water interface, altering the interfacial properties such as interfacial tension, interfacial elasticity and viscosity,[37-40] which thereby influence the interactions between the emulsified droplets. Therefore, a quantitative understanding of the interactions between oil droplets in presence of asphaltenes, under various aqueous solution conditions (e.g. pH, salinity and the presence of multivalent ions like Ca^{2+}), is of vital importance to elucidate the stabilization mechanism of these O/W emulsions.[22, 27, 39, 41]

Experimental tools, such as atomic force microscopy (AFM), surface forces apparatus (SFA), and micropipette have been applied to investigate the molecular interactions of asphaltenes, polyaromatic surfactants (as asphaltene model compounds) and their impacts on emulsion stability.[22, 36, 42-48] Direct force measurements using AFM and SFA showed strong steric repulsion between asphaltene films coated on mica or silica surfaces in toluene, which was believed to play an important role in preventing water droplets from

coalescence and stabilizing W/O emulsion.[1, 45, 49] These previous studies have provided useful information regarding the molecular interactions of asphaltenes under different solvent conditions. However, all the quantitative force results reported have used immobilized asphaltene films coated on solid substrates, and direct force measurements between two emulsion droplets with asphaltenes adsorbed at the oil/water interface is not available, which is directly related to the stabilization mechanism of the emulsions.

Recently, bubble/droplet probe AFM technique has been developed and applied for direct force measurements between two deformable bubbles/droplets and between a bubble/droplet and a solid surface, and various surface interactions involved (*e.g.* electrostatic double layer interaction, hydrophobic interaction, structural force) have been precisely quantified.[10, 15, 18, 19, 50-56] An air bubble or oil droplet anchored on a tipless cantilever was driven to interact with another droplet or a solid surface, and the interaction force was measured by detecting deflection of the cantilever. The surface force involved during bubble/droplet interaction can be quantitatively reconstructed by fitting the measured force curves with a theoretical model based on Reynolds lubrication theory and augmented Young-Laplace equation,[19, 46-48, 53, 56] whose validity has been verified by simultaneously measuring the force and the separation using AFM coupled with reflection interference contrast microscopy (RICM).[50, 57]

In this study, the droplet probe AFM technique was utilized for the first time to directly measure the interaction forces between two oil droplets in the presence of asphaltenes in various aqueous solutions, which were then analyzed with the theoretical model aforementioned. This work provides a useful approach to quantify the interaction behaviors of emulsified oil droplets with asphaltenes adsorbed at the oil/water interface,

88

and the results give insights into the stabilization mechanisms of the O/W emulsions due to asphaltenes.

4.2. Experiment and Theoretical Model

4.2.1. Materials

Crude oil sample was supplied by Shell. Heptane (HPLC grade, Fisher), toluene (HPLC grade, Fisher) and methylene chloride (HPLC grade, Fisher) were used as received. Sodium chloride (NaCl) and calcium chloride (CaCl$_2$) with highest purity were purchased from Fisher Scientific. Milli-Q water (Millipore deionized) with a resistance of $\geqslant$ 18.2 MΩ·cm was used to prepare the aqueous solutions. Hydrochloric acid (HCl, ACS reagent grade, Fisher) and sodium hydroxide (NaOH, ACS reagent grade, Fisher) were used to adjust the pH of the solutions.

4.2.2. Separation of asphaltenes and preparation of asphaltenes solution.

Asphaltenes sample was separated from the crude oil sample using ASTM IP143 procedure.[50] Briefly, crude oil was mixed with heptane at a ratio of 1:30 (g/ml) and then refluxed under stirring for 1 hour. After reflux, the mixture was cooled in fridge for 2.5 hours for precipitation of asphaltenes. The mixture was then filtered to obtain the raw asphaltenes, which was then extracted with heptane for 1 h using a Soxhlet extractor to fully remove the heptane-soluble components. Methylene chloride was then used to extract the asphaltenes from the remaining filtrate. The obtained asphaltene in methylene chloride solution was concentrated and then dried under pure nitrogen flow to get the dry

pure asphaltenes sample. The separated asphaltenes samples were carefully sealed and stored in fridge to avoid oxidation.

To prepare asphaltene solutions, a certain amount of asphaltenes were dissolved in toluene and the solutions were sonicated for 30 min to fully dissolve the asphaltenes. The prepared solutions were then sealed and stored in fridge to avoid solvent evaporation and asphaltenes oxidation. The asphaltenes solutions were sonicated for 30 min prior to each use.

4.2.3. Interfacial tension measurement

Interfacial tension between asphaltenes in toluene solution and different aqueous solutions was measured using drop shape method with a pendent drop tensiometer (Ramé-Hart, USA). For toluene drops in 1 mM and 100 mM NaCl solutions, an interfacial tension of 35.5 ± 0.2 mN/m was measured, indicating purity of the toluene/water system. In presence of asphaltenes, the interfacial tension was measured to decrease with time, the same as previously reported results.[33] The interfacial tension was found to reach equilibrium after 30 min and the values of interfacial tension at equilibrium were taken in the theoretical analysis of the surface force results.

4.2.4 Zeta potential measurement

Zeta potentials of oil droplets in different aqueous conditions were measured using Zetasizer Nano ZSP (Malvern Instruments, UK). Oil-in-water emulsions were prepared by adding 0.5 mL asphaltenes solution into 10 mL aqueous solution. The mixture was tightly sealed using Teflon tape and sonicated for 20 min to obtain stable emulsion.

4.2.5   AFM measurement

Force measurement between two oil droplets was conducted using a MFP-3D AFM system (Asylum Research, Santa Barbara, CA) coupled with a Nikon Ti-U inverted microscope. Oil droplets were generated and immobilized on the glass substrate of an AFM fluid cell using a controlled de-wetting method as reported previously.[51] A custom-made rectangular silicon AFM cantilever (400×70×2 µm) was used to pick up an oil droplet to create an oil droplet probe. The tipless cantilever has a circular gold patch on one end, which is hydrophobized with 1-dodecanethiol for secure anchoring of the oil droplet.[42, 43] The cantilever-anchored oil droplet was then placed above another oil droplet of similar size to conduct force measurement. The two droplets were carefully aligned using the inverted microscope to ensure head-on collision. A schematic of typical experiment setup using the droplet probe AFM technique is shown in Figure 4.1.

Force measurement was conducted by driving the cantilever-anchored oil droplet towards the opposing oil drop on the substrate by lowering the cantilever for a certain distance and then lifting the cantilever up. All force measurements were done with velocity of 1 µm/s to minimize the effects of hydrodynamic force.[42, 43] For experiments in the presence of asphaltenes, force measurements were conducted 30 min after generation of oil droplet for adsorption of asphaltenes onto oil/water interface, in consistency with the interfacial tension measurement. The interaction force was measured by detecting the deflection of the cantilever, whose spring constant was calibrated using Hutter's method before loading of the oil droplet.[52] The measured force F and displacement of the cantilever ΔX were recorded by AFM software, and were used later for theoretical analysis. Force measurements at higher velocities were also conducted and the same

fitting results were obtained which demonstrates the fitted parameters reflect the true properties of the emulsion drops.
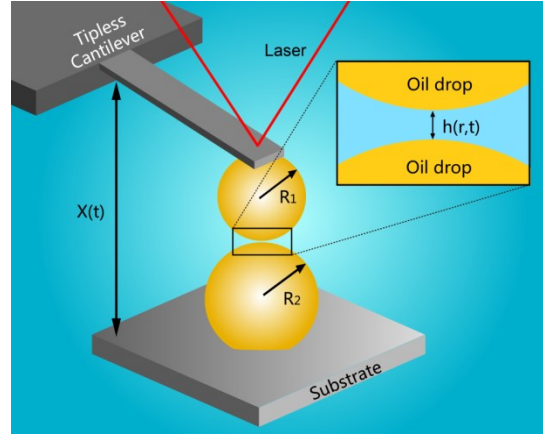
Figure 4.1. Schematic of experiment setup of measuring interaction force between two oil droplets of radii R_1 and R_2 in aqueous solutions using droplet probe AFM technique. The inset shows the schematic of the thin water film with thickness $h(r, t)$ confined between two oil droplets, where t is time and r is the radial coordinate.

4.2.6 Theoretical model

A theoretical model based on Reynolds lubrication theory and Young-Laplace equation was used for AFM results analysis.[42, 43, 46, 47] The local deformation of the interacting droplets due to the Laplace pressure inside the droplets, hydrodynamic pressure p, and disjoining pressure Π can be described by the augmented Young-Laplace equation:

$$\frac{\gamma}{2r}\frac{\partial}{\partial r}\left(r\frac{\partial h}{\partial r}\right) = \frac{2\gamma}{R_0} - p - \Pi \tag{1}$$

where γ is the interfacial tension, R_0 is the harmonic mean of the two droplet radii R_1 and R_2, p is hydrodynamic pressure and Π is disjoining pressure due to surface forces. The disjoining pressure Π generally can arise from electrostatic double layer (EDL) interaction, van der Waals (VDW) interaction, hydrophobic interaction, steric interaction and so on.[12, 14, 42, 43] The disjoining pressure due to VDW interaction is calculated as[12]

$$\Pi_{VDW}[h(r,t)] = -\frac{A_H}{6\pi h^3(r,t)} \tag{2}$$

where A_H is the Hamaker constant between two oil droplets in water. Here, in NaCl solution, the disjoining pressure due to EDL interaction is calculated using equation 3,

$$\Pi_{EDL}[h(r,t)] = 64k_B T \rho_\infty \tanh^2(\frac{e\varphi}{4k_B T}) \exp[-\kappa h(r,t)] \tag{3}$$

where κ is the inverse of the Debye length, φ is the surface potential of the oil/water interface, ρ_∞ is the number density of ions in water, and e is the fundamental charge of an electron. The κ can be calculated as

$$\kappa = (2\rho_0 e^2 / \varepsilon_0 \varepsilon k_B T)^{1/2} \tag{4}$$

where ε_0 is the vacuum permittivity and ε is the dielectric constant of the medium. The overall interaction force $F(t)$ can be calculated by integrating $p(r,t)$ and $\Pi(h(r,t))$ based on Derjaguin approximation as shown in equation 5.

$$F(t) = 2\pi \int_0^\infty [p(r,t) + \Pi(h(r,t))]r dr \tag{5}$$

The dynamic drainage of confined thin water film with thickness h between the oil droplets is described by Reynolds lubrication theory:

$$\frac{\partial h}{\partial t} = \frac{1}{12\mu r}\frac{\partial}{\partial r}\left(rh^3\frac{\partial p}{\partial r}\right) \tag{6}$$

where μ is viscosity of the aqueous solution. Immobile boundary condition at oil/water interface was assumed here, which is consistent with recent reports.[14, 42-44] More details about the theoretical model can be found in recent reports.[15, 42, 43, 48]

4.3 Results and Discussion

4.3.4 Interaction between oil droplets in 1 mM NaCl

Figure 4.2 shows the measured force curves between two toluene droplets with different concentration of asphaltenes in 1 mM NaCl. All the experiment results (blue squares) can be well fitted with the theoretical model (black lines). For interaction between pure toluene droplets, as shown in Figure 4.2A, when the cantilever-anchored droplet approached closely to the opposing drop on the substrate, a strong repulsive force was measured, which is mainly attributed to hydrodynamic interaction and EDL repulsion. When the cantilever was under retraction and the two droplets were in separation, the repulsive force gradually decreased until an attractive maximum was reached, which was also from hydrodynamic origin, so-called "hydrodynamic suction" effect.[9, 14] It should be noted that during the interaction, the two toluene droplets were stable against each other and no coalescence was observed from the force curve and optical microscope. This observation is consistent with DLVO theory and previous studies.[12, 13] According to DLVO theory, in 1 mM NaCl, the Debye length is calculated to be 9.6 nm and the repulsive EDL force between two interfaces dominates the surface interaction, inhibiting coalescence of the two oil droplets. The aforementioned theoretical model incorporating the surface forces between the oil droplets was applied to fit the measured force curves. The Hamaker constant between the two toluene drops in aqueous

solution was calculated to be 0.98×10^{-20} J on the basis of the Lifshitz Theory by taking the refractive indices and dielectric constants of toluene and water.[12] The absolute value of the surface potential of the toluene droplets in 1 mM NaCl was fitted to be -35 $\pm$ 5 mV, which is consistent with the reported values.[53, 54] In contrast to solid particles, the interfacial energetics of deformable oil droplets is governed by interfacial tension and thus the droplets can deform in response to external forces.[12, 43] Figure 4.2D shows the calculated profile of the thin water film confined between the two oil droplets at maximum force load. The flattened central part of the droplets indicates the Laplace pressure inside the droplets is balanced by EDL repulsion (where the hydrodynamic pressure is negligible due to the low approaching velocity). The central separation was calculated to be 30 nm, where the EDL disjoining pressure was about 790 Pa, equal to the Laplace pressure inside the droplets.

Table 4.1. Comparison of measured zeta potential values and theoretically fitted surface potential values of oil droplet

Asphaltenes concentration	Solution condition	Measured zeta potential (mV)	Fitted surface potential (mV)
0 mg/L	1mM NaCl pH = 5.6	-30 $\pm$ 3	-35 $\pm$ 5
10 mg/L	1mM NaCl pH = 5.6	-53 $\pm$ 2	-50 $\pm$ 5
100 mg/L	1 mM NaCl pH = 5.6	-88 $\pm$ 3	-85 $\pm$ 5
10 mg/L	1 mM NaCl pH = 3	-10 $\pm$ 3	-15 $\pm$ 5
10 mg/L	1 mM NaCl pH = 10	-62 $\pm$ 2	-60 $\pm$ 5
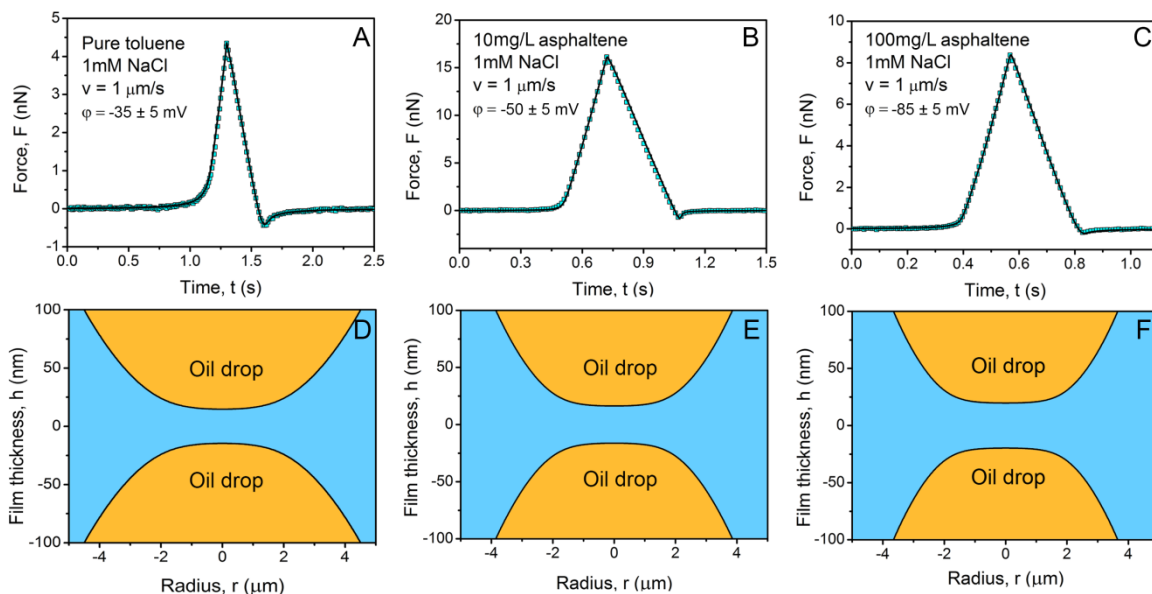
Figure 4.2. Force curves (A-C) and calculated droplet profile at maximum force load (D-F) of interaction between two toluene droplets with 0 mg/L (A and D), 10 mg/L (B and E), and 100 mg/L (C and F) asphaltenes in 1 mM NaCl solution (pH~5.6). The symbols are experiment results and the black solid lines are theoretical fitting results. The nominal velocity is 1 μm/s. The radii of the droplets are 89, 60 and 50 μm for A, B and C, respectively.

Interaction force curves between toluene droplets in the presence of 10 mg/L and 100 mg/L asphaltenes are shown in Figure 4.2B and 4.2C respectively. Similar to the results in Figure 4.2A, the oil droplets were stable against each other and did not coalesce. However, fitting the force curves with the theoretical model shows that the surface potential of the oil droplets changed from -35 ± 5 mV of pure toluene to -50 ± 5 and -85 ± 5 mV, with the addition of 10 mg/L and 100 mg/L asphaltenes, respectively. These fitted values are close to the measured zeta potentials listed in Table 4.1. The enhanced

surface potential can strengthen the EDL repulsion between the oil droplets. The calculated droplet profiles also show that the minimal separation between the oil droplets increased from 30 nm for pure toluene (Figure 4.2D) to 33 nm for 10 mg/L asphaltenes (Figure 4.2E) and 40 nm for 100 mg/L asphaltenes (Figure 4.2F), indicating stronger EDL repulsion with higher asphaltenes concentrations. The strong EDL repulsion can prevent the oil droplets from getting close and thus help stabilize the emulsions. It should be noted that interfacial asphaltenes could lead to rheological response of the oil/water interface particularly at high concentration. However, the agreement between the experiment results and theoretical model here demonstrates that the deformation of the oil/water interface is mainly governed by interfacial tension, which could be most likely due to the relatively low asphaltenes concentrations used in the experiment and low load applied. In addition, the force curves between toluene droplets with different asphaltenes concentration at different nominal velocity (5 μm/s and 10 μm/s) and force load are shown in Figure 3. The fitted results are the same as those obtained at low velocity (1 μm/s), demonstrating that the true properties of the emulsion droplets are reflected by the fitted parameters.

Asphaltenes are known to be surface active and are able to adsorb onto the oil/water interface, changing the interfacial properties. Here, the interfacial tension between 1 mM NaCl and toluene with 0 mg/L, 10 mg/L, and 100 mg/L asphaltenes was measured to be 35.5, 34.0, and 32.0 mN/m, respectively, in agreement with the reported studies that the asphaltenes can lower the interfacial tension.[21, 27, 33] It is also demonstrated here that adsorbed asphaltenes molecules at oil/water interface can enhance the surface potential of the oil droplets. The change of surface potential of oil droplets with asphaltene

97

concentration is most likely due to a change of the adsorbed amount of asphaltenes and their adsorption state at the oil/water interface, as also indicated by the change of the oil/water interfacial tension with increasing the asphaltene concentration in toluene. Figure 4.3 shows the calculated disjoining pressure profiles between two toluene droplets with addition of different concentrations of asphaltenes in 1 mM NaCl, which clearly demonstrate that the addition of asphaltenes significantly strengthens the repulsion between the oil droplets, preventing the drop coalescence and enhancing the emulsion stability.
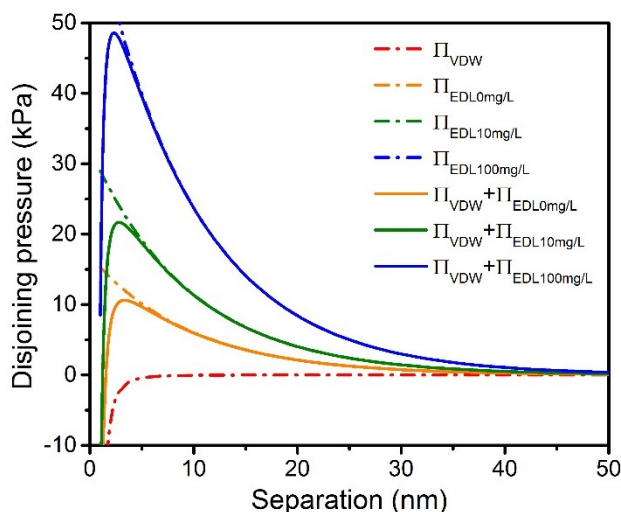
Figure 4.3. Calculated disjoining pressure profiles between two toluene droplets with 0 (orange), 10 (green) and 100 (blue) mg/L asphaltenes in 1 mM NaCl.

4.3.5 Interaction between oil droplets in 100 mM NaCl solution

Figure 4.4A shows measured force curve between two pure toluene droplets in 100 mM NaCl. Different from the force curve shown in Figure 4.2A, a sudden jump-in behavior

was observed when the measured force reached about 0.6 nN, indicating coalescence between the two toluene droplets, which was also verified by the inverted microscopy. The coalescence was induced mainly by the attractive VDW force between the two toluene droplets.[13, 14] It was found here that in the theoretical calculation the attractive VDW interaction was sufficient to induce the coalescence between the droplets and no additional hydrophobic interaction was needed for predicting droplet coalescence, which agreed with previous study on interactions between air bubbles and oil droplets.[9, 14] The mechanism for these phenomena is likely that the hydrophobic attraction between the oil droplets in an aqueous medium is relatively weak (with a decay length of ~0.3 nm) as compared to the VDW attraction.[9, 14] The calculated droplet profile just before coalescence is shown in Figure 4D. The critical separation before coalescence was calculated to be ~6 nm, where the VDW disjoining pressure was -1380 Pa (attractive). The results for two toluene drops interacting in high salt concentration (i.e. 100 mM NaCl) in Figure 4.4A and Figure 4.4D agree with the fact that addition of electrolytes generally destabilizes O/W emulsions.
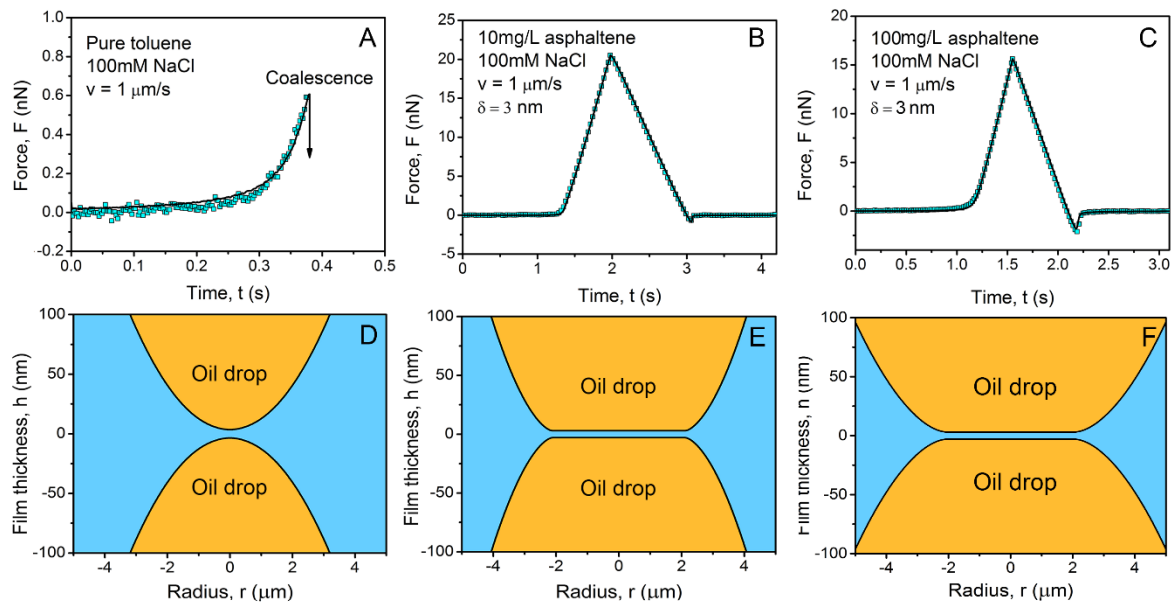
Figure 4.4. Force curves (A-C) and calculated droplet profile at maximum force load (D-F) of interactions between two toluene droplets with 0 mg/L (A and D), 10 mg/L (B and E), and 100 mg/L (C and F) asphaltenes in 100 mM NaCl solution. The symbols are experiment results and the black solid lines are theoretical fitting results. The arrow in A indicates coalescence of the oil droplets. The nominal velocity is 1 μm/s. The radii of the droplets are 52, 40 and 75 μm for A, B and C, respectively.

However, with the addition of small amount of asphaltenes in toluene, as low as 10 mg/L, coalescence between the oil droplets can be effectively inhibited, as shown in Figure 4.4B and 4.4C. Both force curves show no jump-in behavior as observed in Figure 4.4A. Since the EDL force was significantly screened in 100 mM NaCl and the VDW force between the droplets was attractive, an additional repulsive interaction must exist between the droplets to inhibit their coalescence. It has been shown in previous studies that the repulsion measured between two asphaltenes layers in organic solvents is steric-

origin and could be described by the Alexander de Gennes (AdG) model for polymer brushes.[1, 31] Although water is not a good solvent for asphaltenes and the interfacial asphaltenes in water cannot be considered as swelling polymer brushes, the interfacial asphaltene molecules or aggregates and their side chains with functional polar groups may bear some similar properties as polymer brush, resulting in steric repulsion.[31, 37] Herein, the AdG model was used to describe the repulsive interaction measured between the two toluene droplets with asphaltenes, similar to a previous study on interaction between oil droplets in presence of amphiphilic polymers:[44, 55]

$$\Pi_{steric}(h) \approx \frac{kT}{s^3}\left[\left(\frac{2L}{h}\right)^{9/4} - \left(\frac{h}{2L}\right)^{3/4}\right] \text{ for } h < 2L \tag{3}$$

where $\Pi_{steric}(h)$ is the repulsive pressure due to steric interaction, s is the mean distance between anchoring sites of the asphaltene molecules at the interface, L is the length of the brush, T is the temperature, and k is Boltzmann constant.

Here, s was taken as 3 nm based on a previous report.[1] By incorporating the AdG steric interaction into the disjoining pressure in the theoretical model, the measured force curves could be reasonably fitted, with L fitted to be 3 ± 1 nm for both cases with asphaltene concentration of 10 and 100 mg/L respectively. The fitted chain length is reasonable compared with the previously reported size of asphaltenes molecules at the oil/water interface,[27, 32] indicating the repulsion between the oil droplets could be explained by steric interaction described by the AdG model. The calculated droplet profiles at maximum force load are shown in Figure 4.4E and 4.4F, which show thin water films are sustained and confined between the two droplets, due to the steric repulsion.

It was noticed that when the two oil droplets were separated, jump-out behaviors, indicating interfacial adhesion between the droplets, were occasionally observed. These phenomena suggest that the impacts of the interfacial asphaltenes molecules are much more complex than simple steric repulsion described by the AdG model. As shown in Figure 4.4E and 4.4F, the thickness of the confined water film between two toluene droplets was calculated to be ~6 nm, which was about twice of the fitted thickness of asphaltenes. Therefore, the interfacial asphaltene molecules could make contact when the two toluene droplets were brought close under compression, and the adhesion measured could be possibly attributed to electrostatic interaction between the cationic and anionic polar groups on the asphaltenes molecules and the contact/interdigitation/interpenetration of hydrophobic moieties of the opposing asphaltenes molecules or asphaltenes aggregates at the oil/water interfaces.[22, 30, 39]

4.3.6 Effects of pH

The pH of the aqueous solution is believed to affect the adsorption of ions at the oil/water interface and the protonation of functional groups of interfacially adsorbed asphaltene molecules, varying the surface potential of the oil/water interface.[34, 53] The effects of pH on the interactions between two toluene droplets containing 10 mg/L asphaltenes in 1 mM NaCl solution are shown Figure 4.5. Due to the EDL repulsion in aqueous solution with low salt concentration, the oil droplets were stable against each other, and no coalescence was observed from both force curves and optical microscope. The fitted surface potential of the oil droplets is -15 ± 5 and -60 ± 5 mV at pH 3 and pH 10, respectively, which are also comparable to the measured zeta potential in Table 4.1.

At high pH, more of the carboxyl groups on the asphaltenes molecules become ionized, increasing the charge density and surface potential of the oil droplet. At low pH, the carboxyl groups could remain neutral or even be protonated, lowering the surface potential.
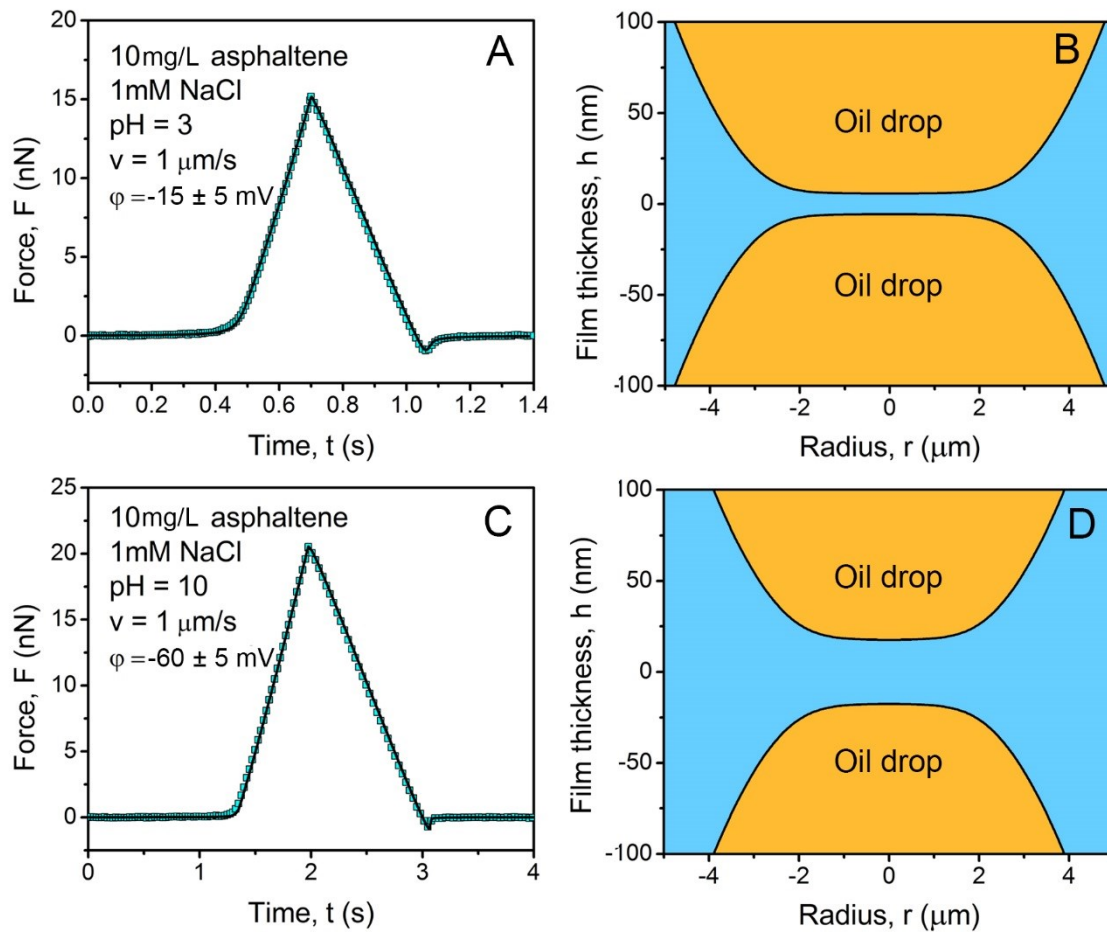
Figure 4.5. Force curves (A and C) and the calculated corresponding droplet profiles at maximum force load (B and D) of interaction between two toluene droplets with 10 mg/L asphatenes in 1mM NaCl at (A) pH = 3 and (C) pH = 10. The symbols are experiment

results and the black solid lines are theoretical fitting results. The nominal velocity is 1 μm/s. The radii of the droplets are 56 and 55 μm for A and C, respectively.

4.4.4. Effects of Ca^{2+}

Ca^{2+} ion has been reported to interact with the functional polar groups of asphaltenes molecules which can affect the properties and conformations of asphaltene molecules adsorbed at oil/water interface.[18, 23, 31] Figure 4.6A and 4.6B show the measured interaction force curves between two toluene droplets containing 100 mg/L asphaltenes in 100 mM NaCl solution, with addition of 1 mM and 10 mM CaCl$_2$, respectively. Figure 4.4 shows that the interfacial asphaltenes molecules could inhibit coalescence of the droplets in 100 mM NaCl solution due to steric repulsion. However, in Figure 4.6, coalescence was observed when the applied force load reached about 8 nN and 2.7 nN in 100 mM NaCl with the addition of 1 mM and 10 mM CaCl$_2$, respectively. The critical force loads required for coalescence in the presence of CaCl$_2$ in Figure 4.6 are much stronger than that (~0.6 nN) between two pure toluene droplets of similar size in 100 mM NaCl (Figure 4.4A), suggesting that the addition of CaCl$_2$ could lead to conformation changes and aggregation of the asphaltenes adsorbed at oil/water interface mainly due to the interaction between Ca^{2+} ions and the carboxyl groups on asphaltene molecules,[28, 30] thus alleviating the steric effects and allowing droplet coalescence. Another possible reason could be the ion bridging effects between Ca^{2+} ions and the carboxyl groups on asphaltenes. The lower critical force load required for coalescence in Figure 4.6B, as compared to that in Figure 4.6A, further demonstrates that higher concentration of Ca^{2+}

could be more effective in weakening the steric effects and therefore destabilizing the emulsion droplets.
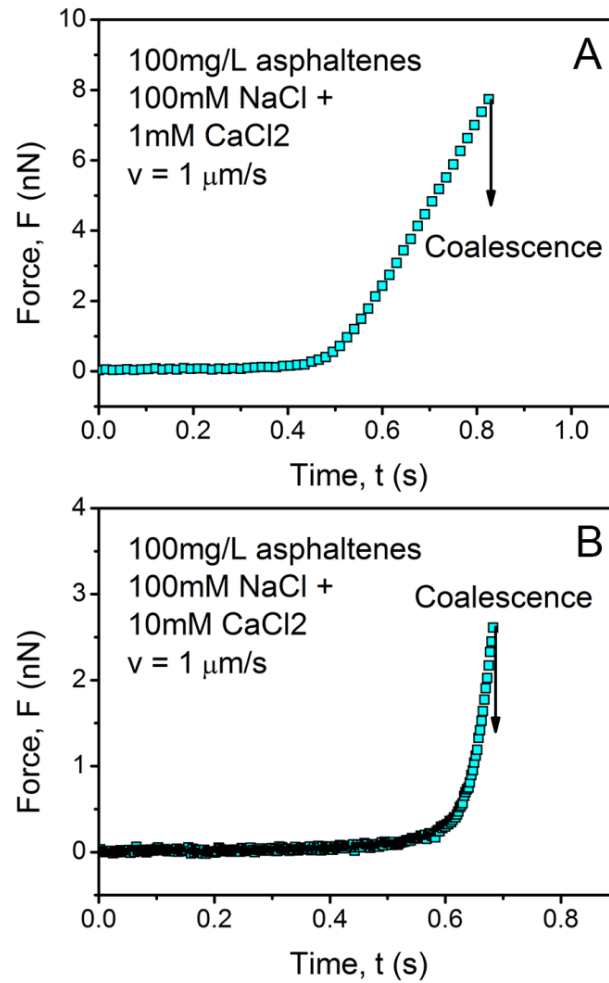
Figure 4.6. Force curves for interaction between two toluene droplets with 100 mg/L asphaltenes in 100 mM NaCl with an addition of (A) 1 mM $CaCl_2$ and (B) 10 mM $CaCl_2$. The arrows indicate coalescence between two oil droplets. The nominal velocity is 1 μm/s. The radii of the droplets are 49 μm and 54 μm for A and B, respectively.
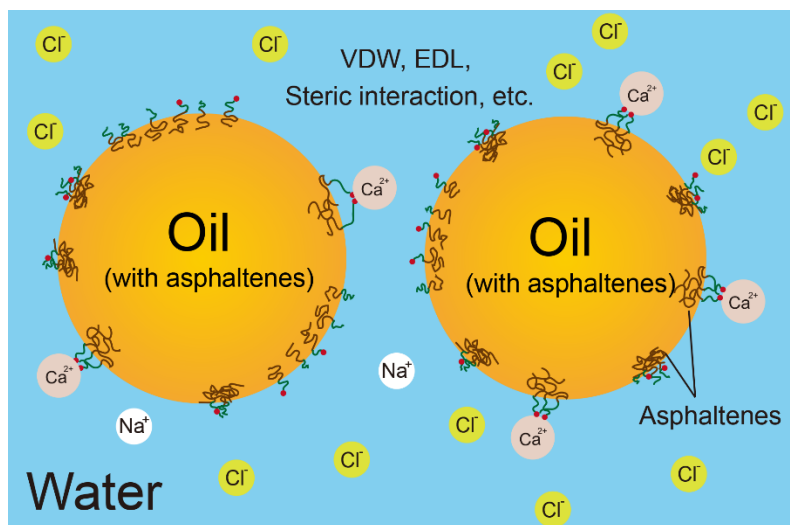
Figure 4.7. Schematic of the interactions between O/W emulsion droplets with asphaltene molecules at the oil/water interface.

4.5. Conclusion

In this study, droplet probe AFM technique was applied for the first time to directly measure the interaction forces between two model oil droplets (i.e. toluene) in water in the presence of asphaltenes, with significant implications in elucidating the stabilization mechanisms of O/W emulsions due to adsorbed asphaltenes at oil/water interface (Figure 4.7). The AFM results between the emulsion droplets were analyzed using a theoretical model based on the Reynolds lubrication theory and Young-Laplace equation by including the influence of disjoining pressure due to surface forces. The measured forces between two bare oil droplets could be well described by the classical DLVO theory; while in the presence of asphaltenes an additional steric interaction should be included in the overall disjoining pressure between the drop surfaces. The measured force results revealed that the stability of oil droplets in water is largely influenced by asphaltenes

106

concentration in oil, salt concentration, pH and presence of divalent ions in water, and a schematic of the interaction between oil drops in aqueous solution is shown in Figure 4.7. Adsorbed asphaltene molecules at oil/water interface can lead to more negative surface potential of oil droplets and also induce strong steric repulsion, inhibiting coalescence between oil droplets and stabilizing the O/W emulsion. Lower pH could lead to less negative surface potential of the oil/water interface and weaken the repulsion between the oil droplets. Addition of divalent ions (Ca^{2+}) was found to induce coalescence between the oil droplets, which could be a potential method to destabilize the O/W emulsion in presence of asphaltenes. Our results provide a useful methodology for quantifying the interaction forces and investigating the behaviors and properties of asphaltenes at the oil/water interface, and provide new insight into the stabilization mechanism of O/W emulsions due to asphaltenes in oil production and water treatment. This method can be extended to other emulsion systems in various industrial processes and help elucidate their stabilization mechanisms.

References

1.   Natarajan, A.; Xie, J.; Wang, S.; Liu, Q.; Masliyah, J.; Zeng, H.; Xu, Z., Understanding Molecular Interactions of Asphaltenes in Organic Solvents Using a Surface Force Apparatus. *J. Phys. Chem. C* **2011,** 115, (32), 16043-16051.

2.   Dai, Q.; Chung, K. H., Hot water extraction process mechanism using model oil sands. *Fuel* **1996,** 75, (2), 220-226.

3.   Kilpatrick, P. K., Water-in-crude oil emulsion stabilization: Review and unanswered questions. *Energy Fuels* **2012,** 26, (7), 4017-4026.

4.   Kovalenko, A.; Jouhannaud, J.; Polavarapu, P.; Krafft, M. P.; Waton, G.; Pourroy, G., Hollow magnetic microspheres obtained by nanoparticle adsorption on surfactant stabilized microbubbles. *Soft Matter* **2014,** 10, (28), 5147-56.

5.   Qu, Y.; Huang, R.; Qi, W.; Su, R.; He, Z., Interfacial Polymerization of Dopamine in a Pickering Emulsion: Synthesis of Cross-Linkable Colloidosomes and Enzyme Immobilization at Oil/Water Interfaces. *ACS Appl. Mater. Interfaces* **2015,** 7, (27), 14954-14964.

6.   Liang, F.; Zhang, C.; Yang, Z., Rational design and synthesis of Janus composites. *Adv. Mater.* **2014,** 26, (40), 6944-6949.

7.   Mura, S.; Nicolas, J.; Couvreur, P., Stimuli-responsive nanocarriers for drug delivery. *Nat Mater* **2013,** 12, (11), 991-1003.

8.   Schutt, E. G.; Klein, D. H.; Mattrey, R. M.; Riess, J. G., Injectable microbubbles as contrast agents for diagnostic ultrasound imaging: the key role of perfluorochemicals. *Angew Chem Int Ed Engl* **2003,** 42, (28), 3218-35.

9.   Vakarelski, I. U.; Manica, R.; Tang, X.; O'Shea, S. J.; Stevens, G. W.; Grieser, F.; Daairtine, R. R.; Chan, D. Y., Dynamic interactions between microbubbles in water. *Proc. Natl. Acad. Sci. U. S. A.* **2010,** 107, (25), 11177-11182.

10.   Clasohm, L. Y.; Vakarelski, I. U.; Daairtine, R. R.; Chan, D. Y.; Stevens, G. W.; Grieser, F., Anomalous pH dependent stability behavior of surfactant-free nonpolar oil drops in aqueous electrolyte solutions. *Langmuir* **2007,** 23, (18), 9335-9340.

11.   Manica, R.; Connor, J. N.; Carnie, S. L.; Horn, R. G.; Chan, D. Y., Dynamics of interactions involving deformable drops: Hydrodynamic dimpling under attractive and repulsive electrical double layer interactions. *Langmuir* **2007,** 23, (2), 626-637.

12.   Israelachvili, J. N., *Intermolecular and surface forces: revised third edition*. Academic press: 2011.

13.   Daairtine, R. R.; Manica, R.; Carnie, S. L.; Chan, D.; Stevens, G. W.; Grieser, F., Dynamic forces between two deformable oil droplets in water. *Science* **2006,** 313, (5784), 210-213.

14.   Tabor, R. F.; Wu, C.; Grieser, F.; Daairtine, R. R.; Chan, D. Y., Measurement of the hydrophobic force in a soft matter system. *J. Phys. Chem. Lett.* **2013,** 4, (22), 3872-3877.

15.   Tabor, R. F.; Grieser, F.; Daairtine, R. R.; Chan, D. Y., Measurement and analysis of forces in bubble and droplet systems using AFM. *J. Colloid Interface Sci.* **2012,** 371, (1), 1-14.

16.   Kralova, I.; Sjöblom, J.; Øye, G.; Simon, S.; Grimes, B. A.; Paso, K., Heavy crude oils/particle stabilized emulsions. *Adv. Colloid Interface Sci.* **2011,** 169, (2), 106-127.

17.   Czarnecki, J.; Moran, K., On the stabilization mechanism of water-in-oil emulsions in petroleum systems. *Energy Fuels* **2005,** 19, (5), 2074-2079.

18.   Liu, J.; Zhang, L.; Xu, Z.; Masliyah, J., Colloidal interactions between asphaltene surfaces in aqueous solutions. *Langmuir* **2006,** 22, (4), 1485-1492.

19.   Gafonova, O. V.; Yarranton, H. W., The stabilization of water-in-hydrocarbon emulsions by asphaltenes and resins. *J. Colloid Interface Sci.* **2001,** 241, (2), 469-478.

20.   Czarnecki, J.; Tchoukov, P.; Dabros, T., Possible role of asphaltenes in the stabilization of water-in-crude oil emulsions. *Energy Fuels* **2012,** 26, (9), 5782-5786.

21.   Yarranton, H. W.; Hussein, H.; Masliyah, J. H., Water-in-hydrocarbon emulsions stabilized by asphaltenes at low concentrations. *J. Colloid Interface Sci.* **2000,** 228, (1), 52-63.

22.   Mullins, O. C., The asphaltenes. *Annu. Rev. Anal. Chem.* **2011,** 4, 393-418.

23.   Liu, J.; Xu, Z.; Masliyah, J., Colloidal forces between bitumen surfaces in aqueous solutions measured with atomic force microscope. *Colloids Surf., A* **2005,** 260, (1), 217-228.

24.   Wu, X.; Laroche, I.; Masliyah, J.; Czarnecki, J.; Dabros, T., Applications of colloidal force measurements using a microcollider apparatus to oil sand studies. *Colloids Surf., A* **2000,** 174, (1), 133-146.

25.   Wu, X.; Czarnecki, J.; Hamza, N.; Masliyah, J., Interaction forces between bitumen droplets in water. *Langmuir* **1999,** 15, (16), 5244-5250.

26.   Ren, S.; Masliyah, J.; Xu, Z., Studying bitumen–bubble interactions using atomic force microscopy. *Colloids Surf., A* **2014,** 444, 165-172.

27.   Pauchard, V.; Rane, J. P.; Zarkar, S.; Couzis, A.; Banerjee, S., Long-Term Adsorption Kinetics of Asphaltenes at the Oil–Water Interface: A Random Sequential Adsorption Perspective. *Langmuir* **2014,** 30, (28), 8381-8390.

28.   Mullins, O. C., The Modified Yen Model†. *Energy Fuels* **2010,** 24, (4), 2179-2207.

29.   McLean, J. D.; Kilpatrick, P. K., Effects of asphaltene aggregation in model heptane–toluene mixtures on stability of water-in-oil emulsions. *J. Colloid Interface Sci.* **1997,** 196, (1), 23-34.

30.   Mullins, O. C.; Sabbah, H.; Eyssautier, J. l.; Pomerantz, A. E.; Barré, L.; Andrews, A. B.; Ruiz-Morales, Y.; Mostowfi, F.; McFarlane, R.; Goual, L., Advances in asphaltene science and the Yen–Mullins model. *Energy Fuels* **2012,** 26, (7), 3986-4003.

31.   Wang, J.; Lu, Q.; Harbottle, D.; Sjöblom, J.; Xu, Z.; Zeng, H., Molecular interactions of a polyaromatic surfactant C5Pe in aqueous solutions studied by a surface forces apparatus. *J. Phys. Chem. B* **2012,** 116, (36), 11187-11196.

32.   Rane, J. P.; Pauchard, V.; Couzis, A.; Banerjee, S., Interfacial rheology of asphaltenes at oil–water interfaces and interpretation of the equation of state. *Langmuir* **2013,** 29, (15), 4750-4759.

33.   Yarranton, H. W.; Alboudwarej, H.; Jakher, R., Investigation of asphaltene association with vapor pressure osmometry and interfacial tension measurements. *Ind. Eng. Chem. Res.* **2000,** 39, (8), 2916-2924.

34.   Das, S.; Thundat, T.; Mitra, S. K., Analytical model for zeta potential of asphaltene. *Fuel* **2013,** 108, 543-549.

35.   Sztukowski, D. M.; Jafari, M.; Alboudwarej, H.; Yarranton, H. W., Asphaltene self-association and water-in-hydrocarbon emulsions. *J. Colloid Interface Sci.* **2003,** 265, (1), 179-186.

36.   Poteau, S.; Argillier, J.-F.; Langevin, D.; Pincet, F.; Perez, E., Influence of pH on stability and dynamic properties of asphaltenes and other amphiphilic molecules at the oil-water interface. *Energy Fuels* **2005,** 19, (4), 1337-1341.

37.   Drummond, C.; Israelachvili, J., Fundamental studies of crude oil–surface water interactions and its relationship to reservoir wettability. *J. Pet. Sci. Eng.* **2004,** 45, (1), 61-81.

38. Drummond, C.; Israelachvili, J., Surface forces and wettability. *J. Pet. Sci. Eng.* **2002,** 33, (1), 123-133.

39. Natarajan, A.; Kuznicki, N.; Harbottle, D.; Masliyah, J.; Zeng, H.; Xu, Z., Understanding Mechanisms of Asphaltene Adsorption from Organic Solvent on Mica. *Langmuir* **2014,** 30, (31), 9370-9377.

40. Wang, J.; van der Tuuk Opedal, N.; Lu, Q.; Xu, Z.; Zeng, H.; Sjöblom, J., Probing Molecular Interactions of an Asphaltene Model Compound in Organic Solvents Using a Surface Forces Apparatus (SFA). *Energy Fuels* **2011,** 26, (5), 2591-2599.

41. Wang, S.; Liu, J.; Zhang, L.; Masliyah, J.; Xu, Z., Interaction forces between asphaltene surfaces in organic solvents. *Langmuir* **2009,** 26, (1), 183-190.

42. Shi, C.; Cui, X.; Xie, L.; Liu, Q.; Chan, D. Y.; Israelachvili, J. N.; Zeng, H., Measuring Forces and Spatiotemporal Evolution of Thin Water Films between an Air Bubble and Solid Surfaces of Different Hydrophobicity. *ACS Nano* **2014**.

43. Shi, C.; Chan, D. Y.; Liu, Q.; Zeng, H., Probing the Hydrophobic Interaction between Air Bubbles and Partially Hydrophobic Surfaces Using Atomic Force Microscopy. *J. Phys. Chem. C* **2014,** 118, (43), 25000-25008.

44. Manor, O.; Chau, T. T.; Stevens, G. W.; Chan, D. Y.; Grieser, F.; Daairtine, R. R., Polymeric stabilized emulsions: Steric effects and deformation in soft systems. *Langmuir* **2012,** 28, (10), 4599-4604.

45. Tabor, R. F.; Manica, R.; Chan, D. Y.; Grieser, F.; Daairtine, R. R., Repulsive van der Waals forces in soft matter: why bubbles do not stick to walls. *Phys. Rev. Lett.* **2011,** 106, (6), 064501.

46.   Vakarelski, I. U.; Li, E. Q.; Thoroddsen, S. T., Soft colloidal probes for AFM force measurements between water droplets in oil. *Colloids Surf., A* **2014,** 462, 259-263.

47.   Xie, L.; Shi, C.; Wang, J.; Huang, J.; Lu, Q.; Liu, Q.; Zeng, H., Probing the Interaction between Air Bubble and Sphalerite Mineral Surface using Atomic Force Microscope. *Langmuir* **2015**.

48.   Chan, D. Y.; Klaseboer, E.; Manica, R., Film drainage and coalescence between deformable drops and bubbles. *Soft Matter* **2011,** 7, (6), 2235-2264.

49.   Schönherr, H., Forces and Thin Water Film Drainage in Deformable Asymmetric Nanoscale Contacts. *ACS Nano* **2015,** 9, (1), 12-15.

50.   Testing, A. S. f.; Materials, ASTM D6560, Standard Test Method for Determination of Asphaltenes (Heptane Insolubles) in Crude Petroleum and Petroleum Products. In ASTM International West Conshohocken, PA: 2005.

51.   Daairtine, R. R.; Prieve, D. C.; White, L. R., Forces between a rigid probe particle and a liquid interface: III. Extraction of the planar half-space interaction energy E (D). *J. Colloid Interface Sci.* **2004,** 269, (1), 84-96.

52.   Hutter, J. L.; Bechhoefer, J., Calibration of atomic-force microscope tips. *Rev. Sci. Instrum.* **1993,** 64, (7), 1868-1873.

53.   Parra-Barraza, H.; Hernández-Montiel, D.; Lizardi, J.; Hernández, J.; Urbina, R. H.; Valdez, M. A., The zeta potential and surface properties of asphaltenes obtained with different crude oil/n-heptane proportions☆. *Fuel* **2003,** 82, (8), 869-874.

54.   Busscher, H.; Van de Belt-Gritter, B.; Van der Mei, H., Implications of microbial adhesion to hydrocarbons for evaluating cell surface hydrophobicity 1. Zeta potentials of hydrocarbon droplets. *Colloids Surf., B* **1995,** 5, (3), 111-116.

55.   De Gennes, P., Polymers at an interface; a simplified view. *Adv. Colloid Interface Sci.* **1987,** 27, (3), 189-209.

Chapter 5 Nanomechanical insights into the stabilization mechanisms of Water-in-Oil Emulsion due to Asphaltenes

5.1. Introduction

Emulsions are essential components of many industrial and biological processes,[1, 2] such as production of conventional petroleum and oil sands,[3, 4] fabrication of advanced materials with complex structures[5-7] and drug delivery in pharmaceutical and bioengineering fields.[8] Thermodynamically, liquid droplets dispersed in another immiscible fluid can readily coalesce with each other, and thereby the mixture will undergo rapid phase separation. Interface-active materials, including surfactants,[9] lipids,[10, 11] amphiphilic polymers,[12] or bi-wetting nano- and micro-particles,[13, 14] are commonly added to create an energy barrier against droplet coalescence, stabilizing the emulsions. Adsorption of these materials at the liquid interfaces can change the interfacial properties (e.g. interfacial tension and rheology) and alter the surface forces (e.g. electrical double layer force, steric repulsion) between emulsion droplets.[2, 10, 11] By controlling the physicochemical properties of the interface-active materials, the functions and behaviors of emulsion droplets can be manipulated, and emulsions with novel complex structures, such as Janus droplets and multiple emulsions,[1, 5] can be fabricated. A systematic understanding of the interaction mechanisms of emulsion droplets with adsorbed interface-active materials is of both fundamental and practical importance, which can facilitate precise manipulation of the emulsion systems.

Extremely stable water-in-oil (W/O) emulsions are commonly encountered in production of crude oil and oil sands. These emulsions are generally undesirable and required to be destabilized before sending for downstream processing, because the presence of ions (e.g. Cl⁻) solids and interfacial compounds in the emulsions can cause severe corrosion and fouling problems.[15-17] It is believed that the adsorbed natural interface-active components, *e.g.* asphaltenes, at the oil/water interface, play an important role in the stabilization of the W/O emulsions.[4, 18-20] Asphaltenes are the heaviest component in crude oil, defined as a solubility class that is soluble in aromatic solvents (e.g. toluene) but insoluble in aliphatic solvents (e.g. heptane).[21, 22] Although the exact chemical compositions still remain unclear, asphaltenes have been proposed to consist of condensed polyaromatic rings with peripheral aliphatic chains and functional polar groups, which render asphaltenes interfacially active.[21-24] Asphaltenes were reported to reversibly adsorb onto oil/water interface in the form of monomers, aggregates and clusters,[25-27] forming a protective layer around water droplet which provides robust mechanical strength to impede coalescence of the water droplets.[16, 18, 28] It has been reported that the environmental conditions (*e.g.* solvent type,[17, 29] temperature,[30, 31] presence of stabilizer[32, 33]) could significantly change interaction behaviors of W/O emulsion droplets with asphaltenes.[32] Generally, strong repulsion between water droplets corresponds to enhanced W/O emulsion stability; while interfacial adhesion can result in droplet agglomeration and flocculation.[2] However, quantitative surface force measurements between W/O emulsion droplets, in the presence of interfacially active components (e.g. asphaltenes in oil production), have not been reported.

116

The interaction mechanisms between asphaltenes or asphaltene model compounds in different organic solvents or aqueous media have been studied using many experiment tools, such as surface forces apparatus (SFA) and atomic force microscopy (AFM).[34-39] The interaction forces between asphaltene surfaces were found to be repulsive in good solvent toluene, which gradually changed to adhesion with increasing the content of a poor alkane solvent (*e.g.* heptane) in the organic medium.[35, 38, 40] These force results imply that the interaction between adsorbed asphaltenes at water/oil interfaces plays an important role in stabilizing the W/O emulsions. Nevertheless, in these previous studies, the asphaltenes were immobilized on a solid substrate, which might not show the same behaviors as at water/oil interface. Direct measurement of the interaction forces of asphaltenes at water/oil interface has never been reported, and their impact on the interaction between W/O emulsion droplets remains unclear. Recently, direct force measurements involving highly deformable air bubble or droplets have been achieved using a bubble/droplet probe AFM technique.[41-46] This technique provides a very useful tool for quantitative understanding of the interaction mechanism at deformable water/oil interfaces and its correlation to stability mechanism of different emulsion systems.[47, 48] In our previous study, the droplet probe AFM was applied to study the impacts of interfacial asphaltenes on the interaction between oil droplets in aqueous media, which could be stabilized through electrical double layer repulsion under low salinity condition with more pronounced steric repulsion effects under high salinity conditions.[49]

In this study, droplet probe AFM technique was applied for the *first* time to directly measure the interaction forces between water droplets in different oil solvents with interfacially adsorbed asphaltenes. This study has quantified the interactions between

117

W/O droplets with absorbed interfacially active asphaltenes, and provides new insights into the stabilization mechanism of the W/O emulsions. This versatile and useful methodology can be extended to many other W/O emulsion systems.

5.2. Experiment

5.2.1. Materials

The asphaltenes used in this work was extracted from crude oil sample provided by Shell based on a well-established standard procedure reported previously.[50] Asphaltenes in toluene solutions were prepared by dissolving a desired amount of extracted asphaltenes in toluene (HPLC, Fisher). The mixtures were then sonicated for 30 min to completely dissolve the asphaltenes. The prepared asphaltene solutions were tightly sealed and stored in fridge to avoid asphaltene oxidation and solvent evaporation. Prior to each force measurement experiment, the asphaltene solutions were sonicated for another 30 min. Heptol solvents, mixture of toluene and heptane, were prepared by mixing toluene and heptane (HPLC, Fisher) with certain volume ratio. Milli-Q water (Millipore deionized) with a resistance ≥18.2 MΩ·cm was used. Octadecyltrichlorosilane (OTS) was purchased from ACROS Organics and used as received.

5.2.2. AFM force measurement

An MFP-3D-Bio AFM system (Asylum Research, Santa Barbara, CA) integrated on an inverted microscope system (Nikon Ti-U) was applied to directly measure the interaction forces between two water droplets. For each measurement, water droplets were injected

into an AFM fluid cell containing asphaltenes in toluene solution using a custom-made ultra-sharp glass pipette. Because the density of water is higher than that of toluene and heptane, the water droplets will spontaneously settle down and immobilize on the glass substrate. The glass substrate of the fluid cell was strongly hydrophobized by immersing in 1 mM OTS in toluene solution for ~2 hours to gain a water contact angle of ~ 90° to facilitate easy lifting of water droplet. It was noted that the water droplets would spread on the glass substrate of low hydrophobicity, which made it difficult to pick up a water droplet to generate a water droplet probe. The water droplets were aged in asphaltene solution for a certain time, and the aging time was 5 min unless specified separately. Afterwards, the asphaltene solution was exchanged with a large amount of pure toluene to completely wash off the free asphaltenes in the solution. Then, the interactions between the water droplets were measured with asphaltenes adsorbed at water/oil interfaces. For force measurements in heptols, the toluene was then exchanged with heptol before tests.

Custom-made tipless rectangular silicon AFM cantilever (400×70×2 µm) was mildly hydrophobized by immersing in 1 mM OTS in toluene solution for ~ 30 s to gain a water contact angle of ~ 45°. Then, the mildly hydrophobized cantilever was used to pick up a water droplet to generate a water droplet probe (denoted as upper water droplet). The spring constant of the cantilever was calibrated using Hutter's thermal method before loading the water droplet.[51] The upper water droplet was then placed above another droplet of similar size on the substrate (denoted as lower water droplet) for force measurements. A schematic illustration of the force measurement setup is shown in Figure 5.1A. Figure 5.1B and Figure 5.1C show a typical optical picture of an upper or

lower water droplet. The two water droplets were then carefully aligned to maintain head-on collision for each force measurement. The upper water droplet was brought down towards the lower one till a desired maximum load force was applied or two water droplets coalesced, and then the cantilever was lifted up to separate the two droplets. For each experiment condition, interaction forces between at least 10 different pairs of water droplets were measured. To investigate the effects of contact time, two water droplets were kept in contact under the maximum load force for a certain time before they were separated. The interaction forces were determined via the Hooke's law by detecting the deflection of the cantilever as recorded in the AFM software. The driving velocity of the upper water droplet was kept at 1 μm/s to minimize the hydrodynamic effects.
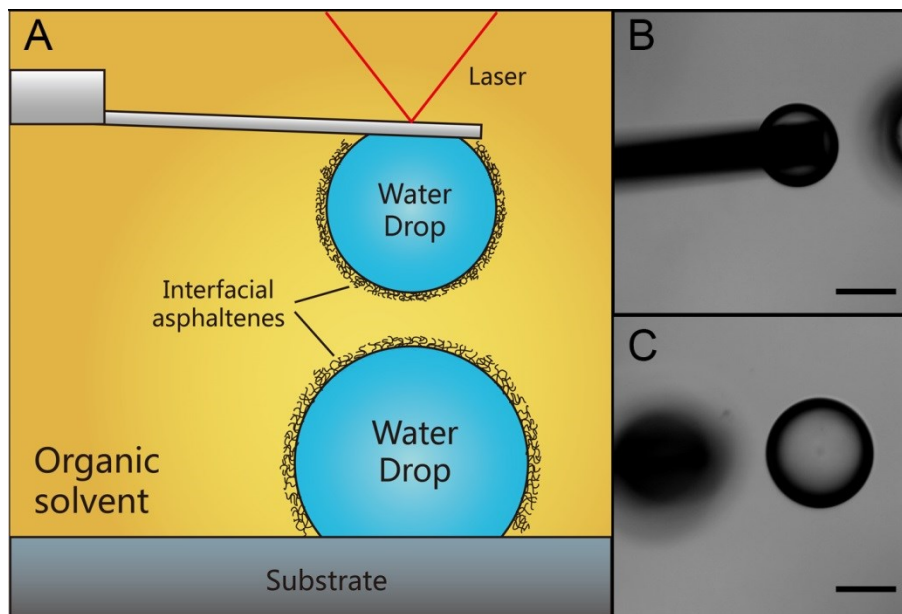
Figure 5.1. (A) Schematic of experiment setup of measuring force between two water droplets in an organic solvent using droplet probe AFM technique; optical pictures of (B)

water droplet anchored on AFM tipless cantilever and (C) water droplet immobilized on a substrate. The scale bar in (B) and (C) is 100 μm.

5.3. Results and discussion

5.3.1. Effects of asphaltenes concentration

Figures 5.2A-E show the measured force curves between two water droplets in toluene after 5 min aging in asphaltene solutions with concentration of 0, 10, 50, 100, and 500 mg/L, respectively. The symbols are the measured force data and the arrows indicate the movement of the water droplets (e.g. approaching, coalescence, or separation). Here, for each measurement, the upper water droplet was brought towards the lower droplet by lowering the cantilever until a maximum load force of ~2 nN or droplet coalescence was detected. Figure 5.2A shows the interaction force between two water droplets without interfacial asphaltenes in pure toluene. The measured forces during approach were slightly repulsive (positive values) due to the weak hydrodynamic repulsion. When the force reached about 0.16 nN, the interaction force suddenly turned attractive and "jump-in" behavior was observed, indicating coalescence between the two water droplets. From the inverted optical microscope, it could be directly observed that the upper water droplet detached from the cantilever and coalesced with the lower one, forming a single larger drop. In pure toluene, only the van der Waals attraction between the water droplets contributes to their surface forces. According to the Lifshitz theory, the Hamaker constant between water surfaces in toluene is calculated to be $9.72 \times 10^{-21} J$, which suggests that the van der Waals attraction is strongly attractive to induce droplet coalescence. The

force results (Figure 5.2A) agree with the commonly observed phenomenon that W/O emulsions without stabilizer are generally unstable and can readily undergo rapid destabilization.
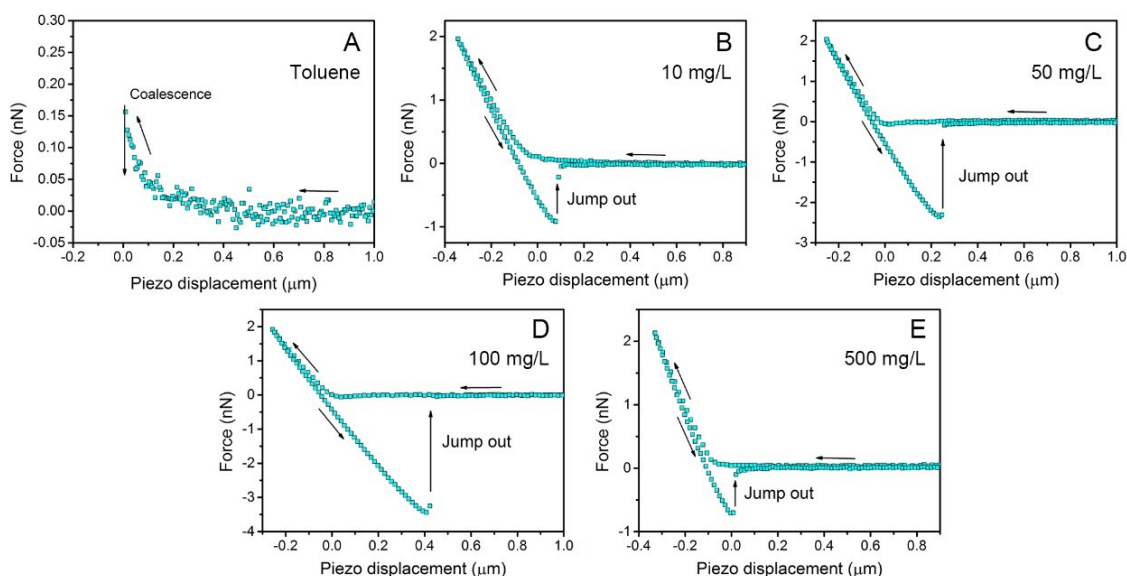
Figure 5.2. Measured force curves of interaction between water droplet in toluene after 5 min aging in asphaltenes solution with concentration of (A) 0 mg/L; (B) 10 mg/L; (C) 50 mg/L; (D) 100 mg/L; (E) 500 mg/L. The arrows show the movement of the water droplet on the cantilever.

Figures 5.2B-5.2E show the force curves between two water droplets in toluene after 5 min aging in asphaltene solutions, which exhibit distinct behaviors from that without asphaltenes (Figure 5.2A). For all the cases, the water droplets were stable against each other, and no "jump-in" or coalescence were observed under a maximum load of 2 nN, as also verified by the inverted optical microscope. Strong repulsion was measured when

two water droplets were brought closer, which was most likely attributed to the steric repulsion between swollen interfacial asphaltenes in toluene, as consistent with previously reported force measurements between solid-supported asphaltene surfaces using SFA and AFM.[35, 38] Such observed stability of water droplets due to adsorbed asphaltenes at oil/water interfaces are consistent with the long-believed fact that asphaltenes can effectively stabilize the W/O emulsions. On the other hand, it was interesting to note that all the force curves in Figures 5.2B-5.2E showed "jump-out" behaviors when the water droplets were separated, which suggested interfacial adhesion between them. The interfacial adhesion measured during separation could be mostly attributed to the interpenetration and local aggregation of the adsorbed asphaltene molecules at water/oil interfaces. It has been widely reported that asphaltenes tend to aggregate even in good solvents (e.g. toluene), through complex intermolecular interactions such as π-π stacking, acid-base interaction, and hydrogen bonding.[23, 26] As a result, when two water droplets were brought into proximity, the confined asphaltene molecules between the water/oil interfaces would contact and interpenetrate with each other, leading to interfacial adhesion between the water droplets.[18] It should be noted that in previous force measurements using AFM and SFA, pure steric repulsion was mostly detected between asphaltene surfaces in toluene, and interfacial adhesion was only detected when a poor solvent like heptane was added.[35, 38] Here, the adhesion between water droplets in toluene due to interfacial asphaltenes molecules was demonstrated and quantified for the first time, which indicates that the impact of asphaltenes on interaction of W/O emulsions would be different from that between solid-supported asphaltene layers in toluene. Such interaction difference is most likely due to the mobility difference

123

of the asphaltenes molecules absorbed at oil/water interfaces and immobilized on solid substrates as used in previous AFM and SFA force measurements. The asphaltene molecules at water/oil interface tend to have relatively higher mobility as compared to those adsorbed on a solid substrate, and could more readily change their conformation, interpenetrate and aggregate when brought into contact, thus showing adhesion during separation of the W/O emulsions.

It has been further found that the adhesion measured between two W/O emulsion droplets with interfacial asphaltenes is dependent on the maximum force load applied, asphaltene concentration of organic solvent where the W/O emulsions were aged, and the contact time. Figure 5.3A shows the measured force curves between two water droplets in toluene after 5 min aging in 100 mg/L asphaltene solutions with different applied force loads F_{max}. With increasing the F_{max} from 1 to 4 nN, higher adhesion can be measured between water droplets. Figures 3B and 3C summarize the effects of maximum force load and contact time, respectively, on the measured adhesion between water droplets. For water drops aged in solutions with relatively low asphaltene concentrations ($\leq$100 mg/L), the measured adhesion F_{ad}/R significantly increases with maximum force load (*e.g.* from 0.049 mN/m to 0.093 mN/m for the case aged in 100 mg/L asphaltenes). When higher F_{max} was applied, the contact area between the two water droplets would be enlarged and more asphaltene molecules would be able to contact, interact and aggregate across the contact interface due to their intermolecular interactions (e.g., π-π stacking, acid-base interaction, and hydrogen bonding), enhancing the interfacial adhesion. However, for the case aged in solution of high asphaltene concentration (i.e. 500 mg/L), the impact of maximum force load was evidently less significant (viz. F_{ad}/R changes only slightly from

0.010 mN/m to 0.015 mN/m with F_{max} increasing from 1 to 4 nN). Under high asphaltene concentration condition, asphaltene molecules tend to form large aggregates and a strong protective layer at oil/water interface, which lowers the mobility of interfacial apshaltene molecules and leads to steric barriers for their interpenetration, thus showing weakened load-dependent adhesion in Figure 5.3B.

Figure 3B also summarized the effects of asphaltene concentration on the normalized interfacial adhesion between water droplets. The measured adhesion force was normalized with the mean radius $R = 2R_1R_2/(R_1+R_2)$ of the two interacting water droplets of radii R_1 and R_2. The error bars represent standard deviations of measured adhesion for 10 different pairs of water droplets for each condition. For relatively low asphaltene concentration cases with maximum load force F_{max} =2 nN, the measured adhesion increased from 0.016 mN/m to 0.061 mN/m with asphaltene concentration increasing from 10 to 100 mg/L. However, for the high concentration case (500 mg/L), the normalized adhesion decreased to 0.012 mN/m, which was even weaker than that measured for the case of 10 mg/L asphaltenes. This concentration-dependent adhesion was most likely attributed to the different aggregation states of asphaltenes under different concentration conditions. As the asphaltene concentration increases, the asphaltene molecules can aggregate from monomer to nanoaggregates and then further to clusters.[23, 26, 52] When the concentration is relatively low (≤100 mg/L), the interfacial asphaltene molecules would not be strongly aggregated, with remaining capacity to interpenetrate and even aggregate with opposing asphaltene molecules during contact, leading to interfacial adhesion which could be strengthened with increasing the asphaltene concentration. For water droplets aged in high asphaltene concentration (i.e.

500 mg/L), the asphaltene molecules at oil/water interface would be mostly aggregated with each other and form a strong protective layer, with limited capacities and mobility for further aggregation or penetration with opposing asphaltenes during contact. Hence, the two interacting water droplets exhibited only weak interfacial adhesion under this condition. Figure 3C shows the results for the effects of contact time under F_{max} on adhesion. Longer contact time resulted in stronger adhesion between water droplets, during which the asphaltene molecules could have more time to adjust their configurations to interact with the opposing molecules to strengthen the adhesion.
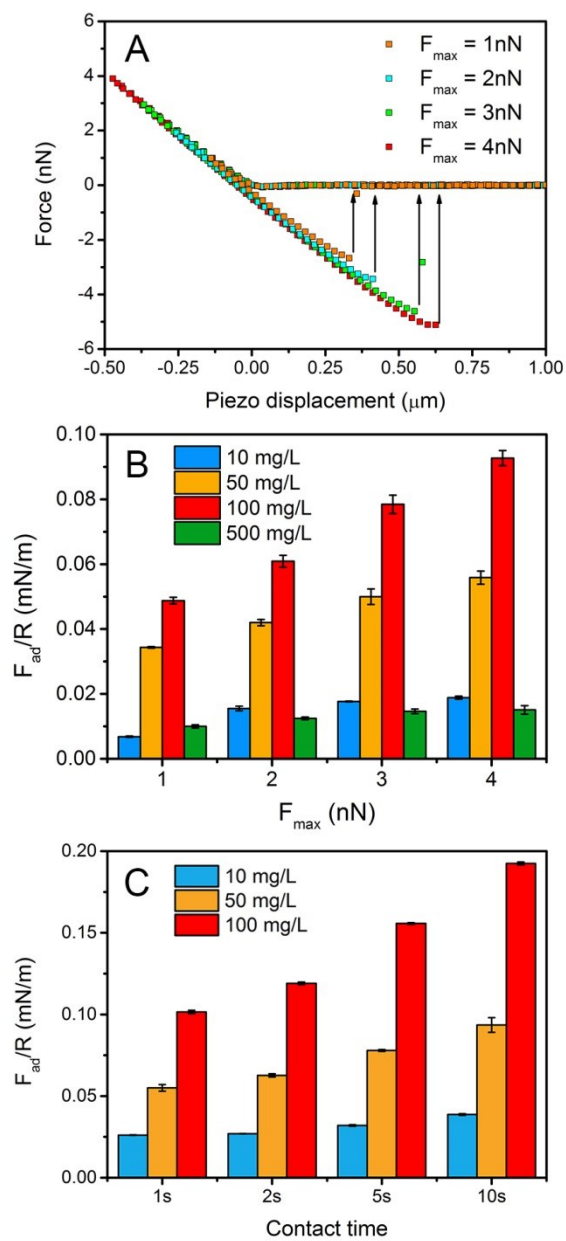
Figure 5.3. Force curves between two water droplets in toluene with (A) different force loads after 5 min aging in 100 mg/L asphaltene solution. Effects of (B) maximum force load and (C) contact time on normalized interfacial adhesion measured between water droplets in toluene after 5 min aging in asphaltene solutions of different concentrations.

5.3.2. Effects of aging time

Aging is a significant factor affecting the aggregation state of asphaltenes and the properties of water/oil interface.[15, 53] During aging process, it has been well demonstrated that the asphaltenes can undergo continuous aggregation both in bulk solution and at water/oil.[26] Interfacial rheology measurements have also demonstrated that the elastic modulus of the water/oil interface with aspahltenes gradually increases with aging time, corresponding to more rigid water/oil interface and stabilized W/O emulsions.[16] Thin liquid film drainage experiments also found that the oil film with asphaltenes confined between water/oil interfaces became thicker and more rigid with increasing aging time.[23, 53, 54] Figure 4 shows the measured force curve between two water droplets in toluene after 15 min aging in 50 mg/L asphaltene solution, and the shape of the force curve shows irregular shape and the adhesive force between water droplets during separation is drastically reduced as compared to the force curve (with 5 min aging in 50 mg/L asphaltene solution) in Figure 5.2C. From the inverted optical microscope, it could be observed that the aged water droplets were attached with lots of tiny water droplets and small particles (Figure 5.4 inset) which were likely large aggregates or clusters of asphaltenes.[54] Previous thin liquid film study showed that the diameter of asphaltene aggregates or clusters at water/oil interface could be as large as about 7.5-12 μm.[18, 54] In contrast, the interface of the water droplets aged in the same asphaltene concentration for 5 min was clean and such large aggregates were not present as shown in Figure 5.1. Therefore, when these "clean" water droplets were brought close, the two water/oil interfaces could relatively easily achieve intimate contact to facilitate the interpenetration and adhesive interaction (e.g. π-π stacking) of the opposing asphaltene molecules at the

contact interface. In contrast, when two longer aged water droplets were brought close, these small particles at water/oil interfaces could provide steric barriers against intimate contact of the two water droplets, inhibiting effective attractive interaction between the interfacial asphaltenes and thereby diminishing the interfacial adhesion. Such weakened interfacial adhesion result with longer aging time is in agreement with previously reported emulsion stability tests that emulsions with longer aging time are more stable than freshly prepared ones.[55, 56]
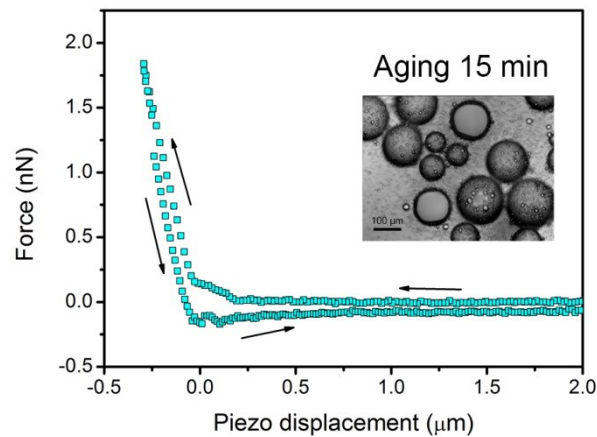
Figure 5.4. Measured force curve between two water droplets in toluene after 15 min aging in 50 mg/L asphaltenes solution. The radii of the water droplets are ~ 60 μm. The inset shows a typical picture of water droplets after 15 min aging in 50 mg/L asphaltene solution.

5.3.3. Qualitative observation on the effects of lateral shearing between water droplets

The above force results all focus on head-on collision between water droplets. In many engineering processes, dynamic flows may induce lateral shearing between W/O

emulsion droplets in collision, which may disrupt the protective coating formed by the interfacial asphaltenes, resulting in coalescence of the water droplets.[57] Figure 5 shows sequential photos of two water droplets in contact in toluene, aged for 5 min in 10 mg/L asphaltene solutions, of which the lower water droplet was laterally dragged by supporting substrate to qualitatively illustrate the effect of later shearing on the stability of W/O emulsions. First, two water droplets were brought in contact and compressed by lowering the cantilever (Figure 5.5A). No coalescence occurred, which confirmed the effective protecting effects of interfacial asphaltenes. Then the bottom substrate was moved laterally. It was observed that the lower water droplet anchored on the substrate remained adhered to the upper drop on the cantilever, attributed to the strong interfacial adhesion measured between the two droplets (Figure 5.5B). However, after several times of dragging and shearing, the protective effects of asphaltene coating was disrupted and the two water droplets suddenly coalesced into a larger one (Figure 5.5C). Detailed video of the interaction between the two water droplets under laterally shearing is given in Supporting Information. It was interesting to notice that the coalesced water droplet still partially retained the original shape of the two water droplets before coalescence, even after the coalesced droplet was lifted up away from the substrate (Figure 5.5D). This non-spherical shape of the coalesced water droplet demonstrated the rigid and more solid-like properties of protective coating formed by interfacial asphaltenes. These results qualitatively demonstrate the protective effects of interfacial asphaltenes on the water droplets and the feasibility to disrupt the protective coating by lateral shearing to destabilize the W/O emulsions, as consistent with our recent report on freely suspending W/O emulsions using an in-house-built computer-controlled 4-mill fluidic device.[58]

130
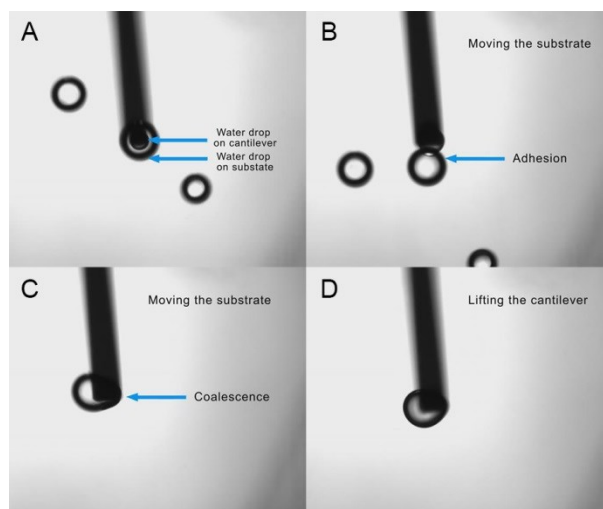
Figure 5.5. Sequential pictures for interactions between two water droplets under laterally shearing in toluene after 5 min aging in 10 mg/L asphaltenes solution: (A) two interacting water droplets in contact; (B) two water droplets adhered to each other; (C) coalescence between two water droplets due to lateral shearing; (D) the coalesced water droplet showing non-spherical shape.

5.3.4. Effects of solvent type

Solvent quality of interfacially active chemicals plays an important role in emulsion stability and emulsion interactions. As a solubility class, asphaltenes can dissolve in aromatic solvents (e.g. toluene) while precipitate in aliphatic solvents (e.g. heptane). Addition of a poor solvent heptane to toluene is expected to affect the interactions of asphaltene molecules at the water/oil interface, eventually impacting the interactions of W/O emulsion droplets.[25, 29, 32]
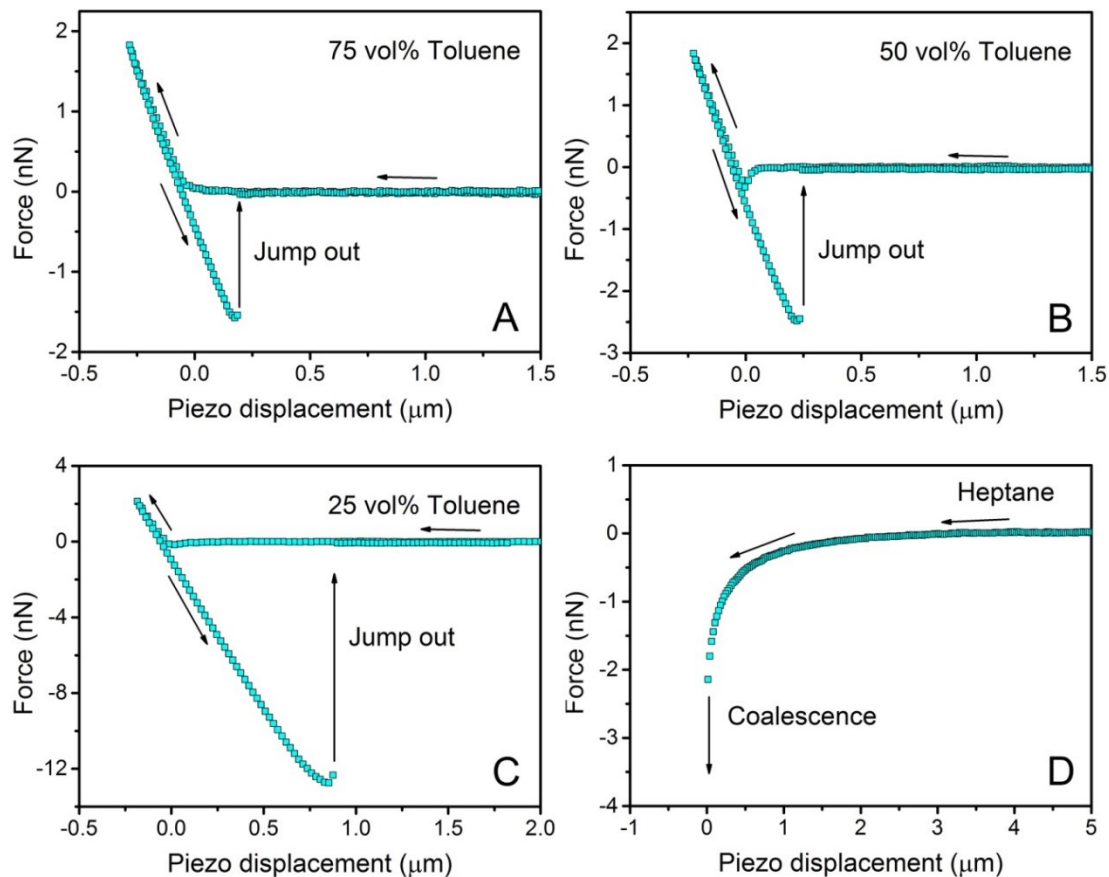
Figure 5.6. Measured force curves of interaction between two water droplets (after 5 min aging in 10 mg/L asphaltene in toluene solution) in heptol solvents with (A) 75 vol% toluene, (B) 50 vol% toluene, (C) 25 vol% toluene, and (D) in pure heptane.

Figures 5.6 and 5.7 show the measured force curves between two water droplets (after 5 min aging in asphaltene solution with concentration of 10 mg/L (Figure 5.6A-5.6D) and 50 mg/L (Figure 5.7A-5.7D)) in heptol solvents with varying volume ratio of toluene in heptol. For water droplets aged in 10 mg/L asphaltene solutions, the adhesion between the two water droplets was measured which increased significantly with increasing the heptane content in heptol (Figure 5.6A-5.6C). While in pure heptane the two water

132

droplets became unstable and readily coalesced when brought close (Figure 5.6D). Figure 5.8 shows that the normalized adhesion F_{ad}/R between water droplets increases significantly from ~0.016 mN/m in toluene to ~0.248 mN/m in heptol with 25 vol% toluene. The force curves during approach also showed distinct difference with different heptol solvents. When the toluene ratio was high (> 75 vol%), the interaction force during approach was purely repulsive, attributed to the steric repulsion by the extended chains of asphaltene molecules at water/oil interface. With increasing heptane content, attraction was measured when the water droplets were brought close, although the droplets still remained stable against coalescence. In pure heptane, however, the two water droplets readily coalesced with each other, demonstrated by the sudden "jump-in" behavior shown in Figure 5.6D. The measured strong attraction was most likely attributed to the solvophobic interaction between the asphaltene molecules in relatively poor solvent.

For the water droplets aged in 50 mg/L asphaltene solution, however, an opposite trend of interfacial adhesion with increasing heptane content was observed (Figure 5.7A-5.7D), as summarized in Figure 5.8. The measured adhesion F_{ad}/R dramatically decreased with addition of heptane, from ~0.042 mN/m in toluene to ~0.007 mN/m in heptol with 25 vol% toluene (Figure 5.8). Coalescence between water droplets was also observed in pure heptane (Figure 5.7D).
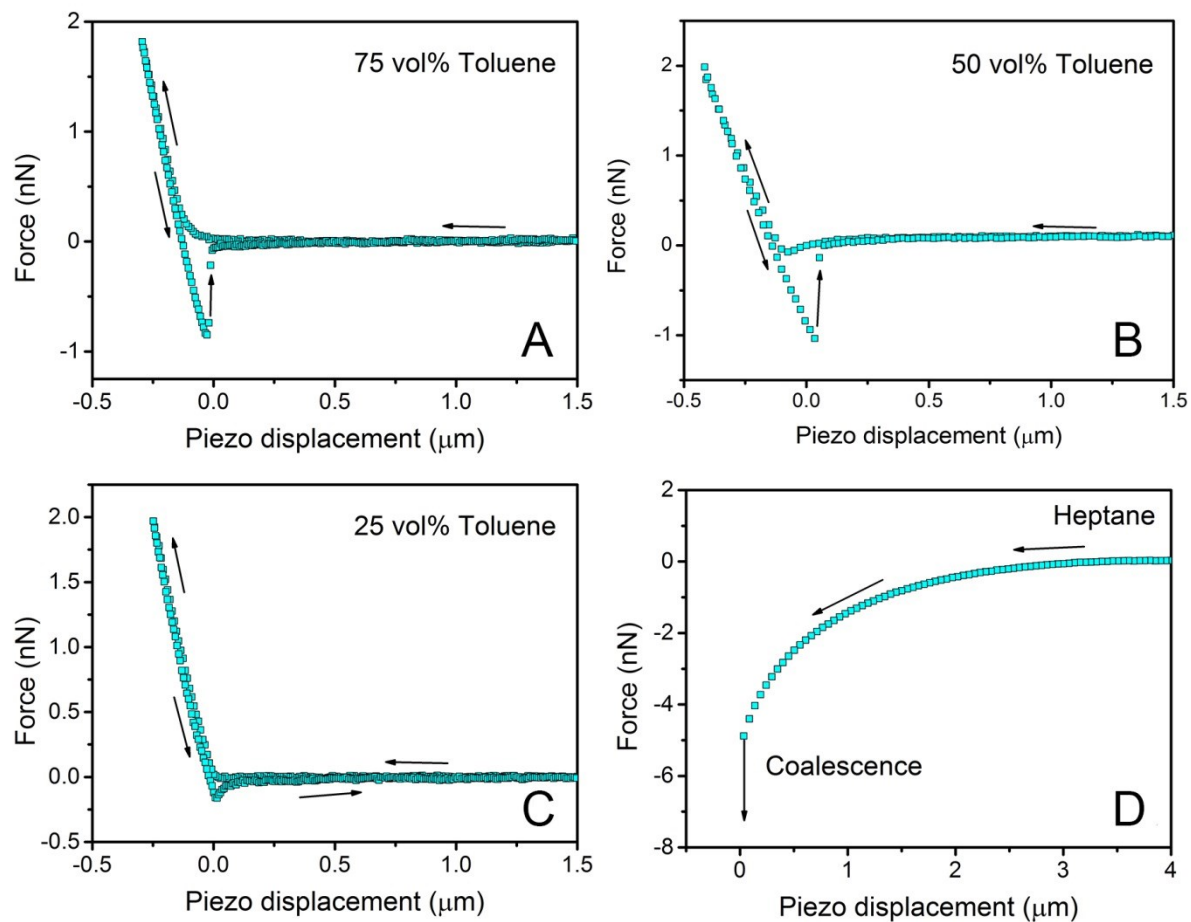
Figure 5.7. Measured force curves of interaction between water droplets (after 5 min aging in 50 mg/L asphaltene in toluene solution) in heptol solvents with (A) 75 vol% toluene, (B) 50 vol% toluene, (C) 25 vol% toluene, and (D) in pure heptane.

Since heptane is a poor solvent of asphaltenes, adding heptane is expected to strengthen the solvophobic attraction between asphaltene molecules and promote aggregation of asphaltenes at oil/water interface.[29, 32] For the two cases (10 mg/L and 50 mg/L asphaltenes) shown in Figure 5.8, the opposite trend of interfacial adhesion with increasing heptane content was mainly attributed to the difference in the amount of

asphaltenes, their aggregation states and mobility at the oil/water interfaces. As compared to the 50 mg/L asphaltenes case, the amount of absorbed asphaltenes at oil/water interface and their aggregation degree would be relatively less for the 10 mg/L case, thus the interfacial asphaltenes had relatively higher mobility for interpenetration and aggregation at the contact interface of the two droplets, contributing to the adhesion measured. For the 10 mg/L asphaltenes case, when two water droplets were brought into contact, addition of heptane enhanced the solvophobic attraction and promoted aggregation between interfacial asphaltene molecules, resulting in higher adhesion between the water droplets. In contrast, for the 50 mg/L asphaltenes case, more asphaltenes were adsorbed at the water/oil interface, and aggregation of these interfacial asphaltenes was significantly enhanced by addition of heptane. The aggregated asphaltenes could not effectively interpenetrate and further aggregate with others at the contact interface of water droplets, and thereby the adhesion decreased with increasing the heptane content in heptol.
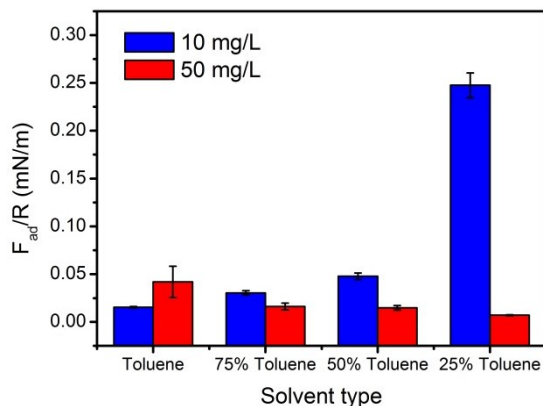
Figure 5.8. Normalized adhesion measured between water droplets in heptol after 5 min aging in 10 mg/L and 50 mg/L asphaltenes in toluene.

5.4. Conclusion

In this study, droplet probe AFM technique was applied for the *first* time to directly measure the interaction forces between W/O emulsion droplets in organic solvents with interfacially adsorbed asphaltenes. The AFM force results revealed that bare water droplets could readily coalesce in oil, while strong steric repulsion due to extended asphaltene chains at oil/water interface could effectively stabilize the droplets and inhibit coalescence. Adsorbed asphaltenes also led to interfacial adhesion between water droplets during their separation, which were mainly attributed to the interpenetration and aggregation of interfacial asphaltene molecules at the contact interface of the droplets. The adhesion strength was largely influenced by asphaltene concentration of the organic solution where the W/O emulsions were aged, aging time, maximum force load, contact time, and solvent type. For low asphaltene concentration cases, the adhesion increased with increasing asphaltenes concentration (≤ 100 mg/L), but it significantly decreased at

136

relatively high asphaltenes concentration (e.g. 500 mg/L). Addition of poor solvent (*e.g.* heptane) could enhance the interfacial adhesion at relatively low asphaltenes concentration, but could weaken the adhesion at relatively high asphaltenes concentration. Lateral shearing was shown to be able to disrupt the protective asphaltene layer and induce coalescence between water droplets. This work has precisely quantified the interactions between W/O emulsion droplets with interfacially adsorbed asphaltenes, and the results provide useful implications into the stabilization mechanisms of W/O emulsions in oil production. The findings also provide useful information regarding the interaction behaviors and properties of W/O emulsion droplets in the presence of interfacially active chemicals in general, and the methodology in this work can be readily extended to other emulsion systems.

References

(1). Zarzar, L. D.; Sresht, V.; Sletten, E. M.; Kalow, J. A.; Blankschtein, D.; Swager, T. M. Dynamically reconfigurable complex emulsions via tunable interfacial tensions. *Nature* **2015,** 518, 520-524.

(2). Israelachvili, J. N., *Intermolecular and surface forces: revised third edition*. Academic press: 2011.

(3). Tsamantakis, C.; Masliyah, J.; Yeung, A.; Gentzis, T. Investigation of the interfacial properties of water-in-diluted-bitumen emulsions using micropipette techniques. *J. Colloid Interface Sci.* **2005,** 284, 176-183.

(4). Czarnecki, J.; Tchoukov, P.; Dabros, T.; Xu, Z. Role of asphaltenes in stabilisation of water in crude oil emulsions. *Can. J. Chem. Eng.* **2013,** 91, 1365-1371.

(5). Villar, G.; Heron, A. J.; Bayley, H. Formation of droplet networks that function in aqueous environments. *Nat. Nanotechnol.* **2011,** 6, 803-808.

(6). Song, Y.; Chan, Y. K.; Ma, Q.; Liu, Z.; Shum, H. C. All-Aqueous Electrosprayed Emulsion for Templated Fabrication of Cytocompatible Microcapsules. *ACS Appl. Mater. Interfaces* **2015,** 7, 13925-13933.

(7). Helgeson, M. E.; Moran, S. E.; An, H. Z.; Doyle, P. S. Mesoporous organohydrogels from thermogelling photocrosslinkable nanoemulsions. *Nat. Mater.* **2012,** 11, 344-352.

(8). Zhang, Y.; Chan, H. F.; Leong, K. W. Advanced materials and processing for drug delivery: the past and the future. *Adv. Drug Delivery Rev.* **2013,** 65, 104-120.

(9). Zhang, L.; Mikhailovskaya, A.; Yazhgur, P.; Muller, F.; Cousin, F.; Langevin, D.; Wang, N.; Salonen, A. Precipitating Sodium Dodecyl Sulfate to Create Ultrastable and Stimulable Foams. *Angew. Chem.* **2015,** 127, 9669-9672.

(10). Yanagisawa, M.; Yoshida, T.-a.; Furuta, M.; Nakata, S.; Tokita, M. Adhesive force between paired microdroplets coated with lipid monolayers. *Soft Matter* **2013,** 9, 5891-5897.

(11). Thiam, A. R.; Bremond, N.; Bibette, J. r. m. From stability to permeability of adhesive emulsion bilayers. *Langmuir* **2012,** 28, 6291-6298.

(12). Li, Y.; Zou, J.; Das, B. P.; Tsianou, M.; Cheng, C. Well-defined amphiphilic double-brush copolymers and their performance as emulsion surfactants. *Macromolecules* **2012,** 45, 4623-4629.

(13). Binks, B. P.; Murakami, R.; Armes, S. P.; Fujii, S. Temperature‐Induced Inversion of Nanoparticle‐Stabilized Emulsions. *Angew. Chem.* **2005,** 117, 4873-4876.

(14). Binks, B. P.; Murakami, R. Phase inversion of particle-stabilized materials from foams to dry water. *Nat. Mater.* **2006,** 5, 865-869.

(15). Yang, F.; Tchoukov, P.; Dettman, H.; Teklebrhan, R. B.; Liu, L.; Dabros, T.; Czarnecki, J.; Masliyah, J.; Xu, Z. Asphaltene Subfractions Responsible for Stabilizing Water-in-Crude Oil Emulsions. Part 2: Molecular Representations and Molecular Dynamics Simulations. *Energy & Fuels* **2015,** 29, 4783-4794.

(16). Li, M.; Xu, M.; Ma, Y.; Wu, Z.; Christy, A. A. Interfacial film properties of asphaltenes and resins. *Fuel* **2002,** 81, 1847-1853.

(17). Long, Y.; Dabros, T.; Hamza, H. Stability and settling characteristics of solvent-diluted bitumen emulsions. *Fuel* **2002,** 81, 1945-1952.

(18). Tchoukov, P.; Yang, F.; Xu, Z.; Dabros, T.; Czarnecki, J.; Sjöblom, J. Role of asphaltenes in stabilizing thin liquid emulsion films. *Langmuir* **2014,** 30, 3024-3033.

(19). Yarranton, H. W.; Hussein, H.; Masliyah, J. H. Water-in-hydrocarbon emulsions stabilized by asphaltenes at low concentrations. *J. Colloid Interface Sci.* **2000,** 228, 52-63.

(20). Wu, X. Investigating the stability mechanism of water-in-diluted bitumen emulsions through isolation and characterization of the stabilizing materials at the interface. *Energy & fuels* **2003,** 17, 179-190.

(21). Schuler, B.; Meyer, G.; Pena, D.; Mullins, O. C.; Gross, L. Unraveling the molecular structures of asphaltenes by atomic force microscopy. *J. Am. Chem. Soc.* **2015,** 137, 9870-9876.

(22). Mullins, O. C. The asphaltenes. *Annu. Rev. Anal. Chem.* **2011,** 4, 393-418.

(23). Langevin, D.; Argillier, J.-F. Interfacial behavior of asphaltenes. *Adv. Colloid Interface Sci.* **2015**, 233, 83-93.

(24). Andersen, S. I.; del Rio, J. M.; Khvostitchenko, D.; Shakir, S.; Lira-Galeana, C. Interaction and solubilization of water by petroleum asphaltenes in organic solution. *Langmuir* **2001,** 17, 307-313.

(25). Mikami, Y.; Liang, Y.; Matsuoka, T.; Boek, E. S. Molecular dynamics simulations of asphaltenes at the oil–water interface: from nanoaggregation to thin-film formation. *Energy & Fuels* **2013,** 27, 1838-1845.

(26). Eyssautier, J.; Levitz, P.; Espinat, D.; Jestin, J.; Gummel, J.; Grillo, I.; Barré, L. Insight into asphaltene nanoaggregate structure inferred by small angle neutron and X-ray scattering. *J. Phys. Chem. B* **2011,** 115, 6827-6837.

(27). Alvarez, G.; Jestin, J.; Argillier, J.; Langevin, D. Small-Angle Neutron Scattering Study of Crude Oil Emulsions: Structure of the Oil− Water Interfaces†. *Langmuir* **2009,** 25, 3985-3990.

(28). Rane, J. P.; Pauchard, V.; Couzis, A.; Banerjee, S. Interfacial rheology of asphaltenes at oil–water interfaces and interpretation of the equation of state. *Langmuir* **2013,** 29, 4750-4759.

(29). McLean, J. D.; Kilpatrick, P. K. Effects of asphaltene solvency on stability of water-in-crude-oil emulsions. *J. Colloid Interface Sci.* **1997,** 189, 242-253.

(30). Hemmingsen, P. V.; Silset, A.; Hannisdal, A.; Sjöblom, J. Emulsions of heavy crude oils. I: Influence of viscosity, temperature, and dilution. *J. Dispersion Sci. Technol.* **2005,** 26, 615-627.

(31). Fortuny, M.; Oliveira, C. B.; Melo, R. L.; Nele, M.; Coutinho, R. C.; Santos, A. F. Effect of salinity, temperature, water content, and pH on the microwave demulsification of crude oil emulsions. *Energy & Fuels* **2007,** 21, 1358-1364.

(32). McLean, J. D.; Kilpatrick, P. K. Effects of asphaltene aggregation in model heptane–toluene mixtures on stability of water-in-oil emulsions. *J. Colloid Interface Sci.* **1997,** 196, 23-34.

(33). Spiecker, P. M.; Gawrys, K. L.; Trail, C. B.; Kilpatrick, P. K. Effects of petroleum resins on asphaltene aggregation and water-in-oil emulsion formation. *Colloids Surf., A* **2003,** 220, 9-27.

(34). Taylor, S. D.; Czarnecki, J.; Masliyah, J. Disjoining pressure isotherms of water-in-bitumen emulsion films. *J. Colloid Interface Sci.* **2002,** 252, 149-160.

(35). Natarajan, A.; Xie, J.; Wang, S.; Liu, Q.; Masliyah, J.; Zeng, H.; Xu, Z. Understanding molecular interactions of asphaltenes in organic solvents using a surface force apparatus. *J. Phys. Chem. C* **2011,** 115, 16043-16051.

(36). Natarajan, A.; Kuznicki, N.; Harbottle, D.; Masliyah, J.; Zeng, H.; Xu, Z. Understanding Mechanisms of Asphaltene Adsorption from Organic Solvent on Mica. *Langmuir* **2014,** 30, 9370-9377.

(37). Wang, J.; Lu, Q.; Harbottle, D.; Sjöblom, J.; Xu, Z.; Zeng, H. Molecular interactions of a polyaromatic surfactant C5Pe in aqueous solutions studied by a surface forces apparatus. *J. Phys. Chem. B* **2012,** 116, 11187-11196.

(38). Wang, S.; Liu, J.; Zhang, L.; Masliyah, J.; Xu, Z. Interaction forces between asphaltene surfaces in organic solvents. *Langmuir* **2009,** 26, 183-190.

(39). Wang, S.; Liu, J.; Zhang, L.; Xu, Z.; Masliyah, J. Colloidal interactions between asphaltene surfaces in toluene. *Energy & Fuels* **2008,** 23, 862-869.

(40). Wu, X.; van De Ven, T.; Czarnecki, J. Colloidal forces between emulsified water droplets in toluene-diluted bitumen. *Colloids Surf., A* **1999,** 149, 577-583.

(41). Shi, C.; Cui, X.; Zhang, X.; Tchoukov, P.; Liu, Q.; Encinas, N.; Paven, M.; Geyer, F.; Vollmer, D.; Xu, Z. Interaction between air bubbles and superhydrophobic surfaces in aqueous solutions. *Langmuir* **2015,** 31, 7317-7327.

(42). Xie, L.; Shi, C.; Wang, J.; Huang, J.; Lu, Q.; Liu, Q.; Zeng, H. Probing the Interaction between Air Bubble and Sphalerite Mineral Surface Using Atomic Force Microscope. *Langmuir* **2015,** 31, 2438-2446.

(43). Shi, C.; Cui, X.; Xie, L.; Liu, Q.; Chan, D. Y.; Israelachvili, J. N.; Zeng, H. Measuring forces and spatiotemporal evolution of thin water films between an air bubble and solid surfaces of different hydrophobicity. *ACS Nano* **2014,** 9, 95-104.

(44). Dagastine, R. R.; Manica, R.; Carnie, S. L.; Chan, D.; Stevens, G. W.; Grieser, F. Dynamic forces between two deformable oil droplets in water. *Science* **2006,** 313, 210-213.

(45). Cui, X.; Shi, C.; Xie, L.; Liu, J.; Zeng, H. Probing Interactions between Air Bubble and Hydrophobic Polymer Surface: Impact of Solution Salinity and Interfacial Nanobubbles. *Langmuir* **2016,** 32, 11236-11244.

(46). Shi, C.; Yan, B.; Xie, L.; Zhang, L.; Wang, J.; Takahara, A.; Zeng, H. Long-Range Hydrophilic Attraction between Water and Polyelectrolyte Surfaces in Oil. *Angew. Chem. Int. Ed.* **2016**, DOI: 10.1002/anie.201608219.

(47). Vakarelski, I. U.; Li, E. Q.; Thoroddsen, S. T. Soft colloidal probes for AFM force measurements between water droplets in oil. *Colloids Surf., A* **2014,** 462, 259-263.

(48). Lockie, H. J.; Manica, R.; Stevens, G. W.; Grieser, F.; Chan, D. Y.; Dagastine, R. R. Precision AFM measurements of dynamic interactions between deformable drops in aqueous surfactant and surfactant-free solutions. *Langmuir* **2011,** 27, 2676-2685.

(49). Shi, C.; Zhang, L.; Xie, L.; Lu, X.; Liu, Q.; Mantilla, C.; van den Berg, F. G.; Zeng, H. Interaction Mechanism of Oil-in-Water Emulsions with Asphaltenes Determined using Droplet Probe AFM. *Langmuir* **2016**, 32, 2302-2310.

(50). Testing, A. S. f.; Materials, ASTM D6560, Standard Test Method for Determination of Asphaltenes (Heptane Insolubles) in Crude Petroleum and Petroleum Products. In ASTM International West Conshohocken, PA: 2005.

(51). Hutter, J. L.; Bechhoefer, J. Calibration of atomic‐force microscope tips. *Rev. Sci. Instrum.* **1993,** 64, 1868-1873.

(52). Evdokimov, I. N.; Fesan, A. A. Multi-step formation of asphaltene colloids in dilute solutions. *Colloids Surf., A* **2016**, 492, 170-180.

(53). Tchoukov, P.; Czarnecki, J.; Dabros, T. Study of water-in-oil thin liquid films: Implications for the stability of petroleum emulsions. *Colloids Surf., A* **2010,** 372, 15-21.

(54). Yang, F.; Tchoukov, P.; Pensini, E.; Dabros, T.; Czarnecki, J.; Masliyah, J.; Xu, Z. Asphaltene subfractions responsible for stabilizing water-in-crude oil emulsions. Part 1: interfacial behaviors. *Energy & Fuels* **2014,** 28, 6897-6904.

(55). Chen, D. C.; Lai, Y. L.; Lee, S. Y.; Hung, S. L.; Chen, H. L. Osteoblastic response to collagen scaffolds varied in freezing temperature and glutaraldehyde crosslinking. *J. Biomed. Mater. Res., Part A* **2007,** 80, 399-409.

(56). Hennink, W.; Van Nostrum, C. F. Novel crosslinking methods to design hydrogels. *Adv. Drug Delivery Rev.* **2012,** 64, 223-236.

(57). Yeung, A.; Moran, K.; Masliyah, J.; Czarnecki, J. Shear-induced coalescence of emulsified oil drops. *J. Colloid Interface Sci.* **2003,** 265, 439-443.

(58). Zhang, L.; Shi, C.; Lu, Q.; Liu, Q.; Zeng, H. Probing Molecular Interactions of Asphaltenes in Heptol Using a Surface Forces Apparatus: Implications on Stability of Water-in-Oil Emulsions. *Langmuir* **2016**, 32, 4886-4895.

Chapter 6 Probing the Interaction Mechanisms between Oil Droplet and Solid Surface using Droplet Probe AFM

6.1. Introduction

Wetting phenomena of a solid surface plays critical roles in many conventional and modern technologies, such as crude oil recovery by water flooding,[1-3] hot-water-based bitumen extraction,[4-6] 3D printing,[7, 8] oil/water separation,[9, 10] surface coating and cleaning and many others.[11-13] It has been previously demonstrated that the wettability of a solid surface is largely determined by the thickness and stability of the water film confined between the surface and the oil, and a thick and stable water film corresponds to the water-wet surface while an unstable water film will lead to contact between oil and surface.[14-17] Intrinsically, the thickness and stability of the confined water film are determined by the surface force between the oil and the surface across the water film. Typically, strong long-ranged electrical double layer (EDL) repulsion can sustain a thick and stable water layer,[3, 17-19] while attractive hydrophobic and van der Waals (VDW) will lead to rupture of the water layer and attachment of oil on the solid surface.[20-22] Therefore, direct quantitative measurement of these surface forces and the interaction mechanism in oil/water/solid systems will facilitate fundamental understanding and practical prediction of the wettability of solid surfaces under complex solution conditions.

In oil industries, understanding the wettability of oil/water/solid systems and its effects on oil recovery has long been a challenging issue for engineers and researchers.[2,

[23-26] In practice, these three phases involved are usually composed of complex chemical mixtures of many components, and their physicochemical properties are influenced by a convoluted interplay among several effects (e.g. temperature, pressure, adsorption of interfacially active components).[27-29] Of all the components in crude oil, asphaltenes, practically defined as a solubility class that is soluble in aromatic solvents (e.g. toluene) but not in aliphatic solvents (e.g. heptane), is believed to be major cause of most critical issues encountered in oil production.[26, 30-33] With the combination of hydrophobic polyaromatic cores and hydrophilic functional polar groups (e.g. amino and carboxyl groups), the asphaltenes is reported to readily adsorb onto both oil/water and solid/water interfaces, which can significantly alter the properties and behaviors of the interfaces and influence the surface forces in the oil/water/solid system.[3, 34-37] Adsorption of asphaltenes on solid surface was reported to change the wettability of the surface,[24, 29, 37-40] and that on oil/water interface could change the interfacial properties such as interfacial tension, surface potential and so on.[3, 25, 31, 35, 41] On the other hand, the water chemistry (e.g. salinity, salt type and pH) is also one of the determining factors of the surface forces in the oil/water/solid system.[3, 25, 41, 42] Therefore, a quantitative understanding of the impacts of asphaltenes on the surface forces and interaction mechanisms of oil/water/solid systems under complex solution conditions is of both fundamental and practical importance, which will eventually help to predict their wetting behavior under specified conditions.

In recent years, a number of publications reported quantification of the interaction forces of asphaltenes or asphaltenes model compounds in different medium using various nanomechanical tools, including surface force apparatus (SFA), atomic force microscopy

146

(AFM), etc.[25, 43-45] Measurement between asphaltenes-coated silica and bare silica surface in aqueous solutions using AFM showed that the adsorbed asphaltenes could alter the surface potential of the silica surface, which also varied with the salinity and pH of the solution.[4, 25] SFA was also applied to quantify the interaction forces between asphaltenes and mica surface in brine solutions, which were correlated with the wettability of mica by oil and brine.[2, 23] Recently, droplet probe AFM was developed to enable direct measurement of interaction force involving deformable oil droplets and air bubbles, which was applied to study the surface interactions of various systems.[3, 20, 46-49] This technique was utilized to directly quantify the interaction force between oil/water droplets in water/oil with presence of interfacially adsorbed asphaltenes, and the measured interaction mechanism of emulsion droplet provided significant implication on elucidating the stabilization mechanism of oil/water and water/oil emulsion from nanoscopic scale.[3, 42]

In this work, droplet probe AFM technique was applied to directly quantify the interaction mechanism between oil droplet and mica surface in presence of asphaltenes. Mica was used as model clay for its molecular smoothness, and the effects of water chemistry (e.g. salinity), oil type, and surface hydrophobicity were investigated. The results provide nanomechanical insightful into the wettability of oil/water mica system with asphaltenes, and this methodology can be readily applied into many other systems to understand the intrinsic wetting mechanism from nanoscopic scale.

6.2. Experiment and Theoretical Model

6.2.1. Materials

Toluene (HPLC grade), heptane (HPLC grade), and methylene chloride (HPLC grade) were purchased from Fisher and used as received. Highest-purity sodium chloride (NaCl) and calcium chloride (CaCl$_2$) were purchased from Fisher Scientific. Brine solutions were prepared using Milli-Q water (Millipore deionized) with a resistance of $\geqslant$ 18.2 MΩ·cm.

6.2.2. Asphaltenes extraction and preparation of asphaltenes solution.

The asphaltenes samples were extracted from crude oil sample supplied by Shell using a previously reported standard ASTM IP143 procedure.[3, 50] Firstly a certain amount of crude oil was refluxed with heptane at a ratio of 1:30 (g/ml) under stirring for 1 hour. Afterwards the crude oil and heptane mixture was cooled in fridge for 2.5 hours for asphaltenes precipitation. Raw asphaltenes was collected by filtering the mixture, and was then Soxhlet-extracted with heptane for 1 h to fully remove the heptane-soluble non-asphaltenes components. After extraction with heptane, the remaining filtrate was dissolved with methylene chloride (DCM) to obtain asphaltenes in DCM solution. The solution was then concentrated and dried under ultra-pure nitrogen flow to get pure asphaltenes.

To prepare asphaltene solutions, a certain amount of asphaltenes were dissolved in toluene or 1:1 heptol (mixture of heptane and toluene with volume ratio of 1:1). The solutions were then sonicated for 30min. After preparation, the solutions were tightly sealed with Teflon tape and stored in fridge to minimize solvent evaporation and

asphaltenes oxidation. Before each experiment, the asphaltenes solutions were re-sonicated for 30 min for full dispersion of asphaltenes.

6.2.3. Interfacial tension measurement

A pendent drop tensiometer (Ramé-Hart, USA) was applied to measure the interfacial tension between asphaltenes solution and different aqueous solutions by analyzing and fitting the drop shape. The interfacial tension between a toluene drop and pure water was measured to be of 35.5 ± 0.2 mN/m, suggesting purity of the toluene/water system. For measurement of asphaltenes solutions, the interfacial tension was found to gradually decrease with time and reached equilibrium after about 30 min, which agreed with our previous reports.[3] These values at equilibrium were used for theoretical analysis of the force results measured using droplet probe AFM.

6.2.4. Preparation of hydrophilic and hydrophobic mica surfaces

Freshly cleaved mica surface was used as model hydrophilic solid surface for its molecular smoothness. To study the effects of surface hydrophobicity on the interaction between oil droplets and solid surfaces, the mica surface was also hydrophobized using octadecyltrichlorosilane (OTS, ACROS Organics) through a previously reported vapor deposition method.[20] Briefly, freshly prepared mica surfaces were exposed to OTS vapor for about 3 days to achieve a water contact angle in air of about 90°. Then the hydrophobized mica surfaces were rinsed with plenty of toluene, ethanol, and Milli-Q water prior to force measurements

6.2.5. Droplet probe AFM measurement

Figure 6.1 shows a schematic of direct measurement of the interaction between an oil droplet and a solid surface using droplet probe AFM. Experiments were done using an MFP-3D AFM system (Asylum Research, Santa Barbara, CA) mounted on a Nikon Ti-U inverted microscopy. For each experiment, a controlled de-wetting method was applied to generate and immobilize oil droplets on the glass disk of an AFM fluid cell, and mica surfaces were then placed into the fluid cell after oil droplets generation.[3, 18, 51] An oil droplet probe was created by picking up an oil droplet with a custom-made rectangular tipless AFM cantilever (400×70×2 μm) made of silicon. The oil droplet was firmly immobilized on a circular gold patch on the end of the tipless cantilever. The gold patch was hydrophobized with 1-dodecanethiol for safe anchor of the hydrophobic oil droplet. Afterwards, the oil droplet probe was moved upon a mica surface, and then force measurement was done by lowering the cantilever for a certain distance and then lifting up. The nominal velocity of the cantilever was chosen to be 1 μm/s to minimize the hydrodynamic interaction. For experiments with asphaltenes, interaction forces were measured after 30 min following oil droplet generation, which was consistent with the interfacial tension measurement. The spring constant of the force-sensing cantilever was calibrated using Hutter's method prior to loading of the oil droplet.[52] The evolution of the measured force F with time t and displacement of the cantilever ΔX were recorded by a computer for analysis using a theoretical model.
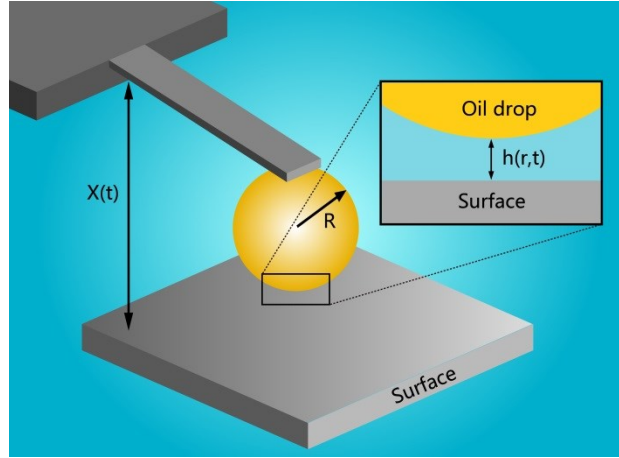
Figure 6.1. Experiment setup of measuring interaction force between an oil droplet of radii R and a solid surface in aqueous solutions using droplet probe AFM. The inset shows the thin water film with thickness $h(r, t)$ confined between the oil droplet and the solid surface.

6.2.6. Theoretical model

The force data measured using droplet probe AFM was analyzed using a theoretical model, which was based on Reynolds lubrication theory and Young-Laplace equation.[53-55] Reynolds lubrication theory describes the dynamic evolution of the thin water film with thickness h confined between the oil droplet and the solid surface:

$$\frac{\partial h}{\partial t} = \frac{1}{12\mu r}\frac{\partial}{\partial r}\left(rh^3\frac{\partial p}{\partial r}\right) \qquad (1)$$

where μ is viscosity of water and p is hydrodynamic pressure. Non-slip boundary condition at both water/oil and water/solid interfaces was applied in this study according to recent reports.

151

The augmented Young-Laplace equation describes the deformation of the oil droplet due to the balancing between the Laplace pressure, hydrodynamic pressure p, and disjoining pressure Π:

$$\frac{\gamma}{2r}\frac{\partial}{\partial r}\left(r\frac{\partial h}{\partial r}\right) = \frac{2\gamma}{R} - p - \Pi \tag{2}$$

where γ is the interfacial tension of oil/water interface, and R is the radius of the oil droplet. The disjoining pressure Π can be due to various surface interactions including electrical double layer (EDL) interaction, van der Waals (VDW) interaction, hydrophobic interaction, and so on. The disjoining pressure arising from VDW interaction can be calculated as[12]

$$\Pi_{VDW}[h(r,t)] = -\frac{A_H}{6\pi h^3} \tag{3}$$

where A_H is the Hamaker constant. And the disjoining pressure due to EDL interaction between the oil droplet and the solid surface in brine solutions is calculated as

$$\Pi_{EDL}(h) = \frac{2\varepsilon_0\varepsilon\kappa^2[(e^{+\kappa h} + e^{-\kappa h}\varphi_o\varphi_s - (\varphi_o^2 + \varphi_s^2)]}{(e^{+\kappa h} - e^{-\kappa h})^2} \tag{4}$$

$$\kappa = (2\rho_0 e^2 / \varepsilon_0\varepsilon k_B T)^{1/2} \tag{5}$$

where φ_o and φ_s are the surface potential of the oil/water interface and water/solid interface respectively, ε_0 is the vacuum permittivity, ε is the dielectric constant of the medium, e is the fundamental charge and ρ_0 is the number density of ions in water.

The interaction force $F(t)$ can be calculated by integrating both p and $\Pi(h)$) over r based on Derjaguin approximation.

$$F(t) = 2\pi\int_0^\infty [p(r,t) + \Pi(h)]rdr \tag{6}$$

6.3. Results and Discussion

6.3.1. Interaction between oil droplet and hydrophilic mica in 1 mM NaCl

Measured interaction force results between a toluene droplet and a hydrophilic mica surface in 1 mM NaCl with presence of different concentrations of asphaltenes are shown as green symbols in Figure 6.2. Positive values of measured force refer to repulsive force, and negative values indicate attraction. The arrows represent the movement of the toluene droplet during force measurement. As shown in Figure 6.2A, strong repulsion was measured when a pure toluene droplet was driven to approach a mica surface, until a maximal repulsion of ~ 40 nN was measured. Afterwards, the toluene droplet was retracted from the mica surface and the repulsive force gradually decreased until a weak attraction was measured, attributed to "hydrodynamic suction" effect. During force measurement, the toluene droplet remained stable on the cantilever and no toluene droplet attachment onto the mica surface was observed from the optical microscopy, even if higher force was applied. It has been reported that both toluene/water interface and mica surface carry negative charge in 1 mM NaCl at natural pH ~ 5.6, and the thereby the EDL interaction is repulsive and may be strong enough to sustain a water layer between the oil/water interface and mica surface. In 1 mM NaCl, the Debye length can be calculated to be 9.6 nm, and the surface potentials of toluene/water interface can be adopted from previous reports to be -35 $\pm$ 5 mV.[3] The Hamaker constant for the VDW interaction between the toluene droplet and the mica surface in water can be calculated to be $1.36 \times 10^{-20} J$ using Lifshitz theory by considering the refractive indices and dielectric constants of toluene, mica, and water.[14] The positive value suggests that the VDW

interaction is attractive. With these parameters, the aforementioned theoretical model was applied to fit the measured force results and also to fit the surface potential of mica. It can be seen that the measured force results (green symbols) can be well fitted using the theoretical model (black curve), and the surface potential of mica is fitted to be -70 ± 8 mV, which is in agreement with previously reported value.[56, 57] Figure 6.2D shows the calculated profile of the toluene droplet at maximum force load. The central region of the toluene droplet is flattened due to the balance between the Laplace pressure inside the toluene droplet and the external EDL repulsion. The thickness of the water film was calculated to be 32.9 nm, indicating that the EDL repulsion sustained a thick water layer and inhibited attachment of the toluene droplet on to the mica surface under this condition.
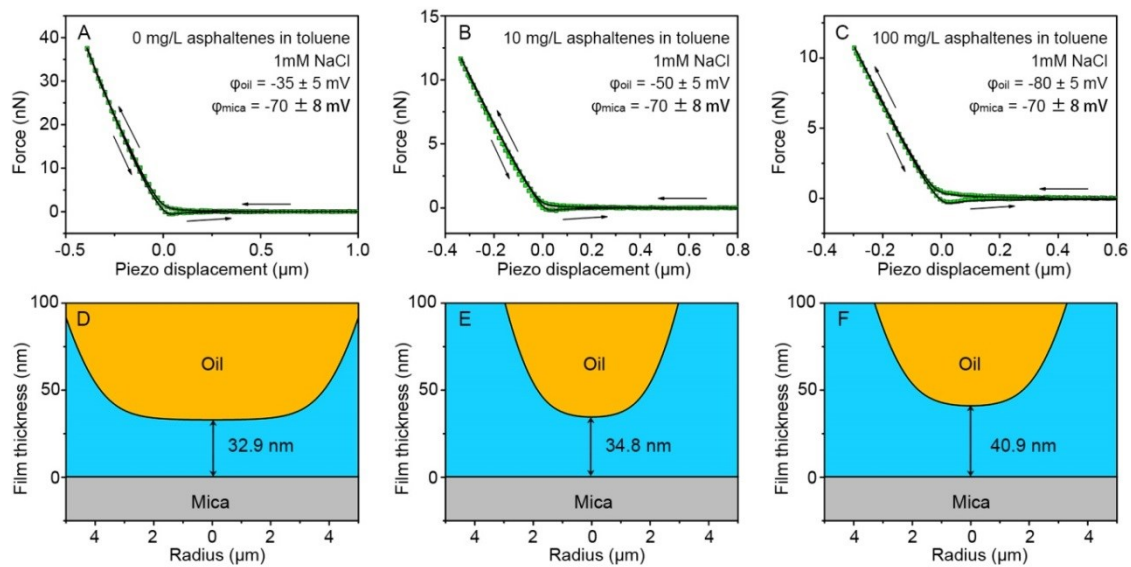
Figure 6.2. Force curves (A-C) and calculated droplet profile at maximum force load (D-F) of interaction between a toluene droplet and a hydrophilic mica surface with 0 mg/L (A and D), 10 mg/L (B and E), and 100 mg/L (C and F) asphaltenes in 1 mM NaCl

solution with natural pH of ~5.6. The green symbols represent experiment data and the black lines are fitting results calculated using theoretical model. The nominal velocity is 1 μm/s. The radii of the droplets are 60, 50 and 48 μm for A, B and C, respectively.

The measured force results with presence of 10 mg/L and 100 mgL asphaltenes in toluene are also shown as green symbols in Figure 6.2B and 6.2C. The interfacial tension between 1 mM NaCl and toluene with addition of 0, 10, and 100 m/L asphaltenes was measured to be 35.5, 34.0 and 32.0 mN/m. The theoretical model was also used to calculate the interaction force curves (black curves) using the previously fitted surface potential of mica surface and the surface potential of oil/water interface adapted from literature (-50 ± 5 and -80 ± 5 mV for 10 and 100 mg/L asphaltenes respectively).[3] The excellent agreement between the measured force data and calculated results verified validity of the fitted surface potential of mica, and suggested the interaction mechanism involved could be well explained by the theoretical model. The more negative surface potential with addition of asphaltenes was reported to be due to adsorption of asphaltenes at the toluene/water interface, which could further strengthen the EDL repulsion between the toluene droplet and the mica surface and sustain a thicker water film. The calculated profiles of toluene droplets at maximal force load clearly demonstrate that the thickness of the confined water film increased to 34.8 and 40.9 nm with addition of 10 and 100 mg/L asphaltenes respectively compared to that of the pure toluene. The calculated profile of disjoining pressure of the toluene/water/mica system is also shown in Figure 6.3. It is evident that the EDL repulsion plays the critical role in sustaining water film and

inhibiting attachment of the toluene droplet. And increasing asphaltenes concentration in oil droplet can strengthen the EDL repulsion and lead to thicker confined water film.
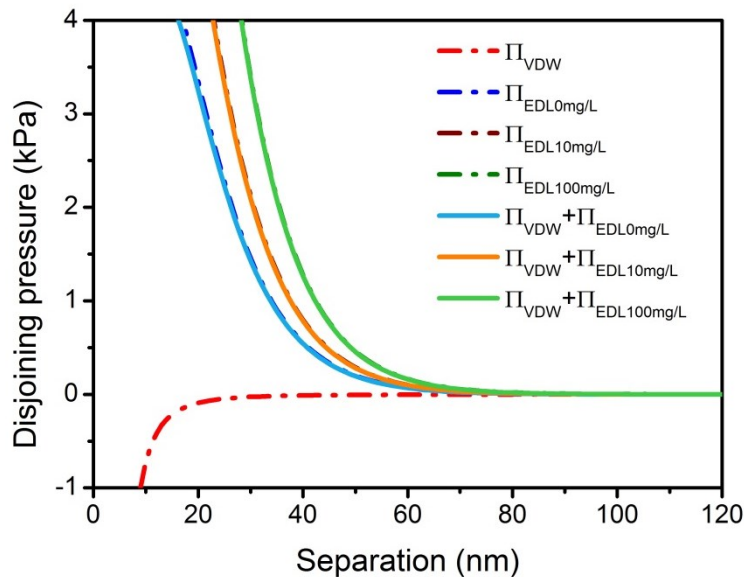
Figure 6.3. Calculated profiles of disjoining pressure between a toluene droplet with 0 (orange), 10 (green) and 100 mg/L (blue) asphaltenes and a hydrophilic mica surface in 1 mM NaCl.

The interaction forces between 1:1 heptol (*i.e.* mixture of heptane and toluene) droplet and mica surface in 1 mM NaCl with presence of 0, 10, and 100 mg/L asphaltenes were also investigated to study the solvent effects on the interaction. Addition of heptane, a poor solvent of asphaltenes, is expected to destabilize the asphaltenes in the oil phase and force more asphaltenes to migrate to the oil/water interface. The interfacial tension between water and heptol with addition of 0, 10, and 100 mg/L asphaltenes was measured to be 40.1, 39.2 and 37.0 mN/m using drop-shape tensiometer. The fitted surface

potential of mica was incorporated in the theoretical model to fit the measured force results and the surface potential of heptol/water interface. In Figure 6.4, it can be seen that all the measured force curves can be well fitted using the theoretical model. The surface potential of pure heptol droplet was fitted to be -37 ± 4 mV, which was close to that of toluene droplet. With addition of 10 and 100 mg/L asphaltenes, the surface potential became -60 ± 5 and -92 ± 7 respectively. The change of surface potential at heptol/water interface is slight larger than that at toluene/water interface, which can be attributed to more asphaltenes adsorbed at the interface due to addition to heptane. However, the change is not very significant, probably due to relatively low asphaltenes concentration.
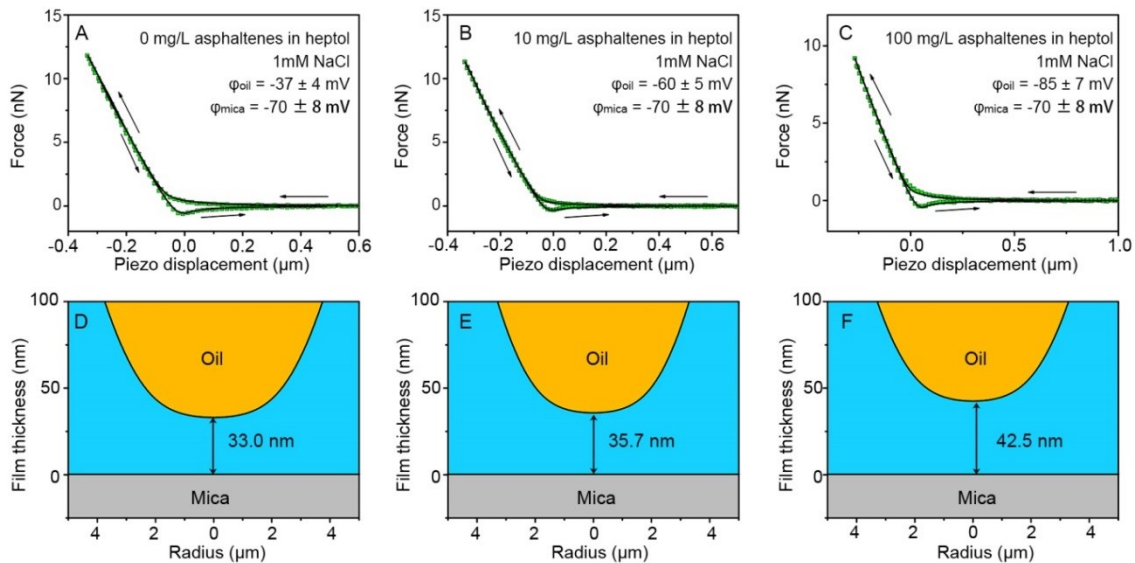
Figure 6.4. Force curves (A-C) and calculated droplet profile at maximum force load (D-F) of interactions between a heptol droplet and a hydrophilic mica surface with 0 mg/L (A and D), 10 mg/L (B and E), and 100 mg/L (C and F) asphaltenes in 1 mM NaCl

solution with natural pH of ~ 5.6. The green symbols are experiment results and the black solid lines are fitting results calculated using theoretical model. The nominal velocity is 1 μm/s. The radii of the droplets are 60, 48 and 55 μm for A, B and C, respectively.

6.3.2. Interaction between oil droplet and hydrophilic mica in 100 mM NaCl

Figure 6.5A shows measured force results between a pure toluene droplet and a hydrophilic mica surface in 100 mM NaCl. A weak jump-in behavior, i.e. a sudden decrease of the measured force, was detected when the repulsive force reached about 3 nN, which suggested attachment of the toluene droplet onto the mica surface. After jump-in, the interaction force first turned slight attractive due to the capillary bridging of the toluene droplet, and then became repulsive again as then cantilever further compressed the droplet. When the droplet was retracted, adhesion was measured before the droplet fully detached from the surface. It was noted that a small satellite droplet of toluene was always left on the mica surface after detachment. The attachment of toluene droplets can be attributed to be VDW attraction. In 100 mM NaCl, the EDL force is highly suppressed, and thereby the attractive VDW force will dominate the interaction force and induce attachment of toluene droplet on the mica surface. Theoretically calculated force curve by considering the VDW attraction was found to agree well with the measured force curve, as shown in Figure 6.5A. It should be noted that the mica surface is highly hydrated in water, and the hydrated ions have been known to cause short-ranged repulsion between mica surfaces in water.[56] In our case, it is likely that a certain amount of hydrated ions may be trapped between the toluene droplet and the mica surface even after observed

158

jump-in behavior. And the hydration repulsion can also prevent the full spreading of toluene droplet on mica surface.
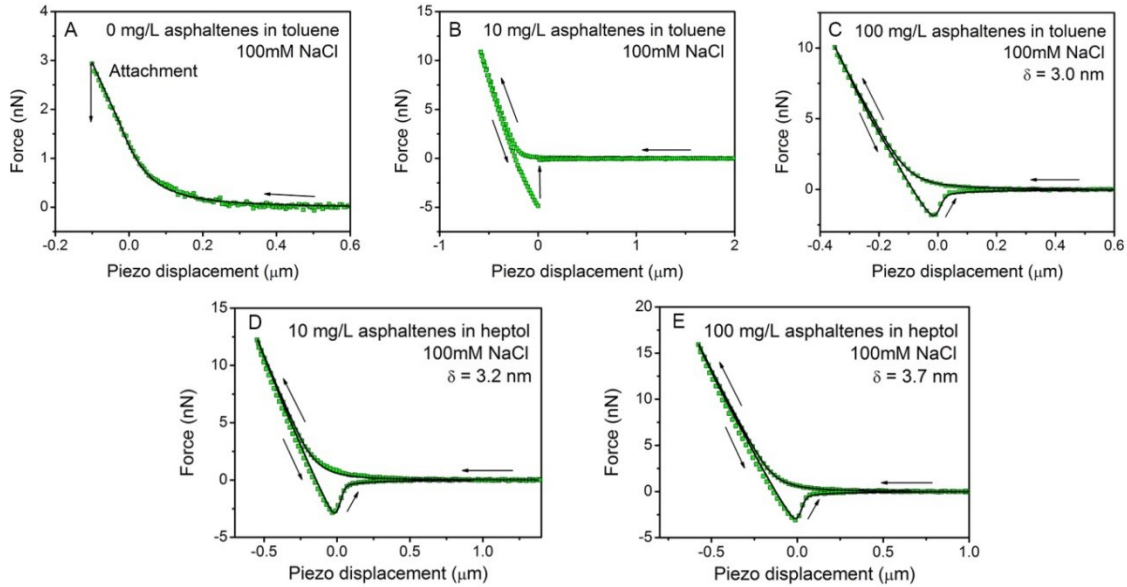
Figure 6.5. Force curves of interaction between a toluene (A~C) or a heptol (D and E) droplet and a hydrophilic mica surface with 0 mg/L (A), 10 mg/L (B and D), and 100 mg/L (C and E) asphatenes in 100 mM NaCl with natural pH ~ 5.6. The green symbols are experiment results and the black solid lines are theoretical fitting results. The nominal velocity is 1 μm/s. The radii of the droplets are 50, 45, 55, 80 and 75 μm for A ~ E, respectively.

With addition of asphaltenes, attachment of toluene droplet on mica surface was found to be largely inhibited (Figure 6.5B~6.5E). For 10 mg/L asphaltenes in toluene, no jump-in behavior was observed when the toluene droplet approached the mica surface, but a weak adhesive force of ~5 nN, indicated by the sudden jump-out behavior, was measured

when the toluene droplet was retracted from the mica surface. When more asphaltenes was added (100 mg/L), the force results became similar to those in Figure 6.4 and no adhesion was measured during retraction. The effects of solvent type were also studied. From Figure 6.5D and 6.5E, it can be seen that even addition of low concentration of asphaltenes (10 mg/L) in heptol can effectively inhibit droplet attachment with no adhesion measured. The inhibition of droplet attachment could be due to the protection from the adsorbed asphaltenes and asphaltenes aggregates at the oil/water interface. It has been reported that the interfacial asphaltenes and asphaltenes aggregates can form a protective layer at oil/water interface, resulting in steric repulsion which can inhibit coalescence between oil droplets, as well as possibly droplet attachment in our case here. When the asphaltenes concentration is low (10 mg/L here), the adsorbed amount of asphaltenes at oil/water interface was not high enough to provide complete protection, and thereby partial attachment of the oil droplet on the mica surface occurred and slight adhesion was detected. However, when the concentration is high, more asphaltenes adsorbs onto the oil/water interface and fully inhibit attachment of oil droplet. Since more asphaltenes are force to migrate to oil/water interface in heptol compared to toluene, even low concentration of asphaltenes is enough to provide complete protection against droplet attachment.

Our previous studies applied the Alexander de Gennes (AdG) model to describe the steric repulsion induced by asphaltenes, and successfully fitted the interaction force curve between two toluene droplets in water with presence of asphaltenes by incorporating the AdG model into the aforementioned theoretical model.[3, 58, 59] The steric repulsion in the AdG model can be described as

$$\Pi_{steric}(h) \approx \frac{kT}{s^3}\left[\left(\frac{2\delta}{h}\right)^{9/4} - \left(\frac{h}{2\delta}\right)^{3/4}\right] \quad \text{for } D < 2L \qquad (7)$$

where δ is the characteristic length, s is the mean distance between anchoring sites of the asphaltene, T is the temperature, and k is Boltzmann constant.

Here we use the AdG model to tentatively calculate the measured force curves in Figure 6.5E~6.5G. By using $s \sim 3$ nm and $\delta \sim 3$ nm adapted from literature,[3] the calculated force curve agreed reasonably well with the measured force curve for 100 mg/L asphaltenes in toluene, indicating the AdG model could satisfactorily describe the steric repulsion induced by asphaltenes. Slightly larger $\delta \sim 3.2$ and 3.4 nm was used for the case of 10 and 100 mg/L asphaltenes in heptol to better fit the force curves. The slight increment in δ might be due to more aggregation induced by addition of heptane. It should be noted that the adhesion measured for 10 mg/L asphaltenes in toluene indicates the effects of asphaltenes on the interaction is much more complex that merely the steric interaction described by AdG model, and more work is still needed to fully uncover the effects of interfacially adsorbed asphaltenes.

6.3.3. Interaction between oil droplet and hydrophobized mica in 100 mM NaCl

Mica surfaces hydrophobized with OTS were used as model hydrophobic surfaces to investigate the impacts of asphaltenes on the interaction between oil droplet and hydrophobic solid surfaces. The green squares in Figure 6.6A show the measured force results between a pure toluene droplet and a hydrophobized mica surface in 100 mM NaCl. A sudden and rapid jump-in behavior indicating toluene droplet attachment was detected when the force reached about 1.5 nN, which was much less than that of

161

hydrophilic mica surface shown in Figure 6.5A. After jump-in, the interaction force rapidly decreased to negative maximum without subsequent increase, and the toluene droplet spontaneously detached from the cantilever and immobilized on the surface during retraction. Both of these phenomena suggested strong adhesion of the toluene droplet on the hydrophobized mica surface. Since EDL interaction is highly suppressed in 100 mM NaCl and the VDW interaction is only weakly attractive to induce weak attachment as shown in Figure 6.5A, the rapid attachment and strong adhesion between the toluene droplet and hydrophobized mica surface are expected to be induced by the strong hydrophobic attraction here.
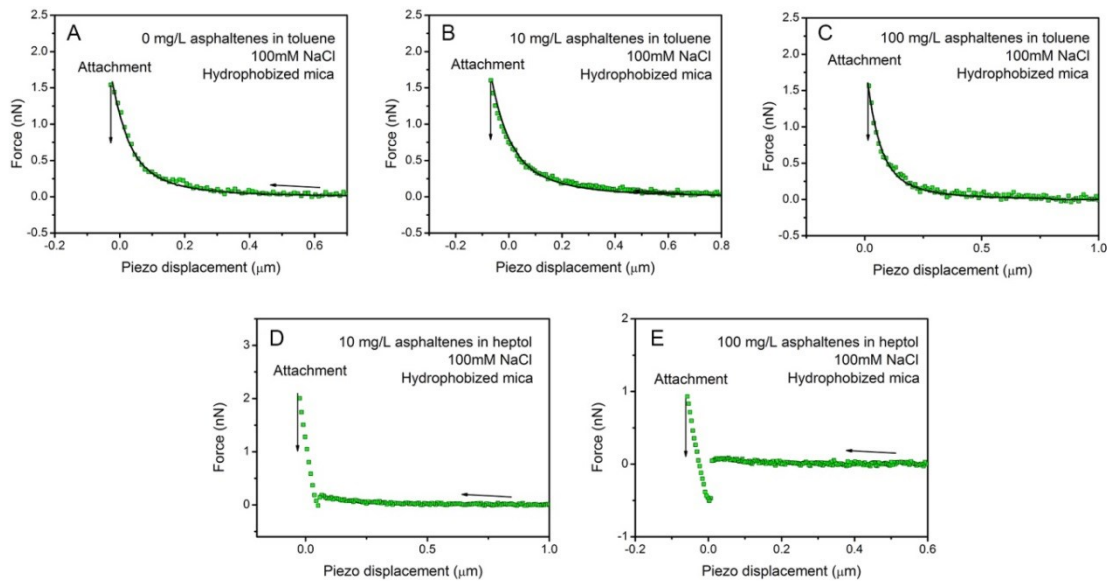
Figure 6.6. Force curves of interaction between a toluene (A~C) or a heptol (D and E) droplet and a hydrophobized mica surface with 0 mg/L (A), 10 mg/L (B and D), and 100 mg/L (C and E) asphatenes in 100 mM NaCl with natural pH ~ 5.6. The green symbols are experiment results and the black solid lines are theoretical fitting results. The nominal

velocity is 1 μm/s. The radii of the droplets are 45, 55, 45, 42 and 44 μm for A ~ E, respectively.

A previously reported exponential equation for hydrophobic interaction potential in asymmetric systems involving deformable surfaces (e.g. air bubble, liquid droplet) was incorporated within the theoretical model to calculate the interaction force between a toluene droplet and a hydrophobized mica surface, which was described as[20, 46]

$$W_{HB}(h) = -\gamma(1-\cos\theta_w)\exp(-h/D_H) \tag{8}$$

where θ_w is the static water contact angle on the surface in oil, and D_H is the characteristic decay length. And hence the disjoining pressure due to hydrophobic interaction can be calculated as

$$\Pi_{HB}(h) = -\gamma(1-\cos\theta_w)/D_H \exp(-h/D_H) \tag{9}$$

Here, the water contact angle on hydrophobized mica surface in toluene was measured to be ~120° using a goniometer and the characteristic length D_H was adapted from previous reports to be 1 nm. The calculated force curve was found to agree quite well with the measured force data, confirming the determining role of hydrophobic interaction in attachment of toluene droplet.

The impacts of asphaltenes on the interactions between oil droplets and hydrophobized mica surfaces were shown in Figure 6.6B~6.6E. With addition of 10 and 100 mg/L asphaltenes, both force curves in Figure 6.6B and 6.6C showed sudden jump-in behaviors when the force reached about 1.5 nN, similar to that in Figure 6.6A. The calculated force curves using theoretical model incorporating impacts of hydrophobic

interaction were in good agreement with measured force results. In previous sections, asphaltenes was found to lead to steric repulsion to inhibit attachment of toluene droplet onto hydrophilic mica surface in 100 mM NaCl. However, the similarity between the force curves with and without asphaltenes in toluene shown in Figure 6.6A~6.6C indicates the hydrophobic attraction dominates over the other surface forces, and induces oil droplet attachment on hydrophobized mica surfaces. Figures 6.6D and 6.6E show the interaction of heptol droplets with addition of 10 and 100 mg/L asphaltenes. It was interesting to note that weak jump-in was first detected after a slight repulsion, and a second severe jump-in were measured after a second linear increment of interaction force. This double jump-in behavior might be due to the steric hindrance of more asphaltenes and asphaltenes aggregates at the heptol/water interface. It is known that asphaltenes can form more aggregates in presence of heptane, leading to stronger steric hindrance. Therefore, when the heptol droplet approaches the surface, the hydrophobic asphaltene aggregates may first attach to the surface, corresponding to the first jump-in. The attached asphaltenes aggregates can provide some steric repulsion preventing further approach of heptol droplet, leading to the increase of interaction force after the first jump-in. Thereafter, the heptol droplet is further compressed towards the surface, and the hydrophobic attraction finally triggers full attachment of the heptol droplet on the hydrophobized mica surface.

6.4. Conclusion

In this work, the interaction mechanism between model oil droplets (i.e. toluene and heptol) and mica surfaces in presence of asphaltenes was investigated using droplet probe AFM, implicating the wetting mechanisms of oil on solid surfaces in presence of adsorbed asphaltenes at oil/water interface. A theoretical model based on the Reynolds lubrication theory and Young-Laplace equation with consideration of the influence of disjoining pressure due to surface forces was applied to analyze the measured AFM force results. The results between pure oil droplets and bare hydrophilic mica surfaces can be well described by the classical DLVO theory. Adsorption of asphaltenes at oil/water interface was found to result in more negative surface potential of oil droplet and also induce steric repulsion, both of which contributed to a stable water film between oil droplets and hydrophilic mica surfaces, inhibiting oil droplet attachment in water with both low and high salinity. Addition of heptane leads to more adsorption of asphaltenes at the interface and strengthens the EDL repulsion and steric repulsion. Attractive hydrophobic interaction between oil droplet and hydrophobized mica surface can overcome the steric hindrance due to interfacial asphaltenes, and induce strong attachment and adhesion of oil droplet. Our results provided nanomechanical insights into the impacts of asphaltenes on the interaction mechanisms between oil droplets and solid surfaces, which can further explain the wetting mechanisms of oil/water/solid systems in oil production and water treatment.

Reference

(1). Morrow, N. R. Wettability and its effect on oil recovery. *J. Pet. Technol.* **1990,** 42, 1,476-1,484.

(2). Drummond, C.; Israelachvili, J. Surface forces and wettability. *J. Pet. Sci. Eng.* **2002,** 33, 123-133.

(3). Shi, C.; Zhang, L.; Xie, L.; Lu, X.; Liu, Q.; Mantilla, C.; van den Berg, F. G.; Zeng, H. Interaction Mechanism of Oil-in-Water Emulsions with Asphaltenes Determined using Droplet Probe AFM. *Langmuir* **2016**.

(4). Liu, J.; Xu, Z.; Masliyah, J. Interaction between bitumen and fines in oil sands extraction system: Implication to bitumen recovery. *Can. J. Chem. Eng.* **2004,** 82, 655-666.

(5). Liu, J.; Xu, Z.; Masliyah, J. Studies on bitumen-silica interaction in aqueous solutions by atomic force microscopy. *Langmuir* **2003,** 19, 3911-3920.

(6). Taylor, S. D.; Czarnecki, J.; Masliyah, J. Disjoining pressure isotherms of water-in-bitumen emulsion films. *J. Colloid Interface Sci.* **2002,** 252, 149-160.

(7). Doudrick, K.; Liu, S.; Mutunga, E. M.; Klein, K. L.; Damle, V.; Varanasi, K. K.; Rykaczewski, K. Different shades of oxide: From nanoscale wetting mechanisms to contact printing of gallium-based liquid metals. *Langmuir* **2014,** 30, 6867-6877.

(8). Ladd, C.; So, J. H.; Muth, J.; Dickey, M. D. 3D printing of free standing liquid metal microstructures. *Adv. Mater.* **2013,** 25, 5081-5085.

(9). Feng, L.; Zhang, Z.; Mai, Z.; Ma, Y.; Liu, B.; Jiang, L.; Zhu, D. A super-hydrophobic and super-oleophilic coating mesh film for the separation of oil and water. *Angew. Chem. Int. Ed.* **2004,** 43, 2012-2014.

(10). Zhang, W.; Shi, Z.; Zhang, F.; Liu, X.; Jin, J.; Jiang, L. Superhydrophobic and superoleophilic PVDF membranes for effective separation of water-in-oil emulsions with high flux. *Adv. Mater.* **2013,** 25, 2071-2076.

(11). He, K.; Duan, H.; Chen, G. Y.; Liu, X.; Yang, W.; Wang, D. Cleaning of Oil Fouling with Water Enabled by Zwitterionic Polyelectrolyte Coatings: Overcoming the Imperative Challenge of Oil–Water Separation Membranes. *ACS Nano* **2015,** 9, 9188-9198.

(12). Li, J.; Wu, R.; Jing, Z.; Yan, L.; Zha, F.; Lei, Z. One-step spray-coating process for the fabrication of colorful superhydrophobic coatings with excellent corrosion resistance. *Langmuir* **2015,** 31, 10702-10707.

(13). Xie, L.; Wang, J.; Shi, C.; Huang, J.; Zhang, H.; Liu, Q.; Liu, Q.; Zeng, H. Probing Surface Interactions of Electrochemically Active Galena Mineral Surface Using Atomic Force Microscope. *J. Phys. Chem. C* **2016**.

(14). Israelachvili, J. N., *Intermolecular and surface forces: revised third edition*. Academic press: 2011.

(15). Boinovich, L.; Emelyanenko, A. Wetting and surface forces. *Adv. Colloid Interface Sci.* **2011,** 165, 60-69.

(16). Ralston, J.; Dukhin, S.; Mishchuk, N. Wetting film stability and flotation kinetics. *Adv. Colloid Interface Sci.* **2002,** 95, 145-236.

(17). Manica, R.; Connor, J. N.; Clasohm, L. Y.; Carnie, S. L.; Horn, R. G.; Chan, D. Y. Transient responses of a wetting film to mechanical and electrical perturbations. *Langmuir* **2008,** 24, 1381-1390.

(18). Lockie, H. J.; Manica, R.; Stevens, G. W.; Grieser, F.; Chan, D. Y.; Daairtine, R. R. Precision AFM measurements of dynamic interactions between deformable drops in aqueous surfactant and surfactant-free solutions. *Langmuir* **2011,** 27, 2676-2685.

(19). Manor, O.; Vakarelski, I. U.; Tang, X.; O'Shea, S. J.; Stevens, G. W.; Grieser, F.; Daairtine, R. R.; Chan, D. Y. Hydrodynamic boundary conditions and dynamic forces between bubbles and surfaces. *Phys. Rev. Lett.* **2008,** 101, 024501.

(20). Shi, C.; Chan, D. Y.; Liu, Q.; Zeng, H. Probing the hydrophobic interaction between air bubbles and partially hydrophobic surfaces using atomic force microscopy. *J. Phys. Chem. C* **2014,** 118, 25000-25008.

(21). Zeng, H.; Shi, C.; Huang, J.; Li, L.; Liu, G.; Zhong, H. Recent experimental advances on hydrophobic interactions at solid/water and fluid/water interfaces. *Biointerphases* **2016,** 11, 018903.

(22). Hsu, P. Y.; Dhinojwala, A. Contact of oil with solid surfaces in aqueous media probed using sum frequency generation spectroscopy. *Langmuir* **2012,** 28, 2567-2573.

(23). Drummond, C.; Israelachvili, J. Fundamental studies of crude oil–surface water interactions and its relationship to reservoir wettability. *J. Pet. Sci. Eng.* **2004,** 45, 61-81.

(24). Natarajan, A.; Kuznicki, N.; Harbottle, D.; Masliyah, J.; Zeng, H.; Xu, Z. Understanding mechanisms of asphaltene adsorption from organic solvent on mica. *Langmuir* **2014,** 30, 9370-9377.

(25). Liu, J.; Zhang, L.; Xu, Z.; Masliyah, J. Colloidal interactions between asphaltene surfaces in aqueous solutions. *Langmuir* **2006,** 22, 1485-1492.

(26). Zhang, L.; Shi, C.; Lu, Q.; Liu, Q.; Zeng, H. Probing Molecular Interactions of Asphaltenes in Heptol Using a Surface Forces Apparatus: Implications on Stability of Water-in-Oil Emulsions. *Langmuir* **2016**.

(27). Tang, G.; Morrow, N. R. Salinity, temperature, oil composition, and oil recovery by waterflooding. *SPE Reservoir Eng.* **1997,** 12, 269-276.

(28). Buckley, J.; Liu, Y.; Monsterleet, S. Mechanisms of wetting alteration by crude oils. *SPE J.* **1998,** 3, 54-61.

(29). Taqvi, S. T.; Almansoori, A.; Bassioni, G. Understanding the Role of Asphaltene in Wettability Alteration Using ζ Potential Measurements. *Energy & Fuels* **2016,** 30, 1927-1932.

(30). Mullins, O. C. The asphaltenes. *Annu. Rev. Anal. Chem.* **2011,** 4, 393-418.

(31). Czarnecki, J.; Tchoukov, P.; Dabros, T.; Xu, Z. Role of asphaltenes in stabilisation of water in crude oil emulsions. *Can. J. Chem. Eng.* **2013,** 91, 1365-1371.

(32). Sabbah, H.; Morrow, A. L.; Pomerantz, A. E.; Zare, R. N. Evidence for island structures as the dominant architecture of asphaltenes. *Energy & Fuels* **2011,** 25, 1597-1604.

(33). Schuler, B.; Meyer, G.; Peña, D.; Mullins, O. C.; Gross, L. Unraveling the molecular structures of asphaltenes by atomic force microscopy. *J. Am. Chem. Soc.* **2015,** 137, 9870-9876.

(34). Rane, J. P.; Pauchard, V.; Couzis, A.; Banerjee, S. Interfacial rheology of asphaltenes at oil–water interfaces and interpretation of the equation of state. *Langmuir* **2013,** 29, 4750-4759.

(35). Langevin, D.; Argillier, J.-F. Interfacial behavior of asphaltenes. *Adv. Colloid Interface Sci.* **2015**.

(36). Harbottle, D.; Chen, Q.; Moorthy, K.; Wang, L.; Xu, S.; Liu, Q.; Sjoblom, J.; Xu, Z. Problematic stabilizing films in petroleum emulsions: Shear rheological response of viscoelastic asphaltene films and the effect on drop coalescence. *Langmuir* **2014,** 30, 6730-6738.

(37). Adams, J. J. Asphaltene adsorption, a literature review. *Energy & Fuels* **2014,** 28, 2831-2856.

(38). Li, M.; Xu, M.; Ma, Y.; Wu, Z.; Christy, A. A. Interfacial film properties of asphaltenes and resins. *Fuel* **2002,** 81, 1847-1853.

(39). Turgman-Cohen, S.; Smith, M. B.; Fischer, D. A.; Kilpatrick, P. K.; Genzer, J. Asphaltene adsorption onto self-assembled monolayers of mixed aromatic and aliphatic trichlorosilanes. *Langmuir* **2009,** 25, 6260-6269.

(40). Turgman-Cohen, S.; Fischer, D. A.; Kilpatrick, P. K.; Genzer, J. Asphaltene adsorption onto self-assembled monolayers of alkyltrichlorosilanes of varying chain length. *ACS Appl. Mater. Interfaces* **2009,** 1, 1347-1357.

(41). Wu, X.; Laroche, I.; Masliyah, J.; Czarnecki, J.; Dabros, T. Applications of colloidal force measurements using a microcollider apparatus to oil sand studies. *Colloids Surf., A* **2000,** 174, 133-146.

(42). Rocha, J.; Baydak, E.; Yarranton, H. W.; Sztukowski, D.; Ali-Marcano, V.; Gong, L.; Shi, C.; Zeng, H. Role of Aqueous Phase Chemistry, Interfacial Film Properties, and Surface Coverage in Stabilizing Water-in-Bitumen Emulsions. *Energy & Fuels* **2016**.

(43). Wang, S.; Liu, J.; Zhang, L.; Xu, Z.; Masliyah, J. Colloidal interactions between asphaltene surfaces in toluene. *Energy & Fuels* **2008,** 23, 862-869.

(44). Wang, S.; Liu, J.; Zhang, L.; Masliyah, J.; Xu, Z. Interaction forces between asphaltene surfaces in organic solvents. *Langmuir* **2009,** 26, 183-190.

(45). Natarajan, A.; Xie, J.; Wang, S.; Liu, Q.; Masliyah, J.; Zeng, H.; Xu, Z. Understanding molecular interactions of asphaltenes in organic solvents using a surface force apparatus. *J. Phys. Chem. C* **2011,** 115, 16043-16051.

(46). Shi, C.; Cui, X.; Xie, L.; Liu, Q.; Chan, D. Y.; Israelachvili, J. N.; Zeng, H. Measuring forces and spatiotemporal evolution of thin water films between an air bubble and solid surfaces of different hydrophobicity. *ACS Nano* **2014,** 9, 95-104.

(47). Xie, L.; Shi, C.; Wang, J.; Huang, J.; Lu, Q.; Liu, Q.; Zeng, H. Probing the Interaction between Air Bubble and Sphalerite Mineral Surface Using Atomic Force Microscope. *Langmuir* **2015,** 31, 2438-2446.

(48). Cui, X.; Shi, C.; Xie, L.; Liu, J.; Zeng, H. Probing Interactions between Air Bubble and Hydrophobic Polymer Surface: Impact of Solution Salinity and Interfacial Nanobubbles. *Langmuir* **2016**.

(49). Shi, C.; Cui, X.; Zhang, X.; Tchoukov, P.; Liu, Q.; Encinas, N.; Paven, M.; Geyer, F.; Vollmer, D.; Xu, Z. Interaction between air bubbles and superhydrophobic surfaces in aqueous solutions. *Langmuir* **2015,** 31, 7317-7327.

(50). Testing, A. S. f.; Materials, ASTM D6560, Standard Test Method for Determination of Asphaltenes (Heptane Insolubles) in Crude Petroleum and Petroleum Products. In ASTM International West Conshohocken, PA: 2005.

(51). Daairtine, R. R.; Manica, R.; Carnie, S. L.; Chan, D.; Stevens, G. W.; Grieser, F. Dynamic forces between two deformable oil droplets in water. *Science* **2006,** 313, 210-213.

(52). Hutter, J. L.; Bechhoefer, J. Calibration of atomic-force microscope tips. *Rev. Sci. Instrum.* **1993,** 64, 1868-1873.

(53). Chan, D. Y.; Klaseboer, E.; Manica, R. Film drainage and coalescence between deformable drops and bubbles. *Soft Matter* **2011,** 7, 2235-2264.

(54). Tabor, R. F.; Grieser, F.; Daairtine, R. R.; Chan, D. Y. Measurement and analysis of forces in bubble and droplet systems using AFM. *J. Colloid Interface Sci.* **2012,** 371, 1-14.

(55). Tabor, R. F.; Chan, D. Y.; Grieser, F.; Daairtine, R. R. Anomalous Stability of Carbon Dioxide in pH-Controlled Bubble Coalescence. *Angew. Chem. Int. Ed.* **2011,** 50, 3454-3456.

(56). Israelachvili, J. N.; Adams, G. E. Measurement of forces between two mica surfaces in aqueous electrolyte solutions in the range 0–100 nm. *J. Chem. Soc., Faraday Trans. 1* **1978,** 74, 975-1001.

(57). Donaldson Jr, S. H.; Das, S.; Gebbie, M. A.; Rapp, M.; Jones, L. C.; Roiter, Y.; Koenig, P. H.; Gizaw, Y.; Israelachvili, J. N. Asymmetric Electrostatic and Hydrophobic–Hydrophilic Interaction Forces between Mica Surfaces and Silicone Polymer Thin Films. *ACS Nano* **2013,** 7, 10094-10104.

(58). de Gennes, P. G. Polymers at an interface; a simplified view. *Adv. Colloid Interface Sci.* **1987,** 27, 189-209.

(59). Manor, O.; Chau, T. T.; Stevens, G. W.; Chan, D. Y. C.; Grieser, F.; Daairtine, R. R. Polymeric Stabilized Emulsions: Steric Effects and Deformation in Soft Systems. *Langmuir* **2012,** 28, 4599-4604.

Chapter 7 Conclusions and Future Work

7.1. Major conclusions

In this study, novel droplet probe AFM technique and theoretical model based on Reynolds lubrication theory and the augmented Young-Laplace equation were developed and applied to directly measure the interaction mechanisms involving deformable droplets and air bubbles, with significant implication in many engineering processes. The droplet probe AFM was coupled with RICM, for the first time, to measure the interaction forces between air bubbles and mica surfaces of different hydrophobicity and synchronously visualize spatiotemporal evolution of the thin drainage process during the interactions. The interaction force and thin film drainage results measured by AFM-RICM were in perfect agreement with the theoretical model, indicating the essential physics behind the interaction between air bubble and solid surfaces could be elucidated. A stable thin water film was found to be sustained by repulsive VDW interaction between air bubble and hydrophilic mica surface, while air bubble attachment was observed on hydrophobized mica surfaces with water contact angle θ_w = 45º and 90º in 0.5 M NaCl. The attachment of the air bubble under various dynamic conditions was found to be quantitatively predicted by the theoretical model incorporating an exponential equation with the form of $W_H(h) = -\gamma(1-\cos\theta_w)\exp(-h/D_H)$ for the hydrophobic interaction in the air/water/hydrophobized mica system. The decay length D_H was fitted to be ~1 nm, equal to the reported value for solid hydrophobic systems.

The droplet probe AFM technique was applied to directly measure interaction between oil droplets in aqueous solutions in presence of asphaltenes, corresponding to the

stabilization mechanisms of O/W emulsions due to adsorption of asphaltenes at oil/water interface. Analyzed using the theoretical model, the AFM force results demonstrated that the interaction and surface forces between two pure oil droplets can well described by the DLVO theory. For oil droplets with adsorbed asphaltenes at oil/water interface, however, additional steric force should be added in the overall surface force to describe the measured force results. The coalescence behavior of oil droplets is largely determined by salt concentration, pH, ion type, and asphaltenes concentration. The surface potential of oil droplets was found to be more negative with adsorbed asphaltenes, which effectively strengthened the EDL repulsion between the oil droplets and inhibited oil droplet coalescence. Both of the enhanced EDL repulsion and the steric repulsion contributed to the stabilization of the O/W emulsions. Less negative surface potential and weaker EDL repulsion were measured at lower pH. Coalescence between oil droplets was found in presence of divalent ions (e.g. Ca^{2+}), which could be due to the bridging interaction between the divalent ions and the carboxyl groups on asphaltenes.

Measured force results between water droplets in oil demonstrated the important role of asphaltenes in stabilizing W/O emulsions. Without interfacial asphaltenes, the pure water droplets could readily coalesce with each other, exhibiting slight repulsion due hydrodynamic interaction. Adsorption of asphaltenes at the oil/water interface induced strong steric repulsion between water droplets, effectively inhibiting droplet coalescence and stabilizing the emulsion. Lateral shearing between water droplets was revealed to disrupt the protective effect of the interfacial asphaltenes layer leading to coalescence between water droplets. Moreover, interfacial adhesion was measured between water droplets during separation, which was most likely attributed to the aggregation and

bridging interaction between interfacial asphaltene molecules. The magnitude of the measured adhesion initially strengthened with increasing asphaltenes concentration, but drastically decreases after the asphaltenes concentration exceeded a certain value (near CNAC). Adding poor solvent like heptane was found to promote the adhesion when asphaltenes concentration was low, but the opposite trend was found at high asphaltenes concentration. Force results between water droplets with adsorbed asphaltenes in heptane showed strong solvophobic attraction during approach and could readily coalescence.

Interaction results between oil droplets (i.e. toluene and heptol) and mica surfaces measured using droplet probe AFM demonstrated that surface forces between pure oil droplets and bare mica surfaces can be explained by the DLVO theory. Interfacially adsorbed asphaltenes resulted in more negative surface potential of oil droplets and induced steric repulsion, supporting water films between oil droplet and mica surface and inhibiting oil droplet attachment. More negative surface potential was found with addition of poor solvent heptane. Hydrophobic attraction was found to dominate over the steric hindrance of asphaltenes and induce oil droplet attachment.

7.2. Original contributions

This work provided the first feasible method for direct synchronous and quantitative measurement of interaction force and thin film drainage process between an air bubble and solid surfaces. This method together with the theoretical model contributed to the understanding of the intrinsic physics behind the interaction between deformable droplets and solid surfaces. The experiment on the interaction between air bubbles and mica

surface with varying hydrophobicity demonstrated the hydrophobic attraction within the system, and an exponential form of hydrophobic attraction was proposed for the first time for the asymmetric air/water/solid systems.

Application of the droplet probe AFM in the interaction of emulsion droplets (i.e. oil droplets in water and water droplets in oil) in presence of asphaltenes provided important contribution to uncovering the molecular interaction mechanisms of asphaltenes at the real oil/water interfaces and the stabilization mechanisms of O/W and W/O due to asphaltenes, which could not be achieved conventional techniques. The results of oil droplets in oil revealed that more asphaltenes changed the surface potential of oil droplets to be more negative and asphaltenes induced steric repulsion at oil/water interfaces. The stability of oil droplets was found to be influenced by asphaltenes concentration and water chemistry. Force results between water droplets in oil with adsorbed asphaltenes at oil/water interface demonstrated that the asphaltenes not only stabilized the water droplets, but also led to strong interfacial adhesion between droplets. This adhesion was found to vary in a wide range depending on the asphaltenes concentration, aging time and solvent type. Lateral shearing was also demonstrated to be a possible method to destabilize the water droplets. Measurements between oil droplets and mica surface in water showed that the asphaltenes could prevent oil droplet attachment on hydrophilic mica surface by strengthening the EDL repulsion and inducing steric repulsion, but hydrophobic attraction strong attracted oil droplet to attach onto the hydrophobized mica surfaces.

Our work applied the unique droplet probe AFM to understand the interaction mechanisms involving deformable droplets and air bubbles, and contributed to the understanding of the molecular interaction mechanisms of asphaltenes at the real oil/water interface, which was not feasible for other conventional techniques. The novel experiment technique developed in this work can also be applied to many other industrial or scientific systems to understand their inherent interaction mechanisms.

7.3. Suggestions for future work

(1) The hydrophobic interaction of deformable oil droplets and air bubbles can be more explored. It is recommended that interaction between air bubbles and much more hydrophobic surfaces, including hydrophobic polymers (e.g. polystyrene, poly(methyl methacrylate)), self-assembled monolayers (e.g. thiols in gold surface) be investigated. More parameters like salt concentrations, ion types, pH, and temperature can be studied to fully understand the hydrophobic interaction within the systems.

(2) To better elucidate the stabilization mechanisms of real O/W emulsion, experiments of interaction between real emulsion droplets are recommended. Moreover, more salt concentration and ion types can be studied. And the effects high asphaltenes concentration can also be an interesting topic.

(3) For the interaction between water droplets in oil, the impacts water chemistry, such as ion effects and pH, should be further investigated. Fine solid particles can also be added into the emulsion systems to study its synergistic effects with asphaltenes. Moreover, sub-fractions of asphaltenes can be individually studied to understand their unique

impacts on stabilization on the W/O emulsions. Finally, the impacts of other components from crude oil products, such as resin, naphthenic acids, can also be further studied.

(4) With all the stabilization mechanisms understood, novel techniques to destabilize the emulsions with asphaltenes can be developed. And the mechanisms of the destabilizer can be directly studied using the same technique.

Bibliography

(1). Ducker, W. A.; Xu, Z.; Israelachvili, J. N. Measurements of hydrophobic and DLVO forces in bubble-surface interactions in aqueous solutions. *Langmuir* **1994,** 10, 3279-3289.

(2). Israelachvili, J. N., *Intermolecular and surface forces: revised third edition*. Academic press: 2011.

(3). Yang, H.; Park, C. C.; Hu, Y. T.; Leal, L. G. The coalescence of two equal-sized drops in a two-dimensional linear flow. *Physics of Fluids (1994-present)* **2001,** 13, 1087-1106.

(4). Lin, C. Y.; Slattery, J. Thinning of a liquid film as a small drop or bubble approaches a solid plane. *AlChE J.* **1982,** 28, 147-156.

(5). Chen, J.-D. Effects of London—van der Waals and electric double layer forces on the thinning of a dimpled film between a small drop or bubble and a horizontal solid plane. *J. Colloid Interface Sci.* **1984,** 98, 329-341.

(6). Klaseboer, E.; Chevaillier, J. P.; Gourdon, C.; Masbernat, O. Film drainage between colliding drops at constant approach velocity: experiments and modeling. *J. Colloid Interface Sci.* **2000,** 229, 274-285.

(7). Zeng, H., *Polymer adhesion, friction, and lubrication*. John Wiley & Sons: 2013.

(8). Zeng, H.; Shi, C.; Huang, J.; Li, L.; Liu, G.; Zhong, H. Recent experimental advances on hydrophobic interactions at solid/water and fluid/water interfaces. *Biointerphases* **2016,** 11, 018903.

(9). Shi, C.; Chan, D. Y.; Liu, Q.; Zeng, H. Probing the hydrophobic interaction between air bubbles and partially hydrophobic surfaces using atomic force microscopy. *J. Phys. Chem. C* **2014,** 118, 25000-25008.

(10). Shi, C.; Cui, X.; Zhang, X.; Tchoukov, P.; Liu, Q.; Encinas, N.; Paven, M.; Geyer, F.; Vollmer, D.; Xu, Z. Interaction between air bubbles and superhydrophobic surfaces in aqueous solutions. *Langmuir* **2015,** 31, 7317-7327.

(11). Shahalami, M.; Wang, L.; Wu, C.; Masliyah, J. H.; Xu, Z.; Chan, D. Y. Measurement and modeling on hydrodynamic forces and deformation of an air bubble approaching a solid sphere in liquids. *Adv. Colloid Interface Sci.* **2015,** 217, 31-42.

(12). Taylor, G. The formation of emulsions in definable fields of flow. *Proceedings of the Royal Society of London. Series A, Containing Papers of a Mathematical and Physical Character* **1934,** 146, 501-523.

(13). Bentley, B.; Leal, L. An experimental investigation of drop deformation and breakup in steady, two-dimensional linear flows. *J. Fluid Mech.* **1986,** 167, 241-283.

(14). Milliken, W.; Leal, L. Deformation and breakup of viscoelastic drops in planar extensional flows. *Journal of non-newtonian fluid mechanics* **1991,** 40, 355-379.

(15). Acrivos, A., The deformation and break-up of single drops in shear fields. In *Physicochemical Hydrodynamics*, Springer: 1988; pp 1-18.

(16). Hsu, A. S.; Roy, A.; Leal, L. G. Drop-size effects on coalescence of two equal-sized drops in a head-on collision. *Journal of Rheology (1978-present)* **2008,** 52, 1291-1310.

(17). Yoon, Y.; Borrell, M.; Park, C. C.; Leal, L. G. Viscosity ratio effects on the coalescence of two equal-sized drops in a two-dimensional linear flow. *J. Fluid Mech.* **2005,** 525, 355-379.

(18). Baldessari, F.; Leal, L. G. Effect of overall drop deformation on flow-induced coalescence at low capillary numbers. *Physics of Fluids (1994-present)* **2006,** 18, 013602.

(19). Dai, B.; Leal, L. G. The mechanism of surfactant effects on drop coalescence. *Physics of Fluids (1994-present)* **2008,** 20, 040802.

(20). Bremond, N.; Thiam, A. R.; Bibette, J. Decompressing emulsion droplets favors coalescence. *Phys. Rev. Lett.* **2008,** 100, 024501.

(21). Weon, B. M.; Je, J. H. Coalescence preference depends on size inequality. *Phys. Rev. Lett.* **2012,** 108, 224501.

(22). Lin, C. Y.; Slattery, J. Thinning of a liquid film as a small drop or bubble approaches a fluid–fluid interface. *AlChE J.* **1982,** 28, 786-792.

(23). Bazhlekov, I.; Chesters, A.; Van de Vosse, F. The effect of the dispersed to continuous-phase viscosity ratio on film drainage between interacting drops. *Int. J. Multiphase Flow* **2000,** 26, 445-466.

(24). Ivanov, I.; Dimitrov, D.; Somasundaran, P.; Jain, R. Thinning of films with deformable surfaces: diffusion-controlled surfactant transfer. *Chem. Eng. Sci.* **1985,** 40, 137-150.

(25). Blake, T.; Kitchener, J. Stability of aqueous films on hydrophobic methylated silica. *J. Chem. Soc., Faraday Trans. 1* **1972,** 68, 1435-1442.

(26). Velev, O.; Constantinides, G.; Avraam, D.; Payatakes, A.; Borwankar, R. Investigation of thin liquid films of small diameters and high capillary pressures by a miniaturized cell. *J. Colloid Interface Sci.* **1995,** 175, 68-76.

(27). Yaminsky, V. V.; Ohnishi, S.; Vogler, E. A.; Horn, R. G. Stability of aqueous films between bubbles. Part 1. The effect of speed on bubble coalescence in purified water and simple electrolyte solutions. *Langmuir* **2010,** 26, 8061-8074.

(28). Yaminsky, V. V.; Ohnishi, S.; Vogler, E. A.; Horn, R. G. Stability of aqueous films between bubbles. Part 2. effects of trace impurities and evaporation. *Langmuir* **2010,** 26, 8075-8080.

(29). Hendrix, M. H.; Manica, R.; Klaseboer, E.; Chan, D. Y.; Ohl, C.-D. Spatiotemporal evolution of thin liquid films during impact of water bubbles on glass on a micrometer to nanometer scale. *Phys. Rev. Lett.* **2012,** 108, 247803.

(30). Tsao, H. K.; Koch, D. L. Observations of high Reynolds number bubbles interacting with a rigid wall. *Physics of Fluids (1994-present)* **1997,** 9, 44-56.

(31). Klaseboer, E.; Chevaillier, J.-P.; Maté, A.; Masbernat, O.; Gourdon, C. Model and experiments of a drop impinging on an immersed wall. *Physics of Fluids (1994-present)* **2001,** 13, 45-57.

(32). Malysa, K.; Krasowska, M.; Krzan, M. Influence of surface active substances on bubble motion and collision with various interfaces. *Adv. Colloid Interface Sci.* **2005,** 114, 205-225.

(33). Manica, R.; Klaseboer, E.; Chan, D. Y. The hydrodynamics of bubble rise and impact with solid surfaces. *Adv. Colloid Interface Sci.* **2016,** 235, 214-232.

(34). Manica, R.; Klaseboer, E.; Chan, D. Y. The impact and bounce of air bubbles at a flat fluid interface. *Soft matter* **2016,** 12, 3271-3282.

(35). Parkinson, L.; Ralston, J. The interaction between a very small rising bubble and a hydrophilic titania surface. *J. Phys. Chem. C* **2010,** 114, 2273-2281.

(36). Manica, R.; Parkinson, L.; Ralston, J.; Chan, D. Y. Interpreting the dynamic interaction between a very small rising bubble and a hydrophilic titania surface. *J. Phys. Chem. C* **2009,** 114, 1942-1946.

(37). Li, E. Q.; Vakarelski, I. U.; Chan, D. Y.; Thoroddsen, S. T. Stabilization of thin liquid films by repulsive van der Waals force. *Langmuir* **2014,** 30, 5162-5169.

(38). Israelachvili, J.; Min, Y.; Akbulut, M.; Alig, A.; Carver, G.; Greene, W.; Kristiansen, K.; Meyer, E.; Pesika, N.; Rosenberg, K. Recent advances in the surface forces apparatus (SFA) technique. *Rep. Prog. Phys.* **2010,** 73, 036601.

(39). Israelachvili, J.; Pashley, R. The hydrophobic interaction is long range, decaying exponentially with distance. **1982**.

(40). Israelachvili, J. N.; Adams, G. E. Measurement of forces between two mica surfaces in aqueous electrolyte solutions in the range 0–100 nm. *J. Chem. Soc., Faraday Trans. 1* **1978,** 74, 975-1001.

(41). Connor, J. N.; Horn, R. G. Measurement of aqueous film thickness between charged mercury and mica surfaces: A direct experimental probe of the Poisson-Boltzmann distribution. *Langmuir* **2001,** 17, 7194-7197.

(42). Connor, J. N.; Horn, R. G. The influence of surface forces on thin film drainage between a fluid drop and a flat solid. *Faraday Discuss.* **2003,** 123, 193-206.

(43). Connor, J. N.; Horn, R. G. Extending the surface force apparatus capabilities by using white light interferometry in reflection. *Rev. Sci. Instrum.* **2003,** 74, 4601-4606.

(44). Pushkarova, R. A.; Horn, R. G. Surface forces measured between an air bubble and a solid surface in water. *Colloids Surf., A* **2005,** 261, 147-152.

(45). Pushkarova, R. A.; Horn, R. G. Bubble− solid interactions in water and electrolyte solutions. *Langmuir* **2008,** 24, 8726-8734.

(46). Horn, R. G.; Asadullah, M.; Connor, J. N. Thin film drainage: hydrodynamic and disjoining pressures determined from experimental measurements of the shape of a fluid drop approaching a solid wall. *Langmuir* **2006,** 22, 2610-2619.

(47). Clasohm, L. Y.; Connor, J. N.; Vinogradova, O. I.; Horn, R. G. The "wimple": rippled deformation of a fluid drop caused by hydrodynamic and surface forces during thin film drainage. *Langmuir* **2005,** 21, 8243-8249.

(48). Meyer, E. Atomic force microscopy. *Prog. Surf. Sci.* **1992,** 41, 3-49.

(49). Binnig, G.; Quate, C. F.; Gerber, C. Atomic Force Microscope. *Phys. Rev. Lett.* **1986,** 56, 930-933.

(50). Cappella, B.; Dietler, G. Force-distance curves by atomic force microscopy. *Surf. Sci. Rep.* **1999,** 34, 1-104.

(51). Hutter, J. L.; Bechhoefer, J. Calibration of atomic-force microscope tips. *Rev. Sci. Instrum.* **1993,** 64, 1868-1873.

(52). Cui, S.; Manica, R.; Tabor, R. F.; Chan, D. Y. Interpreting atomic force microscopy measurements of hydrodynamic and surface forces with nonlinear parametric estimation. *Rev. Sci. Instrum.* **2012,** 83, 103702.

(53). Chan, D.; Dagastine, R.; White, L. Forces between a rigid probe particle and a liquid interface: I. The repulsive case. *J. Colloid Interface Sci.* **2001,** 236, 141-154.

(54). Dagastine, R.; White, L. Forces between a rigid probe particle and a liquid interface: II. The general case. *J. Colloid Interface Sci.* **2002,** 247, 310-320.

(55). Butt, H.-J. A technique for measuring the force between a colloidal particle in water and a bubble. *J. Colloid Interface Sci.* **1994,** 166, 109-117.

(56). Preuss, M.; Butt, H.-J. Direct measurement of forces between particles and bubbles. *Int. J. Miner. Process.* **1999,** 56, 99-115.

(57). Gillies, G.; Kappl, M.; Butt, H.-J. Direct measurements of particle–bubble interactions. *Adv. Colloid Interface Sci.* **2005,** 114, 165-172.

(58). Preuss, M.; Butt, H.-J. Direct measurement of particle-bubble interactions in aqueous electrolyte: Dependence on surfactant. *Langmuir* **1998,** 14, 3164-3174.

(59). Chan, D. Y. C.; Klaseboer, E.; Manica, R. Theory of non-equilibrium force measurements involving deformable drops and bubbles. *Adv. Colloid Interface Sci.* **2011,** 165, 70-90.

(60). Manica, R.; Connor, J. N.; Dagastine, R. R.; Carnie, S. L.; Horn, R. G.; Chan, D. Y. C. Hydrodynamic forces involving deformable interfaces at nanometer separations. *Phys. Fluids* **2008,** 20, 032101.

(61). Vakarelski, I. U.; Manica, R.; Tang, X.; O'Shea, S. J.; Stevens, G. W.; Grieser, F.; Dagastine, R. R.; Chan, D. Y. Dynamic interactions between microbubbles in water. *Proceedings of the National Academy of Sciences* **2010,** 107, 11177-11182.

(62). Tabor, R. F.; Manica, R.; Chan, D. Y.; Grieser, F.; Dagastine, R. R. Repulsive van der Waals forces in soft matter: why bubbles do not stick to walls. *Phys. Rev. Lett.* **2011,** 106, 064501.

(63). Dagastine, R. R.; Manica, R.; Carnie, S. L.; Chan, D.; Stevens, G. W.; Grieser, F. Dynamic forces between two deformable oil droplets in water. *Science* **2006,** 313, 210-213.

(64). Tabor, R. F.; Grieser, F.; Dagastine, R. R.; Chan, D. Y. Measurement and analysis of forces in bubble and droplet systems using AFM. *J. Colloid Interface Sci.* **2012,** 371, 1-14.

(65). Chan, D. Y.; Klaseboer, E.; Manica, R. Film drainage and coalescence between deformable drops and bubbles. *Soft Matter* **2011,** 7, 2235-2264.

(66). Manor, O.; Chan, D. Y. Influence of Surfactants on the force between two Bubbles. *Langmuir* **2009,** 26, 655-662.

(67). Tabor, R. F.; Wu, C.; Grieser, F.; Dagastine, R. R.; Chan, D. Y. Measurement of the hydrophobic force in a soft matter system. *The Journal of Physical Chemistry Letters* **2013,** 4, 3872-3877.

(68). Tabor, R. F.; Chan, D. Y.; Grieser, F.; Dagastine, R. R. Structural forces in soft matter systems. *The Journal of Physical Chemistry Letters* **2011,** 2, 434-437.

(69). Yoon, Y.; Baldessari, F.; Ceniceros, H. D.; Leal, L. G. Coalescence of two equal-sized deformable drops in an axisymmetric flow. *Physics of Fluids (1994-present)* **2007,** 19, 102102.

(70). Manor, O.; Vakarelski, I. U.; Tang, X.; O'Shea, S. J.; Stevens, G. W.; Grieser, F.; Dagastine, R. R.; Chan, D. Y. Hydrodynamic boundary conditions and dynamic forces between bubbles and surfaces. *Phys. Rev. Lett.* **2008,** 101, 024501.

(71). Dagastine, R. R.; Webber, G. B.; Manica, R.; Stevens, G. W.; Grieser, F.; Chan, D. Y. Viscosity effects on hydrodynamic drainage force measurements involving deformable bodies. *Langmuir* **2010,** 26, 11921-11927.

(72). Xie, L.; Shi, C.; Wang, J.; Huang, J.; Lu, Q.; Liu, Q.; Zeng, H. Probing the Interaction between Air Bubble and Sphalerite Mineral Surface Using Atomic Force Microscope. *Langmuir* **2015,** 31, 2438-2446.

(73). Dai, Z.; Fornasiero, D.; Ralston, J. Particle–bubble attachment in mineral flotation. *J. Colloid Interface Sci.* **1999,** 217, 70-76.

(74). Mura, S.; Nicolas, J.; Couvreur, P. Stimuli-responsive nanocarriers for drug delivery. *Nature materials* **2013,** 12, 991-1003.

(75). Chen, Y.; Chen, H.; Zeng, D.; Tian, Y.; Chen, F.; Feng, J.; Shi, J. Core/shell structured hollow mesoporous nanocapsules: a potential platform for simultaneous cell imaging and anticancer drug delivery. *ACS Nano* **2010,** 4, 6001-6013.

(76). Yang, F.; Tchoukov, P.; Dettman, H.; Teklebrhan, R. B.; Liu, L.; Dabros, T.; Czarnecki, J.; Masliyah, J.; Xu, Z. Asphaltene Subfractions Responsible for Stabilizing Water-in-Crude Oil Emulsions. Part 2: Molecular Representations and Molecular Dynamics Simulations. *Energy & Fuels* **2015,** 29, 4783-4794.

(77). Rocha, J.; Baydak, E.; Yarranton, H. W.; Sztukowski, D.; Ali-Marcano, V.; Gong, L.; Shi, C.; Zeng, H. Role of Aqueous Phase Chemistry, Interfacial Film Properties, and Surface Coverage in Stabilizing Water-in-Bitumen Emulsions. *Energy & Fuels* **2016**.

(78). Tchoukov, P.; Yang, F.; Xu, Z.; Dabros, T.; Czarnecki, J.; Sjöblom, J. Role of asphaltenes in stabilizing thin liquid emulsion films. *Langmuir* **2014,** 30, 3024-3033.

(79). Czarnecki, J.; Tchoukov, P.; Dabros, T.; Xu, Z. Role of asphaltenes in stabilisation of water in crude oil emulsions. *Can. J. Chem. Eng.* **2013,** 91, 1365-1371.

(80). Kilpatrick, P. K. Water-in-crude oil emulsion stabilization: Review and unanswered questions. *Energy & Fuels* **2012,** 26, 4017-4026.

(81). Zhang, L.; Shi, C.; Lu, Q.; Liu, Q.; Zeng, H. Probing Molecular Interactions of Asphaltenes in Heptol Using a Surface Forces Apparatus: Implications on Stability of Water-in-Oil Emulsions. *Langmuir* **2016**.

(82). Harbottle, D.; Chen, Q.; Moorthy, K.; Wang, L.; Xu, S.; Liu, Q.; Sjoblom, J.; Xu, Z. Problematic stabilizing films in petroleum emulsions: Shear rheological response of viscoelastic asphaltene films and the effect on drop coalescence. *Langmuir* **2014,** 30, 6730-6738.

(83). Hannisdal, A.; Ese, M.-H.; Hemmingsen, P. V.; Sjöblom, J. Particle-stabilized emulsions: effect of heavy crude oil components pre-adsorbed onto stabilizing solids. *Colloids Surf., A* **2006,** 276, 45-58.

(84). Masliyah, J.; Zhou, Z. J.; Xu, Z.; Czarnecki, J.; Hamza, H. Understanding water-based bitumen extraction from Athabasca oil sands. *Can. J. Chem. Eng.* **2004,** 82, 628-654.

(85). Taylor, S. D.; Czarnecki, J.; Masliyah, J. Disjoining pressure isotherms of water-in-bitumen emulsion films. *J. Colloid Interface Sci.* **2002,** 252, 149-160.

(86). Gu, G.; Xu, Z.; Nandakumar, K.; Masliyah, J. Influence of water-soluble and water-insoluble natural surface active components on the stability of water-in-toluene-diluted bitumen emulsion. *Fuel* **2002,** 81, 1859-1869.

(87). Moran, K.; Yeung, A. Determining bitumen viscosity through drop shape recovery. *Can. J. Chem. Eng.* **2004,** 82, 813-820.

(88). Liu, J.; Xu, Z.; Masliyah, J. Interaction between bitumen and fines in oil sands extraction system: Implication to bitumen recovery. *Can. J. Chem. Eng.* **2004,** 82, 655-666.

(89). Ren, S.; Masliyah, J.; Xu, Z. Studying bitumen–bubble interactions using atomic force microscopy. *Colloids Surf., A* **2014,** 444, 165-172.

(90). He, L.; Lin, F.; Li, X.; Xu, Z.; Sui, H. Effect of solvent addition on bitumen–air bubble attachment in process water. *Chem. Eng. Sci.* **2015,** 137, 31-39.

(91). Strausz, O. P.; Mojelsky, T. W.; Lown, E. M. The molecular structure of asphaltene: an unfolding story. *Fuel* **1992,** 71, 1355-1363.

(92). Yarranton, H. W.; Hussein, H.; Masliyah, J. H. Water-in-hydrocarbon emulsions stabilized by asphaltenes at low concentrations. *J. Colloid Interface Sci.* **2000,** 228, 52-63.

(93). Mullins, O. C. The asphaltenes. *Annu. Rev. Anal. Chem.* **2011,** 4, 393-418.

(94). Schuler, B.; Meyer, G.; Pena, D.; Mullins, O. C.; Gross, L. Unraveling the molecular structures of asphaltenes by atomic force microscopy. *J. Am. Chem. Soc.* **2015,** 137, 9870-9876.

(95). Natarajan, A.; Xie, J.; Wang, S.; Liu, Q.; Masliyah, J.; Zeng, H.; Xu, Z. Understanding molecular interactions of asphaltenes in organic solvents using a surface force apparatus. *J. Phys. Chem. C* **2011,** 115, 16043-16051.

(96). Cimino, R.; Correra, S.; Del Bianco, A.; Lockhart, T. P., Solubility and phase behavior of asphaltenes in hydrocarbon media. In *Asphaltenes*, Springer: 1995; pp 97-130.

(97). Li, M.; Xu, M.; Ma, Y.; Wu, Z.; Christy, A. A. Interfacial film properties of asphaltenes and resins. *Fuel* **2002,** 81, 1847-1853.

(98). Tanaka, R.; Hunt, J. E.; Winans, R. E.; Thiyagarajan, P.; Sato, S.; Takanohashi, T. Aggregates structure analysis of petroleum asphaltenes with small-angle neutron scattering. *Energy & fuels* **2003,** 17, 127-134.

(99). Rane, J. P.; Pauchard, V.; Couzis, A.; Banerjee, S. Interfacial rheology of asphaltenes at oil–water interfaces and interpretation of the equation of state. *Langmuir* **2013,** 29, 4750-4759.

(100). Sztukowski, D. M.; Yarranton, H. W. Rheology of asphaltene-Toluene/water interfaces. *Langmuir* **2005,** 21, 11651-11658.

(101). Yeung, A.; Dabros, T.; Masliyah, J.; Czarnecki, J. Micropipette: a new technique in emulsion research. *Colloids Surf., A* **2000,** 174, 169-181.

(102). Tsamantakis, C.; Masliyah, J.; Yeung, A.; Gentzis, T. Investigation of the interfacial properties of water-in-diluted-bitumen emulsions using micropipette techniques. *J. Colloid Interface Sci.* **2005,** 284, 176-183.

(103). Zhang, L. Y.; Xu, Z.; Masliyah, J. H. Langmuir and Langmuir-Blodgett films of mixed asphaltene and a demulsifier. *Langmuir* **2003,** 19, 9730-9741.

(104). Langevin, D.; Argillier, J.-F. Interfacial behavior of asphaltenes. *Adv. Colloid Interface Sci.* **2015**.

(105). Hu, C.; Garcia, N. C.; Xu, R.; Cao, T.; Yen, A.; Garner, S. A.; Macias, J. M.; Joshi, N.; Hartman, R. L. Interfacial Properties of Asphaltenes at the Heptol–Brine Interface. *Energy & Fuels* **2015,** 30, 80-87.

(106). Yarranton, H. W.; Alboudwarej, H.; Jakher, R. Investigation of asphaltene association with vapor pressure osmometry and interfacial tension measurements. *Industrial & engineering chemistry research* **2000,** 39, 2916-2924.

(107). Yarranton, H.; Sztukowski, D.; Urrutia, P. Effect of interfacial rheology on model emulsion coalescence: I. Interfacial rheology. *J. Colloid Interface Sci.* **2007,** 310, 246-252.

(108). Wang, S.; Liu, J.; Zhang, L.; Xu, Z.; Masliyah, J. Colloidal interactions between asphaltene surfaces in toluene. *Energy & Fuels* **2008,** 23, 862-869.

(109). Liu, J.; Zhang, L.; Xu, Z.; Masliyah, J. Colloidal interactions between asphaltene surfaces in aqueous solutions. *Langmuir* **2006,** 22, 1485-1492.

(110). Wang, S.; Liu, J.; Zhang, L.; Masliyah, J.; Xu, Z. Interaction forces between asphaltene surfaces in organic solvents. *Langmuir* **2009,** 26, 183-190.

(111). Drummond, C.; Israelachvili, J. Surface forces and wettability. *J. Pet. Sci. Eng.* **2002,** 33, 123-133.

(112). Drummond, C.; Israelachvili, J. Fundamental studies of crude oil–surface water interactions and its relationship to reservoir wettability. *J. Pet. Sci. Eng.* **2004,** 45, 61-81.

(113). Durian, D. J.; Weitz, D. A.; Pine, D. J. MULTIPLE LIGHT-SCATTERING PROBES OF FOAM STRUCTURE AND DYNAMICS. *Science* **1991,** 252, 686-688.

(114). Ralston, J.; Fornasiero, D.; Hayes, R. Bubble-particle attachment and detachment in flotation. *Int. J. Miner. Process.* **1999,** 56, 133-164.

(115). Prakash, M.; Gershenfeld, N. Microfluidic bubble logic. *Science* **2007,** 315, 832-835.

(116). Stride, E.; Edirisinghe, M. Novel microbubble preparation technologies. *Soft Matter* **2008,** 4, 2350-2359.

(117). Schutt, E. G.; Klein, D. H.; Mattrey, R. M.; Riess, J. G. Injectable microbubbles as contrast agents for diagnostic ultrasound imaging: The key role of perfluorochemicals. *Angew. Chem., Int. Ed.* **2003,** 42, 3218-3235.

(118). Lindner, J. R. Microbubbles in medical imaging: current applications and future directions. *Nat. Rev. Drug Discovery* **2004,** 3, 527-532.

(119). Prentice, P.; Cuschierp, A.; Dholakia, K.; Prausnitz, M.; Campbell, P. Membrane disruption by optically controlled microbubble cavitation. *Nat. Phys.* **2005,** 1, 107-110.

(120). Wrenn, S. P.; Dicker, S. M.; Small, E. F.; Dan, N. R.; Mleczko, M.; Schmitz, G.; Lewin, P. A. Bursting Bubbles and Bilayers. *Theranostics* **2012,** 2, 1140-1159.

(121). Chen, K.-J.; Chaung, E.-Y.; Wey, S.-P.; Lin, K.-J.; Cheng, F.; Lin, C.-C.; Liu, H.-L.; Tseng, H.-W.; Liu, C.-P.; Wei, M.-C.; Liu, C.-M.; Sung, H.-W. Hyperthermia-Mediated Local Drug Delivery by a Bubble-Generating Liposomal System for Tumor-Specific Chemotherapy. *ACS Nano* **2014,** 8, 5105-5115.

(122). Lentacker, I.; De Smedt, S. C.; Demeester, J.; Van Marck, V.; Bracke, M.; Sanders, N. N. Lipoplex-loaded microbubbles for gene delivery: A Trojan horse controlled by ultrasound. *Adv. Funct. Mater.* **2007,** 17, 1910-1916.

(123). Lentacker, I.; De Smedt, S. C.; Sanders, N. N. Drug loaded microbubble design for ultrasound triggered delivery. *Soft Matter* **2009,** 5, 2161-2170.

(124). Cavalli, R.; Bisazza, A.; Lembo, D. Micro- and nanobubbles: A versatile non-viral platform for gene delivery. *Int. J. Pharm.* **2013,** 456, 437-445.

(125). Soler, L.; Magdanz, V.; Fomin, V. M.; Sanchez, S.; Schmidt, O. G. Self-Propelled Micromotors for Cleaning Polluted Water. *ACS Nano* **2013,** 7, 9611-9620.

(126). Yec, C. C.; Zeng, H. C. Nanobubbles within a Microbubble: Synthesis and Self-Assembly of Hollow Manganese Silicate and Its Metal-Doped Derivatives. *ACS Nano* **2014,** 8, 6407-6416.

(127). Kovalenko, A.; Jouhannaud, J.; Polavarapu, P.; Krafft, M. P.; Waton, G.; Pourroy, G. Hollow magnetic microspheres obtained by nanoparticle adsorption on surfactant stabilized microbubbles. *Soft Matter* **2014,** 10, 5147-5156.

(128). Hower, J. C.; Bernards, M. T.; Chen, S.; Tsao, H.-K.; Sheng, Y.-J.; Jiang, S. Hydration of "nonfouling" functional groups. *The Journal of Physical Chemistry B* **2008,** 113, 197-201.

(129). Belova, V.; Krasowska, M.; Wang, D.; Ralston, J.; Shchukin, D. G.; Moehwald, H. Influence of adsorbed gas at liquid/solid interfaces on heterogeneous cavitation. *Chemical Science* **2013,** 4, 248-256.

(130). Liu, G.; Craig, V. S. J. Improved Cleaning of Hydrophilic Protein-Coated Surfaces using the Combination of Nanobubbles and SDS. *Acs Applied Materials & Interfaces* **2009,** 1, 481-487.

(131). Lozano, M. M.; Longo, M. L. Microbubbles Coated with Disaturated Lipids and DSPE-PEG2000: Phase Behavior, Collapse Transitions, and Permeability. *Langmuir* **2009,** 25, 3705-3712.

(132). Dickinson, E.; Ettelaie, R.; Kostakis, T.; Murray, B. S. Factors controlling the formation and stability of air bubbles stabilized by partially hydrophobic silica nanoparticles. *Langmuir* **2004,** 20, 8517-8525.

(133). Sanchez-Iglesias, A.; Grzelczak, M.; Altantzis, T.; Goris, B.; Perez-Juste, J.; Bals, S.; Van Tendeloo, G.; Donaldson, S. H., Jr.; Chmelka, B. F.; Israelachvili, J. N.; Liz-

Marzan, L. M. Hydrophobic Interactions Modulate Self-Assembly of Nanoparticles. *ACS Nano* **2012,** 6, 11059-11065.

(134). Leckband, D. Measuring the forces that control protein interactions. *Annu. Rev. Biophys. Biomol. Struct.* **2000,** 29, 1-26.

(135). Tirrell, M.; Kokkoli, E.; Biesalski, M. The role of surface science in bioengineered materials. *Surf. Sci.* **2002,** 500, 61-83.

(136). Allan, D. B.; Firester, D. M.; Allard, V. P.; Reich, D. H.; Stebe, K. J.; Leheny, R. L. Linear and nonlinear microrheology of lysozyme layers forming at the air-water interface. *Soft Matter* **2014,** 10, 7051-7060.

(137). Donaldson, S. H.; Røyne, A.; Kristiansen, K.; Rapp, M. V.; Das, S.; Gebbie, M. A.; Lee, D. W.; Stock, P.; Valtiner, M.; Israelachvili, J. Developing a general interaction potential for hydrophobic and hydrophilic interactions. *Langmuir* **2014**.

(138). Lee, M. H.; Reich, D. H.; Stebe, K. J.; Leheny, R. L. Combined Passive and Active Microrheology Study of Protein-Layer Formation at an Air-Water Interface. *Langmuir* **2010,** 26, 2650-2658.

(139). Meyer, E. E.; Rosenberg, K. J.; Israelachvili, J. Recent progress in understanding hydrophobic interactions. *Proc. Natl. Acad. Sci. U. S. A.* **2006,** 103, 15739-15746.

(140). Tabor, R. F.; Grieser, F.; Dagastine, R. R.; Chan, D. Y. C. The hydrophobic force: measurements and methods. *Phys. Chem. Chem. Phys.* **2014,** 16, 18065-75.

(141). Israelachvili, J.; Pashley, R. THE HYDROPHOBIC INTERACTION IS LONG-RANGE, DECAYING EXPONENTIALLY WITH DISTANCE. *Nature* **1982,** 300, 341-342.

(142). Mastropietro, D. J.; Ducker, W. A. Forces between Hydrophobic Solids in Concentrated Aqueous Salt Solution. *Phys. Rev. Lett.* **2012,** 108.

(143). Huang, D. M.; Chandler, D. Temperature and length scale dependence of hydrophobic effects and their possible implications for protein folding. *Proc. Natl. Acad. Sci. U. S. A.* **2000,** 97, 8324-8327.

(144). Pashley, R. M.; McGuiggan, P. M.; Ninham, B. W.; Evans, D. F. ATTRACTIVE FORCES BETWEEN UNCHARGED HYDROPHOBIC SURFACES - DIRECT MEASUREMENTS IN AQUEOUS-SOLUTION. *Science* **1985,** 229, 1088-1089.

(145). Donaldson, S. H., Jr.; Lee, C. T., Jr.; Chmelka, B. F.; Israelachvili, J. N. General hydrophobic interaction potential for surfactant/lipid bilayers from direct force measurements between light-modulated bilayers. *Proc. Natl. Acad. Sci. U. S. A.* **2011,** 108, 15699-15704.

(146). Craig, V.; Ninham, B.; Pashley, R. Direct measurement of hydrophobic forces: A study of dissolved gas, approach rate, and neutron irradiation. *Langmuir* **1999,** 15, 1562-1569.

(147). Faghihnejad, A.; Zeng, H. Hydrophobic interactions between polymer surfaces: using polystyrene as a model system. *Soft Matter* **2012,** 8, 2746-2759.

(148). Donaldson, S. H., Jr.; Das, S.; Gebbie, M. A.; Rapp, M.; Jones, L. C.; Roiter, Y.; Koenig, P. H.; Gizaw, Y.; Israelachvili, J. N. Asymmetric Electrostatic and Hydrophobic-Hydrophilic Interaction Forces between Mica Surfaces and Silicone Polymer Thin Films. *ACS Nano* **2013,** 7, 10094-10104.

(149). Kristiansen, K.; Stock, P.; Baimpos, T.; Raman, S.; Harada, J. K.; Israelachvili, J. N.; Valtiner, M. Influence of molecular dipole orientations on long-range exponential

interaction forces at hydrophobic contacts in aqueous solutions. *ACS Nano* **2014,** 8, 10870-7.

(150). Perkin, S.; Kampf, N.; Klein, J. Long-range attraction between charge-mosaic surfaces across water. *Phys. Rev. Lett.* **2006,** 96.

(151). Faghihnejad, A.; Zeng, H. Interaction Mechanism between Hydrophobic and Hydrophilic Surfaces: Using Polystyrene and Mica as a Model System. *Langmuir* **2013,** 29, 12443-12451.

(152). Carambassis, A.; Jonker, L. C.; Attard, P.; Rutland, M. W. Forces measured between hydrophobic surfaces due to a submicroscopic bridging bubble. *Phys. Rev. Lett.* **1998,** 80, 5357-5360.

(153). Thormann, E.; Simonsen, A. C.; Hansen, P. L.; Mouritsen, O. G. Force trace hysteresis and temperature dependence of bridging nanobubble induced forces between hydrophobic surfaces. *ACS Nano* **2008,** 2, 1817-1824.

(154). German, S. R.; Wu, X.; An, H.; Craig, V. S. J.; Mega, T. L.; Zhang, X. Interfacial Nanobubbles Are Leaky: Permeability of the Gas/Water Interface. *ACS Nano* **2014,** 8, 6193-6201.

(155). Tabor, R. F.; Wu, C.; Grieser, F.; Dagastine, R. R.; Chan, D. Y. C. Measurement of the Hydrophobic Force in a Soft Matter System. *J. Phys. Chem. Lett.* **2013,** 4, 3872-3877.

(156). Preuss, M.; Butt, H. J. Direct measurement of particle-bubble interactions in aqueous electrolyte: Dependence on surfactant. *Langmuir* **1998,** 14, 3164-3174.

(157). Ducker, W. A.; Xu, Z. G.; Israelachvili, J. N. MEASUREMENTS OF HYDROPHOBIC AND DLVO FORCES IN BUBBLE-SURFACE INTERACTIONS IN AQUEOUS-SOLUTIONS. *Langmuir* **1994,** 10, 3279-3289.

(158). Shi, C.; Chan, D. Y.; Liu, Q.; Zeng, H. Probing Hydrophobic Interaction between Air Bubble and Partially Hydrophobic Surfaces Using Atomic Force Microscopy. *J. Phys. Chem. C* **2014,** 118, 25000-25008.

(159). Tabor, R. F.; Manica, R.; Chan, D. Y. C.; Grieser, F.; Dagastine, R. R. Repulsive van der Waals Forces in Soft Matter: Why Bubbles Do Not Stick to Walls. *Phys. Rev. Lett.* **2011,** 106.

(160). Vakarelski, I. U.; Manica, R.; Tang, X.; O'Shea, S. J.; Stevens, G. W.; Grieser, F.; Dagastine, R. R.; Chan, D. Y. C. Dynamic interactions between microbubbles in water. *Proc. Natl. Acad. Sci. U. S. A.* **2010,** 107, 11177-11182.

(161). Manica, R.; Parkinson, L.; Ralston, J.; Chan, D. Y. C. Interpreting the Dynamic Interaction between a Very Small Rising Bubble and a Hydrophilic Titania Surface. *J. Phys. Chem. C* **2010,** 114, 1942-1946.

(162). Hendrix, M. H. W.; Manica, R.; Klaseboer, E.; Chan, D. Y. C.; Ohl, C.-D. Spatiotemporal Evolution of Thin Liquid Films during Impact of Water Bubbles on Glass on a Micrometer to Nanometer Scale. *Phys. Rev. Lett.* **2012,** 108.

(163). Parkinson, L.; Ralston, J. The Interaction between a Very Small Rising Bubble and a Hydrophilic Titania Surface. *J. Phys. Chem. C* **2010,** 114, 2273-2281.

(164). Contreras-Naranjo, J. C.; Ugaz, V. M. A nanometre-scale resolution interference-based probe of interfacial phenomena between microscopic objects and surfaces. *Nat. Commun.* **2013,** 4.

(165). Tabor, R. F.; Grieser, F.; Dagastine, R. R.; Chan, D. Y. C. Measurement and analysis of forces in bubble and droplet systems using AFM. *J. Colloid Interface Sci.* **2012,** 371, 1-14.

(166). Dagastine, R. R.; Manica, R.; Carnie, S. L.; Chan, D. Y. C.; Stevens, G. W.; Grieser, F. Dynamic forces between two deformable oil droplets in water. *Science* **2006,** 313, 210-213.

(167). Manor, O.; Vakarelski, I. U.; Stevens, G. W.; Grieser, F.; Dagastine, R. R.; Chan, D. Y. C. Dynamic Forces between Bubbles and Surfaces and Hydrodynamic Boundary Conditions. *Langmuir* **2008,** 24, 11533-11543.

(168). Ninham, B. W.; Parsegia.Va VANDERWAALS FORCES - SPECIAL CHARACTERISTICS IN LIPID-WATER SYSTEMS AND A GENERAL METHOD OF CALCULATION BASED ON LIFSHITZ THEORY. *Biophys. J.* **1970,** 10, 646-&.

(169). Dagastine, R. R.; Prieve, D. C.; White, L. R. The dielectric function for water and its application to van der Waals forces. *J. Colloid Interface Sci.* **2000,** 231, 351-358.

(170). Grabbe, A. DOUBLE-LAYER INTERACTIONS BETWEEN SILYLATED SILICA SURFACES. *Langmuir* **1993,** 9, 797-801.

(171). Borkent, B. M.; Dammer, S. M.; Schoenherr, H.; Vancso, G. J.; Lohse, D. Superstability of surface nanobubbles. *Phys. Rev. Lett.* **2007,** 98.

(172). Walczyk, W.; Schoenherr, H. Closer Look at the Effect of AFM Imaging Conditions on the Apparent Dimensions of Surface Nanobubbles. *Langmuir* **2013,** 29, 620-632.

(173). Walczyk, W.; Schoen, P. M.; Schoenherr, H. The effect of PeakForce tapping mode AFM imaging on the apparent shape of surface nanobubbles. *J. Phys.: Condens. Matter* **2013,** 25.

(174). Zhang, X. H.; Zhang, X. D.; Lou, S. T.; Zhang, Z. X.; Sun, J. L.; Hu, J. Degassing and temperature effects on the formation of nanobubbles at the mica/water interface. *Langmuir* **2004,** 20, 3813-3815.

(175). Walczyk, W.; Schoenherr, H. Characterization of the Interaction between AFM Tips and Surface Nanobubbles. *Langmuir* **2014,** 30, 7112-7126.

(176). Walczyk, W.; Hain, N.; Schoenherr, H. Hydrodynamic effects of the tip movement on surface nanobubbles: a combined tapping mode, lift mode and force volume mode AFM study. *Soft Matter* **2014,** 10, 5945-5954.

(177). Hutter, J. L.; Bechhoefer, J. CALIBRATION OF ATOMIC-FORCE MICROSCOPE TIPS. *Rev. Sci. Instrum.* **1993,** 64, 1868-1873.

(178). Chan, D. Y. C.; Klaseboer, E.; Manica, R. Film drainage and coalescence between deformable drops and bubbles. *Soft Matter* **2011,** 7, 2235-2264.

(179). Bailey, A. I.; Kay, S. M. MEASUREMENT OF REFRACTIVE INDEX AND DISPERSION OF MICA EMPLOYING MULTIPLE BEAM INTERFERENCE TECHNIQUES. *Br. J. Appl. Phys.* **1965,** 16, 39-44.

(180). Contreras-Naranjo, J. C.; Silas, J. A.; Ugaz, V. M. Reflection interference contrast microscopy of arbitrary convex surfaces. *Appl. Opt.* **2010,** 49, 3701-3712.

(181). Wiegand, G.; Neumaier, K. R.; Sackmann, E. Microinterferometry: three-dimensional reconstruction of surface microtopography for thin-film and wetting studies by reflection interference contrast microscopy (RICM). *Appl. Opt.* **1998,** 37, 6892-6905.

(182). Natarajan, A.; Xie, J.; Wang, S.; Liu, Q.; Masliyah, J.; Zeng, H.; Xu, Z. Understanding Molecular Interactions of Asphaltenes in Organic Solvents Using a Surface Force Apparatus. *J. Phys. Chem. C* **2011,** 115, 16043-16051.

(183). Dai, Q.; Chung, K. H. Hot water extraction process mechanism using model oil sands. *Fuel* **1996,** 75, 220-226.

(184). Kovalenko, A.; Jouhannaud, J.; Polavarapu, P.; Krafft, M. P.; Waton, G.; Pourroy, G. Hollow magnetic microspheres obtained by nanoparticle adsorption on surfactant stabilized microbubbles. *Soft Matter* **2014,** 10, 5147-56.

(185). Guo, S.; Jańczewski, D.; Zhu, X.; Quintana, R.; He, T.; Neoh, K. G. Surface charge control for zwitterionic polymer brushes: Tailoring surface properties to antifouling applications. *J. Colloid Interface Sci.* **2015,** 452, 43-53.

(186). Liang, F.; Zhang, C.; Yang, Z. Rational design and synthesis of Janus composites. *Adv. Mater.* **2014,** 26, 6944-6949.

(187). Mura, S.; Nicolas, J.; Couvreur, P. Stimuli-responsive nanocarriers for drug delivery. *Nat Mater* **2013,** 12, 991-1003.

(188). Schutt, E. G.; Klein, D. H.; Mattrey, R. M.; Riess, J. G. Injectable microbubbles as contrast agents for diagnostic ultrasound imaging: the key role of perfluorochemicals. *Angew Chem Int Ed Engl* **2003,** 42, 3218-35.

(189). Clasohm, L. Y.; Vakarelski, I. U.; Dagastine, R. R.; Chan, D. Y.; Stevens, G. W.; Grieser, F. Anomalous pH dependent stability behavior of surfactant-free nonpolar oil drops in aqueous electrolyte solutions. *Langmuir* **2007,** 23, 9335-9340.

(190). Manica, R.; Connor, J. N.; Carnie, S. L.; Horn, R. G.; Chan, D. Y. Dynamics of interactions involving deformable drops: Hydrodynamic dimpling under attractive and repulsive electrical double layer interactions. *Langmuir* **2007,** 23, 626-637.

(191). Kralova, I.; Sjöblom, J.; Øye, G.; Simon, S.; Grimes, B. A.; Paso, K. Heavy crude oils/particle stabilized emulsions. *Adv. Colloid Interface Sci.* **2011,** 169, 106-127.

(192). Czarnecki, J.; Moran, K. On the stabilization mechanism of water-in-oil emulsions in petroleum systems. *Energy & fuels* **2005,** 19, 2074-2079.

(193). Gafonova, O. V.; Yarranton, H. W. The stabilization of water-in-hydrocarbon emulsions by asphaltenes and resins. *J. Colloid Interface Sci.* **2001,** 241, 469-478.

(194). Czarnecki, J.; Tchoukov, P.; Dabros, T. Possible role of asphaltenes in the stabilization of water-in-crude oil emulsions. *Energy Fuels* **2012,** 26, 5782-5786.

(195). Liu, J.; Xu, Z.; Masliyah, J. Colloidal forces between bitumen surfaces in aqueous solutions measured with atomic force microscope. *Colloids Surf., A* **2005,** 260, 217-228.

(196). Wu, X.; Laroche, I.; Masliyah, J.; Czarnecki, J.; Dabros, T. Applications of colloidal force measurements using a microcollider apparatus to oil sand studies. *Colloids Surf., A* **2000,** 174, 133-146.

(197). Wu, X.; Czarnecki, J.; Hamza, N.; Masliyah, J. Interaction forces between bitumen droplets in water. *Langmuir* **1999,** 15, 5244-5250.

(198). Pauchard, V.; Rane, J. P.; Zarkar, S.; Couzis, A.; Banerjee, S. Long-Term Adsorption Kinetics of Asphaltenes at the Oil–Water Interface: A Random Sequential Adsorption Perspective. *Langmuir* **2014,** 30, 8381-8390.

(199). Mullins, O. C. The Modified Yen Model†. *Energy Fuels* **2010,** 24, 2179-2207.

(200). McLean, J. D.; Kilpatrick, P. K. Effects of asphaltene aggregation in model heptane–toluene mixtures on stability of water-in-oil emulsions. *J. Colloid Interface Sci.* **1997,** 196, 23-34.

(201). Mullins, O. C.; Sabbah, H.; Eyssautier, J. l.; Pomerantz, A. E.; Barré, L.; Andrews, A. B.; Ruiz-Morales, Y.; Mostowfi, F.; McFarlane, R.; Goual, L. Advances in asphaltene science and the Yen–Mullins model. *Energy Fuels* **2012,** 26, 3986-4003.

(202). Wang, J.; Lu, Q.; Harbottle, D.; Sjöblom, J.; Xu, Z.; Zeng, H. Molecular interactions of a polyaromatic surfactant C5Pe in aqueous solutions studied by a surface forces apparatus. *The Journal of Physical Chemistry B* **2012,** 116, 11187-11196.

(203). Das, S.; Thundat, T.; Mitra, S. K. Analytical model for zeta potential of asphaltene. *Fuel* **2013,** 108, 543-549.

(204). Sztukowski, D. M.; Jafari, M.; Alboudwarej, H.; Yarranton, H. W. Asphaltene self-association and water-in-hydrocarbon emulsions. *J. Colloid Interface Sci.* **2003,** 265, 179-186.

(205). Poteau, S.; Argillier, J.-F.; Langevin, D.; Pincet, F.; Perez, E. Influence of pH on stability and dynamic properties of asphaltenes and other amphiphilic molecules at the oil-water interface. *Energy Fuels* **2005,** 19, 1337-1341.

(206). Natarajan, A.; Kuznicki, N.; Harbottle, D.; Masliyah, J.; Zeng, H.; Xu, Z. Understanding Mechanisms of Asphaltene Adsorption from Organic Solvent on Mica. *Langmuir* **2014,** 30, 9370-9377.

(207). Wang, J.; van der Tuuk Opedal, N.; Lu, Q.; Xu, Z.; Zeng, H.; Sjöblom, J. Probing Molecular Interactions of an Asphaltene Model Compound in Organic Solvents Using a Surface Forces Apparatus (SFA). *Energy Fuels* **2011,** 26, 2591-2599.

(208). Shi, C.; Cui, X.; Xie, L.; Liu, Q.; Chan, D. Y.; Israelachvili, J. N.; Zeng, H. Measuring Forces and Spatiotemporal Evolution of Thin Water Films between an Air Bubble and Solid Surfaces of Different Hydrophobicity. *ACS Nano* **2014**.

(209). Manor, O.; Chau, T. T.; Stevens, G. W.; Chan, D. Y.; Grieser, F.; Dagastine, R. R. Polymeric stabilized emulsions: Steric effects and deformation in soft systems. *Langmuir* **2012,** 28, 4599-4604.

(210). Vakarelski, I. U.; Li, E. Q.; Thoroddsen, S. T. Soft colloidal probes for AFM force measurements between water droplets in oil. *Colloids Surf., A* **2014,** 462, 259-263.

(211). Xie, L.; Shi, C.; Wang, J.; Huang, J.; Lu, Q.; Liu, Q.; Zeng, H. Probing the Interaction between Air Bubble and Sphalerite Mineral Surface using Atomic Force Microscope. *Langmuir* **2015**.

(212). Schönherr, H. Forces and Thin Water Film Drainage in Deformable Asymmetric Nanoscale Contacts. *ACS Nano* **2015,** 9, 12-15.

(213). Testing, A. S. f.; Materials, ASTM D6560, Standard Test Method for Determination of Asphaltenes (Heptane Insolubles) in Crude Petroleum and Petroleum Products. In ASTM International West Conshohocken, PA: 2005.

(214). Dagastine, R. R.; Prieve, D. C.; White, L. R. Forces between a rigid probe particle and a liquid interface: III. Extraction of the planar half-space interaction energy E (D). *J. Colloid Interface Sci.* **2004,** 269, 84-96.

(215). Parra-Barraza, H.; Hernández-Montiel, D.; Lizardi, J.; Hernández, J.; Urbina, R. H.; Valdez, M. A. The zeta potential and surface properties of asphaltenes obtained with different crude oil/n-heptane proportions☆. *Fuel* **2003,** 82, 869-874.

(216). Busscher, H.; Van de Belt-Gritter, B.; Van der Mei, H. Implications of microbial adhesion to hydrocarbons for evaluating cell surface hydrophobicity 1. Zeta potentials of hydrocarbon droplets. *Colloids Surf., B* **1995,** 5, 111-116.

(217). De Gennes, P. Polymers at an interface; a simplified view. *Adv. Colloid Interface Sci.* **1987,** 27, 189-209.

(218). Zarzar, L. D.; Sresht, V.; Sletten, E. M.; Kalow, J. A.; Blankschtein, D.; Swager, T. M. Dynamically reconfigurable complex emulsions via tunable interfacial tensions. *Nature* **2015,** 518, 520-524.

(219). Villar, G.; Heron, A. J.; Bayley, H. Formation of droplet networks that function in aqueous environments. *Nature nanotechnology* **2011,** 6, 803-808.

(220). Song, Y.; Chan, Y. K.; Ma, Q.; Liu, Z.; Shum, H. C. All-Aqueous Electrosprayed Emulsion for Templated Fabrication of Cytocompatible Microcapsules. *ACS Appl. Mater. Interfaces* **2015,** 7, 13925-13933.

(221). Helgeson, M. E.; Moran, S. E.; An, H. Z.; Doyle, P. S. Mesoporous organohydrogels from thermogelling photocrosslinkable nanoemulsions. *Nature materials* **2012,** 11, 344-352.

(222). Zhang, L.; Mikhailovskaya, A.; Yazhgur, P.; Muller, F.; Cousin, F.; Langevin, D.; Wang, N.; Salonen, A. Precipitating Sodium Dodecyl Sulfate to Create Ultrastable and Stimulable Foams. *Angew. Chem.* **2015,** 127, 9669-9672.

(223). Yanagisawa, M.; Yoshida, T.-a.; Furuta, M.; Nakata, S.; Tokita, M. Adhesive force between paired microdroplets coated with lipid monolayers. *Soft Matter* **2013,** 9, 5891-5897.

(224). Thiam, A. R.; Bremond, N.; Bibette, J. r. m. From stability to permeability of adhesive emulsion bilayers. *Langmuir* **2012,** 28, 6291-6298.

(225). Li, Y.; Zou, J.; Das, B. P.; Tsianou, M.; Cheng, C. Well-defined amphiphilic double-brush copolymers and their performance as emulsion surfactants. *Macromolecules* **2012,** 45, 4623-4629.

(226). Binks, B. P.; Murakami, R.; Armes, S. P.; Fujii, S. Temperature-Induced Inversion of Nanoparticle-Stabilized Emulsions. *Angew. Chem.* **2005,** 117, 4873-4876.

(227). Binks, B. P.; Murakami, R. Phase inversion of particle-stabilized materials from foams to dry water. *Nature materials* **2006,** 5, 865-869.

(228). Long, Y.; Dabros, T.; Hamza, H. Stability and settling characteristics of solvent-diluted bitumen emulsions. *Fuel* **2002,** 81, 1945-1952.

(229). Wu, X. Investigating the stability mechanism of water-in-diluted bitumen emulsions through isolation and characterization of the stabilizing materials at the interface. *Energy & fuels* **2003,** 17, 179-190.

(230). Andersen, S. I.; del Rio, J. M.; Khvostitchenko, D.; Shakir, S.; Lira-Galeana, C. Interaction and solubilization of water by petroleum asphaltenes in organic solution. *Langmuir* **2001,** 17, 307-313.

(231). Mikami, Y.; Liang, Y.; Matsuoka, T.; Boek, E. S. Molecular dynamics simulations of asphaltenes at the oil–water interface: from nanoaggregation to thin-film formation. *Energy & Fuels* **2013,** 27, 1838-1845.

(232). Eyssautier, J.; Levitz, P.; Espinat, D.; Jestin, J.; Gummel, J.; Grillo, I.; Barré, L. Insight into asphaltene nanoaggregate structure inferred by small angle neutron and X-ray scattering. *The Journal of Physical Chemistry B* **2011,** 115, 6827-6837.

(233). Alvarez, G.; Jestin, J.; Argillier, J.; Langevin, D. Small-Angle Neutron Scattering Study of Crude Oil Emulsions: Structure of the Oil− Water Interfaces†. *Langmuir* **2009,** 25, 3985-3990.

(234). McLean, J. D.; Kilpatrick, P. K. Effects of asphaltene solvency on stability of water-in-crude-oil emulsions. *J. Colloid Interface Sci.* **1997,** 189, 242-253.

(235). Hemmingsen, P. V.; Silset, A.; Hannisdal, A.; Sjöblom, J. Emulsions of heavy crude oils. I: Influence of viscosity, temperature, and dilution. *J. Dispersion Sci. Technol.* **2005,** 26, 615-627.

(236). Fortuny, M.; Oliveira, C. B.; Melo, R. L.; Nele, M.; Coutinho, R. C.; Santos, A. F. Effect of salinity, temperature, water content, and pH on the microwave demulsification of crude oil emulsions. *Energy & Fuels* **2007,** 21, 1358-1364.

(237). Spiecker, P. M.; Gawrys, K. L.; Trail, C. B.; Kilpatrick, P. K. Effects of petroleum resins on asphaltene aggregation and water-in-oil emulsion formation. *Colloids Surf., A* **2003,** 220, 9-27.

(238). Wu, X.; van De Ven, T.; Czarnecki, J. Colloidal forces between emulsified water droplets in toluene-diluted bitumen. *Colloids Surf., A* **1999,** 149, 577-583.

(239). Shi, C.; Cui, X.; Xie, L.; Liu, Q.; Chan, D. Y.; Israelachvili, J. N.; Zeng, H. Measuring forces and spatiotemporal evolution of thin water films between an air bubble and solid surfaces of different hydrophobicity. *ACS Nano* **2014,** 9, 95-104.

(240). Evdokimov, I. N.; Fesan, A. A. Multi-step formation of asphaltene colloids in dilute solutions. *Colloids Surf., A* **2016**.

(241). Tchoukov, P.; Czarnecki, J.; Dabros, T. Study of water-in-oil thin liquid films: Implications for the stability of petroleum emulsions. *Colloids Surf., A* **2010,** 372, 15-21.

(242). Yang, F.; Tchoukov, P.; Pensini, E.; Dabros, T.; Czarnecki, J.; Masliyah, J.; Xu, Z. Asphaltene subfractions responsible for stabilizing water-in-crude oil emulsions. Part 1: interfacial behaviors. *Energy & Fuels* **2014,** 28, 6897-6904.

(243). Chen, D. C.; Lai, Y. L.; Lee, S. Y.; Hung, S. L.; Chen, H. L. Osteoblastic response to collagen scaffolds varied in freezing temperature and glutaraldehyde crosslinking. *Journal of Biomedical Materials Research Part A* **2007,** 80, 399-409.

(244). Hennink, W.; Van Nostrum, C. F. Novel crosslinking methods to design hydrogels. *Advanced drug delivery reviews* **2012,** 64, 223-236.

(245). Yeung, A.; Moran, K.; Masliyah, J.; Czarnecki, J. Shear-induced coalescence of emulsified oil drops. *J. Colloid Interface Sci.* **2003,** 265, 439-443.

(246). Morrow, N. R. Wettability and its effect on oil recovery. *J. Pet. Technol.* **1990,** 42, 1,476-1,484.

(247). Shi, C.; Zhang, L.; Xie, L.; Lu, X.; Liu, Q.; Mantilla, C.; van den Berg, F. G.; Zeng, H. Interaction Mechanism of Oil-in-Water Emulsions with Asphaltenes Determined using Droplet Probe AFM. *Langmuir* **2016**.

(248). Liu, J.; Xu, Z.; Masliyah, J. Studies on bitumen-silica interaction in aqueous solutions by atomic force microscopy. *Langmuir* **2003,** 19, 3911-3920.

(249). Doudrick, K.; Liu, S.; Mutunga, E. M.; Klein, K. L.; Damle, V.; Varanasi, K. K.; Rykaczewski, K. Different shades of oxide: From nanoscale wetting mechanisms to contact printing of gallium-based liquid metals. *Langmuir* **2014,** 30, 6867-6877.

(250). Ladd, C.; So, J. H.; Muth, J.; Dickey, M. D. 3D printing of free standing liquid metal microstructures. *Adv. Mater.* **2013,** 25, 5081-5085.

(251). Feng, L.; Zhang, Z.; Mai, Z.; Ma, Y.; Liu, B.; Jiang, L.; Zhu, D. A super-hydrophobic and super-oleophilic coating mesh film for the separation of oil and water. *Angew. Chem. Int. Ed.* **2004,** 43, 2012-2014.

(252). Zhang, W.; Shi, Z.; Zhang, F.; Liu, X.; Jin, J.; Jiang, L. Superhydrophobic and superoleophilic PVDF membranes for effective separation of water-in-oil emulsions with high flux. *Adv. Mater.* **2013,** 25, 2071-2076.

(253). He, K.; Duan, H.; Chen, G. Y.; Liu, X.; Yang, W.; Wang, D. Cleaning of Oil Fouling with Water Enabled by Zwitterionic Polyelectrolyte Coatings: Overcoming the Imperative Challenge of Oil–Water Separation Membranes. *ACS Nano* **2015,** 9, 9188-9198.

(254). Li, J.; Wu, R.; Jing, Z.; Yan, L.; Zha, F.; Lei, Z. One-step spray-coating process for the fabrication of colorful superhydrophobic coatings with excellent corrosion resistance. *Langmuir* **2015,** 31, 10702-10707.

(255). Xie, L.; Wang, J.; Shi, C.; Huang, J.; Zhang, H.; Liu, Q.; Liu, Q.; Zeng, H. Probing Surface Interactions of Electrochemically Active Galena Mineral Surface Using Atomic Force Microscope. *J. Phys. Chem. C* **2016**.

(256). Boinovich, L.; Emelyanenko, A. Wetting and surface forces. *Adv. Colloid Interface Sci.* **2011,** 165, 60-69.

(257). Ralston, J.; Dukhin, S.; Mishchuk, N. Wetting film stability and flotation kinetics. *Adv. Colloid Interface Sci.* **2002,** 95, 145-236.

(258). Manica, R.; Connor, J. N.; Clasohm, L. Y.; Carnie, S. L.; Horn, R. G.; Chan, D. Y. Transient responses of a wetting film to mechanical and electrical perturbations. *Langmuir* **2008,** 24, 1381-1390.

(259). Lockie, H. J.; Manica, R.; Stevens, G. W.; Grieser, F.; Chan, D. Y.; Dagastine, R. R. Precision AFM measurements of dynamic interactions between deformable drops in aqueous surfactant and surfactant-free solutions. *Langmuir* **2011,** 27, 2676-2685.

(260). Hsu, P. Y.; Dhinojwala, A. Contact of oil with solid surfaces in aqueous media probed using sum frequency generation spectroscopy. *Langmuir* **2012,** 28, 2567-2573.

(261). Tang, G.; Morrow, N. R. Salinity, temperature, oil composition, and oil recovery by waterflooding. *SPE Reservoir Eng.* **1997,** 12, 269-276.

(262). Buckley, J.; Liu, Y.; Monsterleet, S. Mechanisms of wetting alteration by crude oils. *SPE J.* **1998,** 3, 54-61.

(263). Taqvi, S. T.; Almansoori, A.; Bassioni, G. Understanding the Role of Asphaltene in Wettability Alteration Using ζ Potential Measurements. *Energy & Fuels* **2016,** 30, 1927-1932.

(264). Sabbah, H.; Morrow, A. L.; Pomerantz, A. E.; Zare, R. N. Evidence for island structures as the dominant architecture of asphaltenes. *Energy & Fuels* **2011,** 25, 1597-1604.

(265). Schuler, B.; Meyer, G.; Peña, D.; Mullins, O. C.; Gross, L. Unraveling the molecular structures of asphaltenes by atomic force microscopy. *J. Am. Chem. Soc.* **2015,** 137, 9870-9876.

(266). Adams, J. J. Asphaltene adsorption, a literature review. *Energy & Fuels* **2014,** 28, 2831-2856.

(267). Turgman-Cohen, S.; Smith, M. B.; Fischer, D. A.; Kilpatrick, P. K.; Genzer, J. Asphaltene adsorption onto self-assembled monolayers of mixed aromatic and aliphatic trichlorosilanes. *Langmuir* **2009,** 25, 6260-6269.

(268). Turgman-Cohen, S.; Fischer, D. A.; Kilpatrick, P. K.; Genzer, J. Asphaltene adsorption onto self-assembled monolayers of alkyltrichlorosilanes of varying chain length. *ACS Appl. Mater. Interfaces* **2009,** 1, 1347-1357.

(269). Cui, X.; Shi, C.; Xie, L.; Liu, J.; Zeng, H. Probing Interactions between Air Bubble and Hydrophobic Polymer Surface: Impact of Solution Salinity and Interfacial Nanobubbles. *Langmuir* **2016**.

(270). Tabor, R. F.; Chan, D. Y.; Grieser, F.; Dagastine, R. R. Anomalous Stability of Carbon Dioxide in pH-Controlled Bubble Coalescence. *Angew. Chem. Int. Ed.* **2011,** 50, 3454-3456.

(271). Donaldson Jr, S. H.; Das, S.; Gebbie, M. A.; Rapp, M.; Jones, L. C.; Roiter, Y.; Koenig, P. H.; Gizaw, Y.; Israelachvili, J. N. Asymmetric Electrostatic and Hydrophobic–Hydrophilic Interaction Forces between Mica Surfaces and Silicone Polymer Thin Films. *ACS Nano* **2013,** 7, 10094-10104.

(272). de Gennes, P. G. Polymers at an interface; a simplified view. *Adv. Colloid Interface Sci.* **1987,** 27, 189-209.

(273). Manor, O.; Chau, T. T.; Stevens, G. W.; Chan, D. Y. C.; Grieser, F.; Dagastine, R. R. Polymeric Stabilized Emulsions: Steric Effects and Deformation in Soft Systems. *Langmuir* **2012,** 28, 4599-4604.